Quantum Theory of Amplifying Random Media

Dissertation
zur Erlangung des Grades
Doktor der Naturwissenschaften
(Dr. rer. nat.)
vorgelegt am Fachbereich Physik der
Universität Duisburg–Essen

von

Carlos L. Viviescas Ramírez
aus Medellín

Essen, Juni 2004

1. Gutachter: PD Dr. G. Hackenbroich
2. Gutachter: Prof. Dr. R. Graham
Tag der Disputation: 21. Juni 2004

abstract

A quantum theory of lasing in random media is presented. The theory constitutes a generalization of the standard laser theory, accounting for lasing in resonators with spectrally overlapping modes due to large outcoupling losses, and incorporating in a natural fashion the statistical properties of chaotic modes when apply to lasers in random media or inside chaotic resonators.

We study the photocount statistics of the radiation emitted from a chaotic laser resonator in the regime of single-mode lasing. The random spatial variations of the resonator eigenfunctions are incorporated in the theory, and showed to lead to strong mode-to-mode fluctuations of the laser emission. The distribution of the mean photocount over an *ensemble of modes* changes qualitatively at the lasing transition, and displays up to three peaks above the lasing threshold.

We then address the quantization of the electromagnetic field in weakly confining resonators using Feshbach's projection technique. We consider both inhomogeneous dielectric resonators with a scalar dielectric constant $\epsilon(\boldsymbol{r})$ and cavities defined by mirrors of arbitrary shape. The field is quantized in terms of a set of resonator and bath modes. We rigorously show that the field Hamiltonian reduces to the system-and-bath Hamiltonian of quantum optics. The field dynamics is investigated using the input-output theory of Gardiner and Collet. In the case of strong coupling to the external radiation field we find spectrally overlapping resonator modes. The mode dynamics is coupled due to the damping and noise inflicted by the external radiation field. We derived Langevin equations and a master equation for the resonator modes. For linear optical systems, including gain/loss contributions, it is shown that the field dynamics is described by the system S matrix. For wave chaotic resonator the dynamics is determined by a non-Hermitian random matrix.

After including an amplifying medium, we use the open-resonator dynamics to construct a quantum theory for lasing in random media. We investigate the emission spectrum of lasers in cavities with overlapping modes operating in the single-mode regime. The noise properties of such lasers are seen to differ from traditional lasers due to the presence of excess noise. Our theory not only accounts for the Petermann linewidth enhancement, but predicts deviations of the laser line from a Lorentzian shape. To conclude, the emission spectrum of random lasers is discussed.

A Olga

Contents

Chapter 1

Introduction

Random lasers are a novel class of nonlinear amplifiers realized in disordered dielectrics with a dielectric function $\epsilon(\boldsymbol{r})$ that varies randomly in space. In contrast to standard lasers in which the confinement of light is achieved by means of mirrors, random lasers are cavities without mirrors in which the feedback of light results from multiple scattering in the random media (see Fig. 1.1). Light amplification is provided by an active optical medium. Due to chaotic scattering, light is trapped inside the material for long enough times for the amplification to become efficient. Laser oscillations emerge when the amplification exceeds the loss rate due to escape from and absorption in the medium.

In this thesis we present a quantum theory for lasing in random media. Our theory applies to random lasers as well as to chaotic laser cavities, hereafter called chaotic lasers, in which randomness is the consequence of the irregular shape of the cavity or of artificial scatters inside of it. The two types of random media considered in this thesis are shown in Fig. 1.1.

In recent years several experiments have demonstrated random laser action (for a review see Refs. [1, 2]). Important contributions were made by H. Cao and her group in an extensive series of experiments on amplifying random media using dielectric films [3, 4, 5], disordered dielectric cluster [6], and suspensions of scattering particles in dye solutions [7]. Figure 1.2 reproduces measured emission spectra of a suspension of zinkoxide microparticles in a dye solution of rhodamine 640; the pump strength increases from bottom to top. The dye solution is used as amplifying medium while the zinkoxide particles act as scatterers. The density of scatterers determine the strength of the disorder. The samples were optically pumped and the emitted light was collected by a photodetector. For small pumping one observes a smooth emission spectrum with a broad maximum due to amplified spontaneous emission. However, at a critical pump the spectrum changes dramatically. Depending on the disorder two different behaviors are found: For weak disorder a single maximum is present but its linewidth shrinks very fast (Fig. 1.2(a)). For strong disorder, in contrast, a number of sharp peaks appear (Fig. 1.2(b)). Both phenomena signal the onset of lasing. This interpretation is confirmed by measurements of the photon statistics [8, 9]. They show a crossover from thermal statistics $P(n) \sim [\bar{n}/(1+\bar{n})]^n$ below threshold to a Poissonian statistics $P(n) = [\bar{n}^n/n!]\exp(-\bar{n})$ above threshold, where $P(n)$ is the occupation probability of the lasing mode with n photons, and $\bar{n}$ the mean photon number. The Poissonian

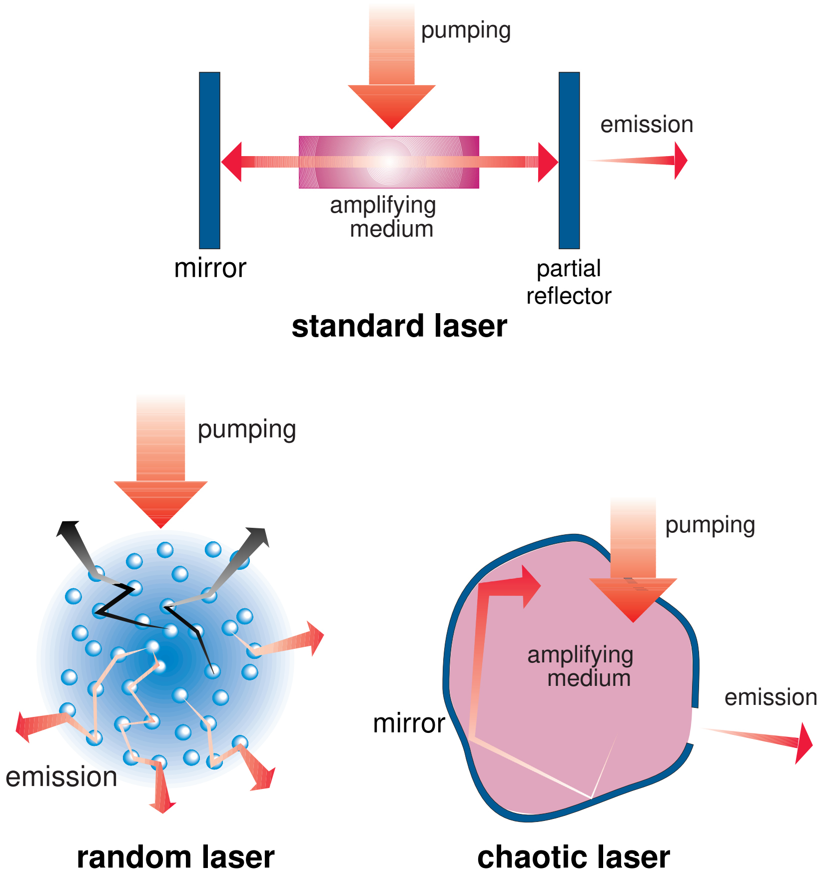

Figure 1.1: Comparison between a standard laser and the two type of random lasers considered in this thesis. In a standard laser a simple geometry of mirrors forms the cavity. The mirrors confined the light inside the resonator providing the feedback to produce laser. In a random laser there are no mirrors but due to multiple scattering the light is trapped inside the material long enough to give rise to laser. In a chaotic laser photons are confined inside the resonator by an irregular shaped configuration of mirrors long enough to ergodically explore the resonator volume.

statistics is the result expected for a single-mode laser far above threshold.

The above mentioned features of the emission spectra of random lasers cannot be explained by the standard laser theory [10, 11, 12]. The reasons are twofold: First, in random lasers the resonant modes and their frequencies depend on the statistical properties of the underlying random medium. Random lasers, therefore, must be analyzed in a statistical fashion, in contrast to standard lasers for which the simple mirrors geometry allows for an explicit determination of the resonant modes and their frequencies. Second, due to the absence of mirrors, random laser light is only weakly confined. This gives rise to spectrally overlapping modes. Standard lasers, in contrast, usually display well-isolated modes with high-Q. In order to attain a complete understanding of random lasers both effects, random scattering of light and mode overlap, must be included in a theory of random lasers. In this thesis we show how this can be done in the framework of a quantum theory of random lasing. The following introduction

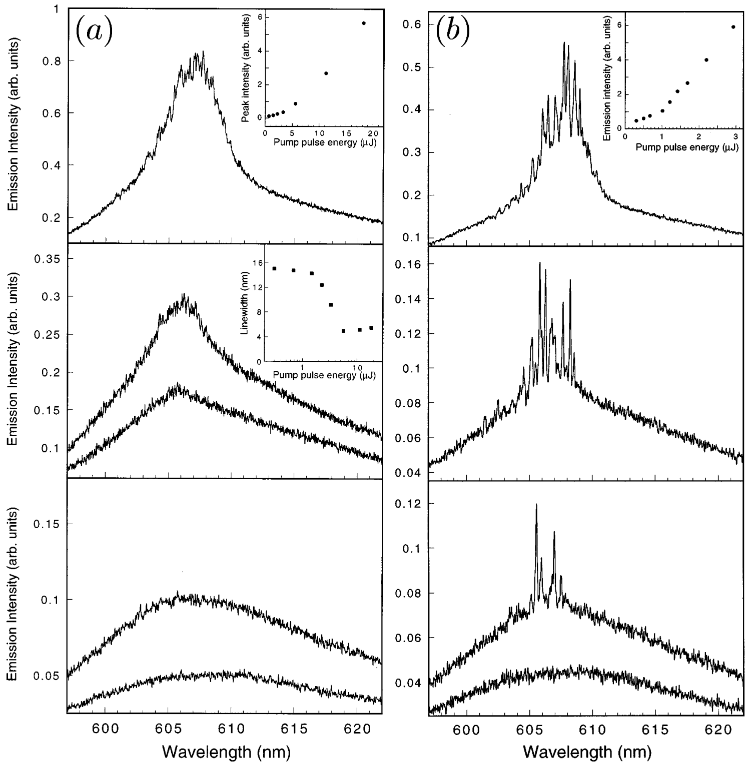

Figure 1.2: Emission spectra from rhodamine 640 dye solution containing ZnO nanoparticles as measured by Cao et al [7]. (a) Random laser with weak disorder. The ZnO particle density is $\sim 3 \times 10^{11}\mathrm{cm}^{-3}$. The incident pump-pulse energy is (from bottom to top) 0.68, 1.5, 2.3, 3.3, and 5.6 μJ. The laser threshold corresponds to a pump-pulse of $\sim 3\,\mu$J. The upper inset is the emission intensity at the peak wavelength versus the pump pulse energy. The lower inset shows the emission linewidth versus the pump pulse energy. (b) Random laser with strong disorder. The ZnO particle density is $\sim 1 \times 10^{12}\mathrm{cm}^{-3}$. The incident pump pulse energy is (from bottom to top) 0.68, 1.1, 1.3, and 2.9 μJ. The laser threshold corresponds to a pump-pulse of $\sim 1\,\mu$J. The inset shows the emission intensity versus the pump-pulse energy.

provides a short review of early theoretical ideas and recent semiclassical approaches to random lasing. We discuss the consequences of mode overlap and summarize previous approaches to the field quantization in media with overlapping modes. The fact, that none of these approaches allows to include random scattering of light partly motivated our work on random lasers.

1.1 Early Ideas

The theoretical study of random lasing was initiated in a seminal paper by Letokhov [13]. He introduced the concept of feedback by diffusive scattering and stated the feasibility of random lasing. Letokhov considered a disordered medium in which light scatters irregularly. The disorder strength can be characterized by the (transport) mean free path l_t. Light propagates diffusively provided $L \gg l_\mathrm{t} \gg \lambda$, where L is the linear size of the medium and λ the wavelength of light. Assuming a uniform linear gain, the spectral density of photons follows a diffusion type of equation [13, 14],

$$\frac{\partial W(\boldsymbol{r},\omega,t)}{\partial t} = D\nabla^2 W(\boldsymbol{r},\omega,t) + \frac{v}{l_\mathrm{g}} W(\boldsymbol{r},\omega,t)\,, \tag{1.1}$$

where v is the transport velocity of light inside the scattering medium, l_g is the gain length, and $D = vl_\mathrm{t}/3$ the diffusion constant. Note that l_g is frequency dependent; it reaches its maximum at the frequency of the laser transition. Equation (1.1) must be complemented by boundary conditions. Clearly, the density of photons vanishes far away from the medium. At the boundary it cannot be zero as photons cross the boundary upon emission from the sample. Exact solutions of the emission problem for simple geometries show that the photon density, linearly extrapolated from the boundary, vanishes at a distance of order l_t [15]. As l_t is much smaller than the system size L, we may impose the condition $W(\boldsymbol{r},\omega,t) = 0$ directly at the boundary, yielding a very good approximation to the true boundary conditions. The general solution to Eq. (1.1) is then easily seen to be given by

$$W(\boldsymbol{r},\omega,t) = \sum_n a_n \Psi_n(\boldsymbol{r}) \mathrm{e}^{-(DB_n^2 - v/l_g)t}\,, \tag{1.2}$$

where $\Psi_n(\boldsymbol{r})$ and B_n are the eigenfunctions and eigenvalues, respectively, of the Helmholtz equation

$$\nabla^2 \Psi_n(\boldsymbol{r}) + B_n^2 \Psi_n(\boldsymbol{r}) = 0\,, \tag{1.3}$$

with boundary conditions $\Psi_n = 0$ at the boundary of the scattering medium.

The laser threshold is defined by the crossover of the photon density in Eq. (1.2) from a decaying solution to a solution that increases exponentially in time. The threshold condition then follows at once from Eq. (1.2),

$$DB_1^2 - v/l_g = 0\,, \tag{1.4}$$

where $B_1 \approx 1/L$ is the lowest eigenvalue. At the threshold the typical path length $L_\mathrm{pat} \sim vL^2/D$ of light propagating inside the active material matches or exceeds the gain length; then, on average, each emitted photon will generate another photon before escaping from the medium. Based on this threshold condition, Letokhov predicted a critical volume for the onset of lasing

$$V_\mathrm{cr} \approx L^3 \approx \left(\frac{l_\mathrm{t} l_\mathrm{g}}{3}\right)^{3/2}\,. \tag{1.5}$$

As the proliferation of light in amplifying random media is similar to the generation of neutrons in nuclear reactors and atomic bombs, early theoretical work coined the term photonic bomb.

1.2 Lasing: Nonlinear Equations

Clearly, the exponential increase predicted by the diffusion equation (1.1) is not found in actual media. In reality, the gain length does depend on the photon intensity: for large photon density the gain is eventually depleted and $l_{\rm g}$ increases. The description of laser emission should combine the concept of diffusive feedback with nonlinear gain saturation. Letokhov [14] and John and Pang [16] implemented a set of nonlinear diffusive equations for the photon density in the scattering medium with a photon density-dependent gain length. Their theory proved to account for the linewidth shrinking of the spectrum. Focusing on the spectral line narrowing, Balachandran, Lawandy, and Moon [17] proposed a laser model based on nonlinear rate equations for the inversion population N of a two-level atomic medium and the mean field intensity $W(\omega)$,

$$\frac{\mathrm{d}N(t)}{\mathrm{d}t} = [1 - N(t)]B_p\Lambda(t) - N(t)\int \mathrm{d}\omega\, B_l(\omega)W(\omega, t) - N(t)\Gamma\,, \tag{1.6a}$$

$$\frac{\partial W(\omega, t)}{\partial t} = c[\gamma_0(\omega)N(t) - \gamma_{\rm th}]W(\omega, t) + \eta(\omega)N(t)\,, \tag{1.6b}$$

where Λ is the pump intensity, and B_p and B_l are the Einstein coefficients for the pump and the laser emission, respectively. The noise terms $N\Gamma$ and ηN were added phenomenologically to mimic spontaneous emission. The set of equations describe many phenomena that were found in early experiments [18, 19, 20, 21] on random media (see Fig 1.2(a)): A threshold pumping with a much stronger increase of the emission output above threshold, a collapse of the emission linewidth at threshold, relaxation oscillations of the emission intensity. In contrast to the experiments of Cao et al such early experiments did not reveal quasi–discrete emission peaks. The respective devices are sometimes called lasers with non–resonant feedback.

1.3 Petermann Excess Noise

The theoretical approaches to random lasing discussed above are based on a classical description of the electromagnetic field. The laser dynamics is then describe by semi-classical equations: They characterize the mean values of the spectral photon density and the atomic inversion. Quantum effects such as spontaneous emission and vacuum fluctuations are taken into account phenomenologically by including noise terms. In lasers, spontaneous emission noise is ultimately responsible for the laser linewidth, below the laser threshold it gives rise to amplified spontaneous emission. A proper description of noise can only be provided by a quantum laser theory.

It has long been known that lasers with overlapping modes exhibit unusual noise properties. In his investigations on gain-guided lasers, Petermann [22] found that these lasers exhibit a greatly increased linewidth $\delta\omega$, whose enhancement with respect to the Schawlow–Townes limit $\delta\omega_{\rm ST}$ [23] can be described by an excess noise factor $K \geq 1$ known as the Petermann factor,

$$\delta\omega = K\delta\omega_{\rm ST}. \tag{1.7}$$

Later, Siegman demonstrated [24, 25] that this effect was not restricted to gain-guided lasers, but was present in all laser cavities with spectrally overlapping modes. He noticed that due to mode overlap the cavity modes do not form an orthogonal set but a biorthogonal set. Thus, generically, one can associate to each cavity resonance a left mode $\langle L_l|$ and a right mode $|R_l\rangle$. The biorthogonality condition then reads

$\langle L_l | R_k \rangle = \delta_{lk}$. Excess noise is generated as noise corresponding to different cavity modes is correlated; Petermann excess noise is thus intrinsically a multi-mode phenomenon. The net result, however, can be observed in a single mode laser as an increase in the amplitude and phase fluctuations by the Petermann factor. For the laser oscillation in mode l, the Petermann factor takes the form

$$K_l = \langle L_l | L_l \rangle \langle R_l | R_l \rangle \geq 1 \, ; \tag{1.8}$$

where use was made of the Schwartz' inequality.

Excess noise has been experimentally well established: It has been detected in stable cavities with large losses [26, 27, 28], unstable resonators with nonorthogonal transverse modes [29, 30], and lasers with nonorthogonal polarization modes [31, 32]. Despite of large theoretical and experimental evidence for excess noise, a quantum theory of the phenomenon has long been missing. The quantum theory of random laser presented in this thesis provides also a quantum description of excess noise. Recently, alternatively to our work [33] other quantum approaches to excess noise have been reported [34, 35].

1.4 Field Quantization of Leaky Cavities

The development of a quantum theory of excess noise has been hampered for a long time by the lack of a proper quantization method of the electromagnetic field in open resonators. Conventionally the electromagnetic field in a leaky cavity is quantized in terms of modes of a *closed* resonator, while the cavity losses are modeled by coupling each mode to an external bath that provides both damping and noise [11, 36]. That traditional formulation of the system-and-bath model [37, 38, 39] assumes spectrally isolated sharp resonator modes, and therefore applies successfully to the high-Q modes of traditional laser cavities. However, that description fails when the cavity losses become so large that modes overlap. Mode overlap is expected, in particular, for unstable laser cavities and mirrorless random lasers. For such lasers a quantization scheme suitable for open laser resonators must be used.

Developing appropriate quantization methods has been a fundamental problem of quantum optics and has generated a substantial amount of literature. In their classical paper [40], Fox and Li numerically studied open resonators taking into account diffractive losses. They found that open resonators support a well-defined set of modes which due to the losses generally differ from the eigenmodes of closed cavities. In particular, they do not form an orthogonal set. The Fox-Li modes correspond to the Gamov states [41] of scattering theory. Lang, Scully and Lamb [42] proposed the first rigorous quantization procedure for the field in open optical cavities. Their so-called modes-of-the-universe approach consist in quantizing the eigenmodes of Maxwell's equations in the whole space comprising the resonator and the external world. Their method has been applied to a number of open resonators problems [43, 44, 45, 46, 47, 48, 49, 50, 51]. Although the modes-of-the-universe approach provides an exact quantum description of the electromagnetic field, it makes no distinction between the cavity and its environment. Therefore it fails to single out explicit information about the dynamics of the field inside the cavity.

In recent years, studies on excess noise renewed the interest in open cavities and several new field quantization schemes were proposed. They are either based on mode expansions or they altogether abandon the idea of cavity modes. The quasimodes of Dalton, Barnett, and Knight [52, 53] provide a complete basis of field modes satisfying idealized boundary conditions at the resonator surface. Quasimode expansions have been successfully applied in cavity quantum electrodynamics [54, 55, 56, 57, 58]. Fundamentally, however, the quasimode method suffers from the same problem as the modes-of-the-universe approach: The quasimodes are defined throughout the whole space and therefore provide no specific information about the cavity field. In order to overcome this structural disadvantage, methods involving nonorthogonal (Fox–Li) modes have been developed. Most remarkable are the works by Young and collaborators [59, 60] and by Lamprecht and Ritsch [61, 62, 34]. These last authors introduced an *ad hoc* master equation for open cavities in order to describe the field damping. Since that equation was not derived from first principles, its status remained unclear. Fox–Li expansions of both the cavity and the external field were developed in Refs. [63, 64]. Both approaches claim to constitute a starting point for a quantum theory of excess noise, however, to the best of our knowledge, up to now none of them has been used for that purpose.

Alternative approaches not based on mode expansions were developed by Gruner and Welsch [65, 66] and by Artoni and Loudon [67]. Their quantization methods are based on Green functions and allow to include complex, frequency and spatially dependent dielectric functions. These approaches have been used in connection with *linear* random media in the papers of Beenakker [68, 69] (see Sec. 1.5). Since the method is based on Green functions it can not be extended to include nonlinear phenomena like lasers.

In this thesis we address the problem of the quantization of the electromagnetic field in open optical cavities. Our approach provides a first principle derivation of a system-and-bath type Hamiltonian. In contrast to previous approaches, we derive microscopic expressions for all mode frequencies and coupling amplitudes. The quantization procedure allows for a microscopic description of atom-field interactions. In connection with random matrix theory, our method provides a basis for a statistical theory of random lasers.

1.5 Linear Random Media

For weak pumping, below the laser threshold, random lasers behave like linear random amplifiers. A comprehensive quantum theory of light propagation in linear active random media was recently presented by Beenakker and coworkers [68, 69, 70]. Based on a scattering quantization of the electromagnetic field [65, 66, 67], they implemented an input-output relation for the propagating field. The emission intensity was then showed to be completely determined by the system S matrix. Since the medium is active the S matrix is generally not unitary, but becomes sub-unitary in absorbing media and super-unitary in amplifying media (cf. Eq. (4.47)). The statistical properties of the emitted light follow from the statistics of the S matrix. When applied to random media, the statistical properties of the S matrix are known from random matrix theory. A major prediction of the theory was the characterization of the super-Poissonian noise of a random medium as corresponding to a black body with a reduced number of degrees of freedom [68]. In addition Beenakker and co-workers computed the photon noise spectrum [71] and investigated the effects of photon localization [72] in linear random media.

Most noticeable, Beenakker's theory of light propagation naturally included both the statistical nature of the random modes and the mode overlapping due to the weak confinement of light in random media. It allows for an investigation of the noise enhancement in linearly amplifying media below the laser threshold, and for an statistical treatment of the Petermann factor for linear disordered media [73, 74, 75]. The theory for random lasing proposed in this thesis reduces to Beenakker's for amplifying media below the lasing threshold.

1.6 About this Thesis

The physics of amplifying random media involves both chaotic scattering and weak confinement of light. Theoretically, therefore, methods and concepts coming from both quantum optics and quantum chaos theory must be used. We study first the consequences of chaotic scattering. To this end, we investigate in *Chapter 2* the photocount statistics of the radiation emitted from an almost closed chaotic laser cavity in the regime of single-mode lasing. Chaotic scattering causes strong mode-to-mode fluctuations of the laser losses, giving rise to additional fluctuations of the photocount statistics *on top* of the quantum fluctuations inherent to the quantized electromagnetic field. For cavities with a small number of escape channels the distribution of the mean photocount number is shown to be broad, revealing up to three peaks.

In *Chapter 3* we address the quantization of the electromagnetic field in weakly confining resonators. We present and discuss an exact quantization procedure for *open* cavities. Our method is based on a technique from nuclear and condensed-matter physics known as the Feshbach projection formalism [76]. We rigorously derive a system-and-bath Hamiltonian for the electromagnetic field starting from Maxwell's equations. The Hamiltonian is shown to correctly describe damping and even overdamping in open resonators (when the damping rates become of the order of the oscillation frequencies). In the limit of small outcoupling losses our field Hamiltonian reduces to the well-known independent oscillator model of quantum optics. Randomness can be naturally included in our formulation employing random matrix theory. We conclude by illustrating the quantization method in a series of frequently used optical resonators.

The dynamics of optical fields in open cavities is studied in *Chapter 4*. For linear optical systems we show that the field dynamics can be completely described by the S matrix of the open resonator which may include gain/loss contributions. Taking into account the multi-mode nature of the field, we derive and clarify the status of stochastic equations for the field dynamics in resonators with overlapping resonances. Our equations provide for a quantum picture of excess noise. Upon inclusion of an active medium, our quantization technique constitutes the basis of our laser theory for open lasers with overlapping modes.

A quantum theory for lasing in random media is formulated in *Chapter 5*. A set of quantum lasers equations is derived that includes the atomic-field interactions on a microscopic level. The noise properties of such lasers is seen to differ from traditional lasers. To explore the differences we consider the emission spectra of linear random media below the laser threshold, and postpone a complete discussion on excess noise to *Chapter 6*.

Although the semiclassical picture of excess noise has been known for some time, a quantum theory of it was lacking. In *Chapter 6* we show that our lasers equations provide a quantum description of excess noise. We concentrate on a laser operating above threshold in the regime of single-mode lasing. Our theory not only accounts for the Petermann linewidth enhancement due to excess noise, but predicts the deviation of the laser line from a Lorentzian shape. We conclude with a discussion on the consequences of such deviations in the emission spectra of random lasers.

Chapter 2

Photocount Statistics of Chaotic Lasers

It has been known since the early days of the quantum theory of laser, that the nonlinear interactions between the optical field and the active medium in a single-mode laser leads to drastic changes in the statistics of the photon field [10, 36, 77, 78]: Below the laser threshold, losses outweigh the gain by linear amplification such that nonlinear saturation is negligible. Then the photon statistics is well represented by a thermal distribution, and the probability P_n for the occupation of the mode with n photons decays as the power law $P_n \sim [\bar{n}/(1+\bar{n})]^n$ ($\bar{n}$ is the mean photon number). Above threshold nonlinear interactions stabilize the field intensity. The (relative) intensity fluctuations are strongly reduced below the value found for a thermal distribution, and far above threshold P_n approaches the Poissonian distribution $P_n = [\bar{n}^n/n!]\exp(-\bar{n})$ characteristic for a coherent state.

Recent experiments on random lasers [1] as well as on laser in chaotic resonator with irregularly shaped boundary [79] have dragged considerable interest on the characterization of the properties of light emitted by these novel devises. Contrary to the profusion of theoretical investigations [68, 69, 72, 71] on the linear optical regime of such systems, theoretical studies on the nonlinear optical regime are still scarce. In particular, little is known about the photocount statistics above the laser threshold in random media. In this Chapter we address that problem in the regime of single-mode lasing in an almost closed chaotic resonator. This problem provide us with an excellent opportunity to get familiar with the kind of mixing of ideas and concepts coming from quantum optics and quantum chaos theory, that the study of light in random media requires. We show that the chaotic nature of the cavity modes gives rise to fluctuations of the photocount *on top* of the quantum optical fluctuations known from laser theory. Chaos-induced fluctuations are found when a single-mode photodetection is performed over an *ensemble* of modes. The ensemble may be obtained from a single resonator upon varying suitable parameters or from different resonators with small variations in shape. Two kind of ensembles are considered depending on the strength of the pumping: An above threshold ensemble, in which the system gain exceeds the ensemble average loss for the laser mode; and a below threshold ensemble in which all lasers of the ensemble operates below the laser threshold. The factorial moments of the photocount display strong fluctuations from one mode to another. We evaluate numerically

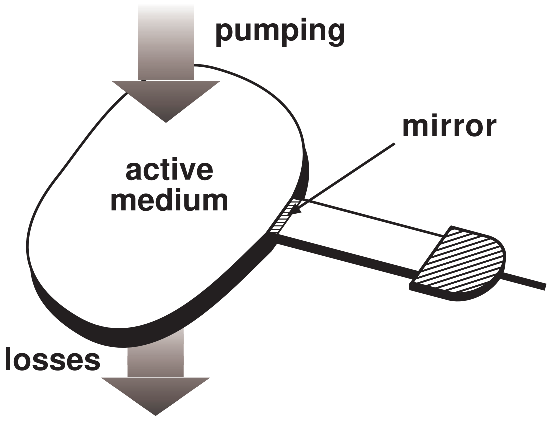

Figure 2.1: Sketch of chaotic laser cavity with a partly transmitting mirror. The cavity is connected to a waveguide and a frequency selective photodetector.

the distribution of the mean photocount and show that for the case of a chaotic cavity with a small number of escape channels this distribution is broad, differing significantly from a Gaussian.

Most of the results presented in this chapter have been reported in Ref. [80].

2.1 Chaotic Lasers

We consider a chaotic laser: a chaotic resonator with an irregular shaped boundary homogeneously filled with an amplifying medium. In this chapter we concentrate on the study of the simple case of laser oscillation in a single cavity mode which is in resonance with the amplifying medium at frequency ω_0. A sketch of the system is shown in Fig. 2.1. The cavity has an opening and is coupled to a waveguide that supports M transverse modes at frequency ω_0. A partly transmitting mirror reflects impinging radiation with mean probability R back into the resonator. The fraction $T = 1 - R$ of radiation is transmitted and injected into the waveguide. A frequency selective photodetector counts the transmitted photons with efficiency 1 at the other end of the waveguide. Due to the opening the modes acquire finite widths Γ. We restrict ourselves to the case of weak outcoupling to the outside world, defined by the condition

$$\overline{\Gamma} \ll \Delta\omega_0 \,, \tag{2.1}$$

where $\Delta\omega_0$ is the cavity mean mode separation. The cavity then has a quasidiscrete spectrum and the mode wavefunctions can be approximated by the eigenfunctions of the closed cavity $u(\boldsymbol{r})$ (for simplicity, in this chapter, we neglect the field polarization and work with an scalar amplitude for the field). Since the mean cavity escape rate $\overline{\Gamma} = MT\Delta\omega/2\pi$, in the weak coupling regime the mirror transmission coefficient T must be small, $MT \ll 1$. The counting time t of photons arriving at the photodector will be assumed large enough that the radiation from individual cavity modes can be resolved, $t\Delta\omega \gg 1$.

As for the active medium, we allow for $\mathcal{N}$ active two-level atoms with transition frequency ω_0. The p-th atom "sees" the field mode through a coupling constant g_p proportional to both the atomic dipole matrix element d and the value of the lasing mode at the location of the atom, $g_p \propto d\,u(\boldsymbol{r}_p)$. We only consider the simplest situation in which the characteristic times for atomic pump and losses are short compared to the mean life time of a photon in the cavity, so that we can adiabatically eliminate the medium variables from the equations of motion for the system.

2.1.1 Single-Mode Laser

A laser oscillation in a single-mode is characterized by three parameters comprising the effect of the atoms on the field mode: A, B, C that characterize the linear gain, the nonlinear saturation, and the total loss, respectively. The first two parameters depend on the atomic-field coupling constants as [10, 77, 78]

$$A \sim \sum_{p=1}^{\mathcal{N}} g_p^2, \qquad B \sim \sum_{p=1}^{\mathcal{N}} g_p^4\,, \tag{2.2}$$

while the total loss rate

$$C = \Gamma + \kappa \tag{2.3}$$

is the sum of the photon escape rate Γ, due to the cavity opening, and the absorption rate κ, that accounts for all other loss mechanisms of the the radiation field inside the cavity. While here κ may be considered fixed, both the coupling amplitudes g_p and the photon escape rate Γ depend on the resonator mode, and inasmuch as the resonator mode represents wave chaos these two quantities become random numbers. We may then ask for the effect of the chaotic wavefunction nature on the parameters A, B, and C; this problem will be considered in the following section.

As an illustration of the way these three parameters determined the laser state, we write down the steady–state photon number distribution for a single-mode laser [10, 77, 78]

$$P_n = \mathsf{N}\frac{[An_s/C]^{n+n_s}}{(n+n_s)!}\,, \tag{2.4}$$

which gives the probability to find n photons at a time t in the laser field. The symbol N represents a normalization constant and the nonlinear saturation B enters through the so-called saturation photon number $n_s = A/B$. Two limits of the distribution (2.4) sufficiently far from threshold will be of relevance for us: The below threshold limit, $A < C$, in which the photon number distribution can be shown to reduce to a thermal distribution. And the above threshold limit, $A > C$, where the distribution (2.4) is well approximated by a Poissonian distribution characteristic of a coherent state. The mean photon number in this two limits is then given by

$$\overline{n} = \begin{cases} \frac{A}{C-A} & \text{for } A < C\,, \\ n_s\frac{A-C}{C} & \text{for } A > C\,. \end{cases} \tag{2.5}$$

2.1.2 Chaotic Modes

If the cavity is weakly coupled to the outside world we may use the modes of the closed cavity to describe the electromagnetic field inside the resonator. Let $u_\lambda(\boldsymbol{r})$ be the amplitude of the closed cavity mode at frequency ω_λ, normalized according to $\int \mathrm{d}\boldsymbol{r}\, |u_\lambda(\boldsymbol{r})|^2 = 1$. In a chaotic cavity the amplitude $u_\lambda(\boldsymbol{r})$ at the point $\boldsymbol{r}$ behaves like a random Gaussian variable, and is uncorrelated with the amplitude at any other point provided it lies further apart than an optical wave length λ [81, 82, 83]. The chaotic modes $u_\lambda(\boldsymbol{r})$ are then mimicked by a random superposition of plane waves with wave number $k_\lambda = \omega_\lambda/c$ [84, 85, 86].

At this point we determined the consequences that considering a chaotic wavefunction may have on the laser parameters A, B, and C. The coupling amplitudes g_p, being proportional to the mode wavefunction, behave like random Gaussian variables. It follows from Eq. (2.2) for the linear gain and the nonlinear saturation that for a large number of atoms, $\mathcal{N} \gg 1$, the distributions for the parameters A and B become sharp due to central limit theorem. The total loss rate C, on the other hand, depends on the photon escape rate, $\Gamma = \sum_{i=1}^{M} |\gamma_i|^2$. The latter, like the g_p, is also a random variable, as will be revealed presently. The outcoupling amplitude γ_i of the field mode into the ith transverse channel of the waveguide are independent random quantities with Gaussian statistics, since they represent the local fluctuations of the resonator mode across the outcoupling mirror. In fact, their randomness constitutes the principle effect of the wave chaos within the resonator on the ensemble fluctuations of the laser output (see Eq. (2.8)). The Gaussian statistics of the γ's implies that the distribution of Γ over an *ensemble of modes* is the χ^2_ν distribution

$$P(\Gamma) = \mathsf{A}_\nu \Gamma^{\nu/2-1} \exp(-\nu\Gamma/2\overline{\Gamma}) \tag{2.6}$$

well known from random–matrix theory [87]. Here, $\nu = \beta M$ is an integer and A_ν a normalization constant. The value of the parameter β depends on whether the system is time-reversal invariant ($\beta = 1$) or whether time-reversal invariance is broken ($\beta = 2$) [87, 85]. The special case $M = \beta = 1$ is known as the Porter–Thomas distribution. We have thus shown that in a single-mode laser the effects of the chaotic nature of the wave functions are contained in the fluctuations of the loss C given by Eq. (2.6).

2.2 Photodetection Statistics

A photocount experiment gives a statistical measure of the arrival frequency of photons at the photodetector in a given time interval. As is usually the case, the photodetector is placed outside the cavity. Thus, although the photons registered at the detector correspond to the state of the field outside the resonator, we may use the input–output relations to relate the results of a photocount experiment to the intracavity field.

2.2.1 Input-Output Relation

The photons arriving at the photodector correspond to the field in the wave guide and do not provide direct information about the state of the field inside the cavity. In order to relate the measurements made by the photodector to the state of the field inside the cavity, we use the input–output theory of Gardiner and Collet [88, 39, 77] (see also *Chapter 4* for a detail discussion). Waves entering and leaving the waveguide are described by M annihilation and creation operators $b_i^{\rm in}$, $b_i^{\rm in\dagger}$, $b_i^{\rm out}$, $b_i^{\rm out\dagger}$, which obey the commutation relations

$$[b_i(t), b_j^\dagger(t')] = \delta_{ij}\delta(t-t'), \qquad [b_i(t), b_j(t')] = 0\,. \tag{2.7}$$

Here, $i, j = 1, \ldots, M$ label the transverse modes of the waveguide and $b = b^{\rm in}$ or $b = b^{\rm out}$. The boundary condition

$$b_i^{\rm in}(t) + b_i^{\rm out}(t) = \gamma_i a(t)\,, \tag{2.8}$$

connects incoming and outgoing radiation in each transverse mode with the annihilation operator a of the cavity mode. While the boundary condition (2.8) results from assuming a linear coupling between the waveguide and the cavity field, *no* restriction is imposed on the intracavity dynamics. Therefore, the input-output relation (2.8) holds both below and above threshold.

In the linear regime below threshold, one can eliminate the cavity operators from Eq. (2.8) and express the outgoing radiation in terms of the incoming radiation, the intracavity noise, and the S-matrix [77, 68, 69] (cf. Eq. (4.42)). One thus obtains the photocount fluctuations [68, 69] through the S-matrix statistics known for chaotic scattering.

2.2.2 Photocount Distribution

For times t larger than $1/\Delta\omega_0$ the photodector performs a frequency resolved measurement and individual modes of the cavity can be identify. We assume that all outgoing modes in the waveguide are detected with unit efficiency by the photodector. The probability $p(n)$ that n photons are counted in the time interval t is given by [89, 90, 78]

$$p(n) = \frac{1}{n!}\langle :W^n \mathrm{e}^{-W}: \rangle\,, \tag{2.9}$$

$$W = \int_0^t \mathrm{d}t' \sum_{i=1}^{M} b_i^{\rm out\dagger}(t') b_i^{\rm out}(t')\,. \tag{2.10}$$

Here $\langle \cdots \rangle$ denote the quantum steady–state average and the colons demand normal and a certain time ordering. The photocount distribution may be evaluated using the state of the field inside the cavity. For this we use the input-output relation (2.8), which for the case of vacuum input, allow us to write Eq. (2.10) as

$$W = \Gamma I\,, \tag{2.11}$$

where I is the integrated cavity field intensity

$$I = \int_0^t \mathrm{d}t'\, a^\dagger(t') a(t')\,. \tag{2.12}$$

We characterize $p(n)$ through its factorial moments

$$\mu_r = \sum_{n=0}^{\infty} n(n-1)\cdots(n-r+1)p(n). \tag{2.13}$$

Combining Eqs. (2.9), (2.11), and (2.13) one obtains for the factorial moments

$$\mu_r = \Gamma^r \langle : I^r : \rangle \,. \tag{2.14}$$

Clearly, the first moment alias mean photocount, $\mu_1 = \Gamma t \overline{n}$, is a purely static quantity as it is proportional to the stationary mean photon number inside the cavity .

2.3 Factorial Moments Distribution

In what follows we will show that for an ensemble of chaotic cavity modes the moments of the photocount distribution become random variables, and evaluate numerically the distribution of the mean photocount. The factorial moments μ_r specify the output statistics of a single cavity mode with the escape rate Γ. For an ensemble of chaotic modes the escape rate is a random quantity and due to Eq. (2.14) the μ_r become also random quantities. Their distribution is given by

$$\mathcal{P}(\mu_r) = \int \mathrm{d}\Gamma \, P(\Gamma) \, \delta(\mu_r - \Gamma^r \langle : I^r : \rangle) \,. \tag{2.15}$$

Note that the right hand side involves a twofold average, the quantum optical average (represented by the brackets $\langle \cdots \rangle$) and the ensemble average over the cavity modes (represented by the integral with the probability distribution $P(\Gamma)$). We emphasize that the quantum optical average $\langle : I^r : \rangle$ depends on Γ through the total loss rate C. We now discuss the result (2.15) in various limiting cases.

Large Number of Escape Channels

We first consider the case $M \gg 1$ of many transverse modes in the waveguide. The diameter of the waveguide is then much larger than the wavelength of the cavity mode. A simple saddle point argument shows that $P(\Gamma)$ for large M approaches a Gaussian distribution with mean $\overline{\Gamma} \sim M$ and standard deviation $\Delta\Gamma = \overline{\Gamma}/\sqrt{\beta M}$ [87]. The relative fluctuations are small, $\Delta\Gamma/\overline{\Gamma} \sim 1/\sqrt{M} \to 0$ for $M \to \infty$, and the same is true for the fluctuations of all factorial moments. For cavities with large outcoupling mirrors we thus recover the sharp factorial moments one is used to from non-chaotic resonators.

Vanishing Photocount

Second, we investigate the limit of vanishing photocount, $\mu_r \to 0$. According to Eq. (2.14), this is the weak–coupling limit $\Gamma \to 0$ for which the photons in the cavity field can hardly escape into the waveguide. The laser dynamics becomes independent of the outcoupling loss as the total cavity loss C is fully dominated by the absorption loss, $\kappa > \overline{\Gamma}$. All cavity field moments become independent of Γ, and Eq. (2.14) reduces to $\mu_r \sim \Gamma^r$. Substitution into Eq. (2.15) yields the power-law behavior

$$\mathcal{P}(\mu_r) \sim \mu_r^{(\beta M)/(2r)-1}, \tag{2.16}$$

for $\mu_r \to 0$. A special case of this result is $M = \beta = 1$ for which the distribution of the first and second moment diverge as $\mu_1^{-1/2}$ and $\mu_2^{-3/4}$ for μ_1, $\mu_2 \to 0$, respectively.

Short Time Regime

The third case is the short–time regime $t \ll t_c$ where t_c is the correlation time of the intensity fluctuations of the cavity mode. During counting intervals that short the field intensity cannot vary appreciably. Therefore, the integrated intensity I becomes the product of t with the instantaneous photon number $\hat{n} = a^\dagger a$ in the cavity. The factorial moments of the output take the simple form

$$\mu_r = (\Gamma t)^r \langle \hat{n}^{(r)} \rangle . \tag{2.17}$$

That is, the factorial moments of the photocount distribution become proportional to the factorial moments $\langle \hat{n}^{(r)} \rangle$ of the photon number distribution. To obtained Eq. (2.17) we used $\langle \hat{n}^{(r)} \rangle = \langle : \hat{n}^r : \rangle$ [78], which is easily proved using the optical equivalence theorem.

2.3.1 Mean Photocount

We restrict now our analysis to the distribution of the mean photocount μ_1. According to Eq. (2.14), the calculation of the mean photocount reduces to the evaluation of the steady-state average

$$\mu_1 = \Gamma t \overline{n} , \tag{2.18}$$

for arbitrary counting time t. We calculated μ_1 numerically as a function of Γ using the distribution (2.4). Substituting the result $\mu_1(\Gamma)$ into Eq. (2.15) and carrying out the integration over Γ, we obtained $\mathcal{P}(\mu_1)$. The results for time-reversal invariant cavities connected to a waveguide supporting $M = 1, 2, 3, 6, 10$ transverse modes are plotted in Figs. 2.2 and 2.3, for $\nu = M$ and different sets of laser parameters. The distribution for cavities with broken time-reversal invariance[1] and M' escape channels are obtained from those for time-reversal invariance by making $M' = M/2$ with M even in Figs. 2.2 and 2.3. All distributions in Fig. 2.2 correspond to $A > \overline{C}$, i.e., to lasers above threshold in the ensemble average. By contrast, $A < \kappa$ for the distributions of Fig. 2.3; all lasers of those ensembles are below threshold irrespective of the escape rate Γ. While for a large number of the escape channels the distributions get sharper around $\mu_1(\bar{\Gamma})/\mu_{\max}$, in agreement with our previous analysis for $M \gg 1$, we note that for small number of escape channels the distributions are strongly non–Gaussian. In particular, for $M = 1$ they are all peaked as $\mu_1^{-1/2}$ at small mean photocount, in accord with the general argument presented above for the asymptotics at $\mu_1 \to 0$. Two further features spring to the eye and demand explanation: First, above threshold but not below we encounter an additional peak at maximum photocount; second, for certain cases (Figs. 2.2(a) and 2.3(a)) the distribution $\mathcal{P}(\mu_1)$ displays a shoulder for submaximal μ_1.

[1]the case $\beta = 2$ can be realized in microwave cavities containing magnetized ferrites

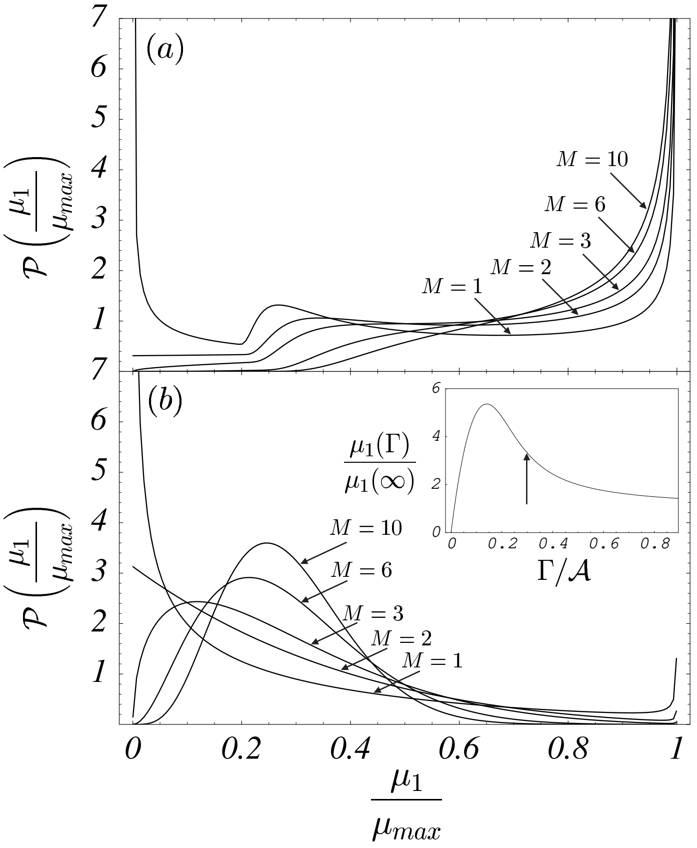

Figure 2.2: Distribution $\mathcal{P}(\mu_1/\mu_{\max})$ as a function of the dimensionless mean photocount $\mu_1/\mu_{\max}$ for $\beta = 1$ in an ensemble above the laser threshold on average. We consider two set of laser parameters. Rates are given in units of $A \equiv 1$, the nonlinearity is $B = 0.005$: (a) $\kappa = 0.7$, $\overline{\Gamma} = 0.2$, and (b) $\kappa = 0.7$, $\overline{\Gamma} = 0.02$. The inset shows μ_1 as a function of Γ/A. The function maximum occurs at $\Gamma^* \sim 0.13$. The arrow indicates the threshold–value of Γ below which lasing takes place.

The origin of these structures lies in the Γ dependence of the mean photocount μ_1. That dependence is depicted in the insets in Figs. 2.2 and 2.3, and seen to be qualitatively different above and below threshold. While μ_1 increases monotonically with Γ in the below threshold case, it develops a maximum at an intermediate value of Γ when the laser is above threshold. This behavior can be understood from the simple analytic expressions

$$\frac{\mu_1}{t} = \begin{cases} \Gamma n_s \frac{A-C}{C} & \text{for } C = \Gamma + \kappa < A, \\ \frac{\Gamma A}{C-A} & \text{for } C = \Gamma + \kappa > A. \end{cases} \tag{2.19}$$

that follow from the photon number average results (2.5) sufficiently far from threshold. According to Eq. (2.19), μ_1 rises linearly with Γ out of the origin and approaches an asymptotic plateau for very large Γ, as visible in the insets in Figs. 2.2 and 2.3. The rise to the plateau is monotonic when $A < \kappa$ since the below-threshold case of (2.19) applies for all values of Γ; the maximum photocount $\mu_{\max}$ is then just the plateau

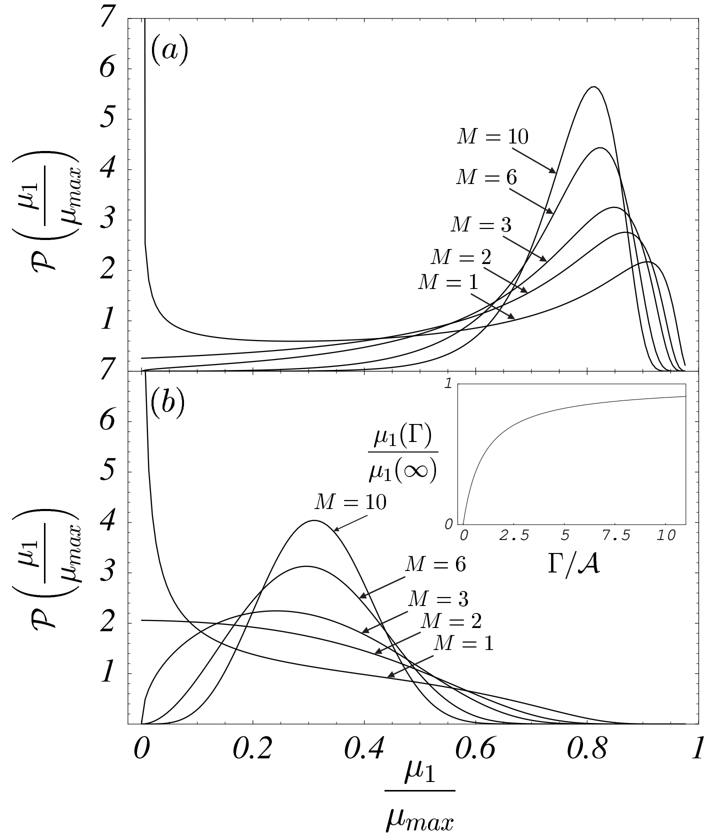

Figure 2.3: Distribution $\mathcal{P}(\mu_1/\mu_{\max})$ as a function of the dimensionless mean photocount $\mu_1/\mu_{\max}$ for $\beta = 1$ in an ensemble bellow threshold. We consider two sets of laser parameters. Rates are given in units of $A \equiv 1$, the nonlinearity is $B = 0.005$: (a) $\kappa = 2.0$, $\overline{\Gamma} = 4.0$, and (b) $\kappa = 2.0$, $\overline{\Gamma} = 0.5$. The inset shows μ_1 as a function of Γ/A.

value. The laser of Fig. 2.2 is above threshold for small Γ but below for large Γ. The maximum photocount $\mu_{\max}$ then arises for an intermediate value Γ^*. A simple argument can be employed to determine the border between the below- and the above-threshold ensemble. The argument follows from the observation that $\mu_1(\Gamma)$ approaches its plateau value from above for the above-threshold ensemble while the plateau is approached from below when the ensemble is below threshold. From the lower case of Eq. (2.19), which becomes exact for $\Gamma \to \infty$, this yields the threshold condition $A = \kappa$. To estimate the value of Γ^* we may employ the above-threshold case of Eq. (2.19) and find $\Gamma^* = \sqrt{A\kappa} - \kappa$.

Based on this understanding of $\mu_1(\Gamma)$ one can appreciate the above-threshold peak of $\mathcal{P}(\mu_1)$ at $\mu_1 = \mu_{\max}$. Substituting $\mu_1(\Gamma) = \mu_{\max} + \frac{1}{2}\mu''(\Gamma^*)(\Gamma - \Gamma^*)^2$ in the photocount distribution (2.15) we find that $\mathcal{P}(\mu_1)$ has a square–root singularity $|\mu_1 - \mu_{\max}|^{-1/2}$ which is precisely the peak depicted in Fig. 2.2. This peak, contrary to the peak at μ_1, is independent of the number of channels on the waveguide, and is a genuine signature of the laser nonlinearity. We note that in Fig. 2.2(a) the width of the peak at $\nu_{\max}$ is enhanced with increasing number of channels. The opposite happens in Fig. 2.2(b), where for $M > 2$ the peak cannot be resolved. The explanation for this behavior again follows from our previous analysis for the general case $M \gg 1$. For increasing M the distribution $P(\Gamma)$ narrows around $\overline{\Gamma}$ and is enhanced for values of Γ close to $\overline{\Gamma}$, on the contrary, values of Γ far from $\overline{\Gamma}$ are strongly suppressed. Thus in Fig. 2.2(a), where $\overline{\Gamma} \sim \Gamma^*$, definition (2.15) implies an enhancement of the probability of μ_1 around the peak at $\mu_{\max}$; while in Fig. 2.2(b) the small mean value of $\overline{\Gamma}$ accounts for the narrowing of $\mathcal{P}(\mu_1)$ around $\mu_{\max}$.

Clearly, no such peak can arise in the below–threshold case of Fig. 2.3 as the photocount increases monotonically with Γ. For the set of parameters in Fig. 2.3 the mean photocount is well approximated by the second line in Eq. (2.19) and we can analytically evaluate $\mathcal{P}(\mu_1)$. Defining $y = \mu_1/\mu_{\max}$, we obtain

$$\mathcal{P}(y) = \mathsf{B}_\nu \frac{y^{\nu/2-1}}{(1-y)^{\nu/2+1}} \exp\left(-\frac{\nu}{2\beta}\frac{y}{1-y}\right) . \tag{2.20}$$

Here B_ν is a normalization constant. The analytical curves obtained using (2.20) do not differed appreciably from the numerical results, therefore, for clarity, in Fig. 2.3 we have only plotted the numerical results for $\mathcal{P}(y)$. The suppression of the peak at $\mu_{\max}$ can be appreciated in Eq. (2.20), where for $y \to 1$ ($\mu \to \mu_{\max}$) we see that $\mathcal{P}(y)$ vanishes.

The shoulders at submaximal photocount are caused by amplified spontaneous emission below the laser threshold. Formally, the shoulders arise from the asymptotic plateau of μ_1 for large Γ. The definition (2.15) immediately implies enhanced probability for photocounts μ_1 in the vicinity of that plateau. Note that the shoulder is invisible for the distributions shown in Fig. 2.2(b), and it disappear for increasing M in Fig. 2.2(a). In the first case, large values of Γ are strongly suppressed by the small mean value $\overline{\Gamma}$; this suppression is however a general feature of the distribution $\mathcal{P}(\mu_1)$ for increasing number of channels M, explaining the disappearance of the shoulder in the second case. Further note that the shoulders for all curves in Fig. 2.3 with $M \sim 1$ lie closer to $\mu_{\max}$ than for the curves in Fig. 2.2(a) since $\mu \to \mu_{\max}$ coincides with $\Gamma \to \infty$ in the regime below threshold.

In contrast to the mean photocount, which can be expressed in terms of the stationary distribution of the laser, all μ_r with $r \geq 2$ involve dynamical information through correlation functions with $r-1$ time arguments; their behavior will not be discussed here.

2.4 Discussion and Outlook

In this chapter we derived the photocount statistics of the radiation emitted from a laser inside a chaotic resonator in the regime of single-mode laser. The new ingredient added to the standard laser theory came from the chaotic nature of the cavity modes. We considered two possible kind of laser ensembles: One corresponding to laser operation on the ensemble average, the other corresponding to all lasers on the ensemble being below threshold. The spatial fluctuations of the resonator eigenfunctions induced a strong mode-to-mode fluctuations of the laser emission. However, we showed that the probability density for each factorial moment depends only on general symmetries of the ensemble and on four parameters describing the laser dynamics; these are the coefficients of linear gain, mean escape loss, absorption loss and saturation of the amplifying medium. The distribution of the mean photocount over the *ensemble of modes* was shown to change qualitatively at the lasing transition, and display up to three peaks above the lasing threshold.

We now compare our results with related fluctuation phenomena in other areas of physics and discuss possible experimental tests. In nuclear physics the Porther–Thomas distribution describes level–width fluctuations in neutron scattering [87]. The amplitude fluctuations of Coulomb blockade oscillations in semiconductor quantum dots are also of the Porther–Thomas type [91]. In both cases, as well as for the chaotic lasers studied in this chapter, the fluctuations result from the chaotic nature of wavefunctions. However, in chaotic lasers new interesting features arise due to the interplay of wave chaos with the nonlinear dynamics of the laser. As a consequence of this interplay, the distribution of the mean photocount can strongly deviate from the Porter–Thomas distribution. To test the predicted mode-to-mode fluctuations experimentally, one must study the photocount statistics for an ensemble of chaotic modes. It seems feasible to generate such ensembles in tunable lasers e.g. by shape variations, or by the injection and displacement of artificial scatterers in the case of microwave cavities.

Finally let us mention that in contrast to the wealth of results for random linear amplifiers, little is known about the photon statistics of random media above the lasing threshold. Our study addressed this problem for the simple case of single-mode laser in a chaotic cavity with isolated modes. The observed generic operation regime of random lasers, and the one expected for lasers in chaotic resonators, corresponds nevertheless to multi-mode lasing. Recently Patra [92] showed numerically that in this regime, due to the mode competition, the statistics of the laser emission change: a laser mode above threshold will show an increment on the photon number fluctuations depending on the total number of lasing modes operating above threshold for a given value of pump. In a related work, Mishchenko [93] considered a multi-mode laser in a chaotic cavity with overlapping resonances, which allowed him to described the field through a uniform density of photons over the cavity volume employing a transfer equation. Although his analysis is restricted to the below threshold case, the nonlinear character of the equations of motion for the field and the active medium are kept, allowing for the evaluation of corrections to previous results for linear amplifiers close to the laser threshold [68, 69].

Chapter 3

Electromagnetic Field Quantization for Open Optical Cavities

A fundamental problem in quantum optics is the description of the radiation damping due to leakage out of an open cavity. Conventionally this problem is treated on a phenomenological level by adopting the system-and-bath model [37, 38, 39] to describe the resonator losses: The resonator field is modeled by a discrete set of independent quantum harmonic oscillators associated with the normal modes of the closed cavity. Each mode is *weakly* coupled to its own bath represented by a continuous set of oscillators. The coupling to the reservoir introduces both losses and noise for the resonator field dynamics. Baths corresponding to different modes are statistically independent [11]. In spite of its intuitive appeal and it success in applications, this model of damping has been criticized. The model lacks a microscopic justification as the coupling amplitudes between the system and bath only enter as phenomenological parameters. Moreover, the model is only reliable for almost closed cavities with very high-Q for which the spectrum has well-isolated resonances.

In the last decade the interest on a quantum description of the electromagnetic field inside open optical cavities has reemerged as consequence of the experimental observation of lasing in random media [1] and the need for a quantum theory of excess noise [94]. In this chapter we address this problem and develop a quantization method for open optical cavities which provides an exact description of the cavity field leakage for spectrally-overlapping resonances. Our method is of significance for several reasons: it provides a quantum description of excess noise, it allows for multi-mode lasing, and upon combination with a description of wave chaos it can account for lasing in random media.

Our quantization method applies both to open cavities defined by mirrors of arbitrary shape and quality, and to dielectric media characterized by a real dielectric constant which might be spatially nonuniform. The system may be coupled to an arbitrary number of escape channels. The quantization of the field is performed in terms of the exact eigenmodes of Maxwell's equation defined in the whole space [95]. The essence of the proposed quantization method lies in the use of a technique known in nuclear and condensed-matter physics as the Feshbach projection formalism [76]. The projection formalism separates the field into two contributions corresponding, respectively, to the cavity region and its exterior. Each region entails a set of normal modes in terms of which the electromagnetic field can be represented by associating to each mode standard creation and annihilation operators. In the resonator region the modes form a discrete set and vanish outside the cavity, while there is a continuous set of external modes which vanish inside the resonator and fulfill scattering-type boundary conditions at infinity. The separation of the field allows for a rigorous representation of the system Hamiltonian by a bilinear form in the cavity and exterior operators, with the same structure as the system-and-bath Hamiltonian used in phenomenological approaches [37, 38, 39]. In contrast to these approaches, our derivation provides explicit expressions for the coupling amplitudes. The field Hamiltonian generally includes both resonant and non-resonant terms. When both are kept, the quantization method accounts for overdamping (when the field damping rate becomes of the order of the frequency). In the case of weak damping (when the field damping rate is much smaller that the mean frequency separation) our approach reduces to the well-known field quantization of the phenomenological approach.

We note that our system-and-bath representation of the open resonator dynamics is not unique but depends on the choices made in the separation of the space into two subregions. This arbitrariness is usually encountered with the projection technique [96]; its origin goes back to the freedom to chose the "inside" and "outside" subregions in which to separate the space. Consider for example a cavity with an opening, i.e., a hole in the material walls of the cavity boundary. Any choice of a fictitious surface covering the hole yields its own inside/outside separation. Moreover, different boundary conditions may be imposed at the chosen separating surface. Nevertheless, each such surface and boundary condition entail eigenmodes allowing to represent the electromagnetic field almost everywhere. We emphasize that the field expansion cannot be expected to converge uniformly or even pointwise, and in particular not on an arbitrarily chosen boundary. Still the system-and-bath representation is exact in the L^2 sense required by quantum mechanics. The freedom in the choice of the separating surface and the boundary conditions manifests itself in the Hamiltonian and the field expansions, as the coupling amplitudes, and the internal and external basis sets, all depend explicitly on these choices. However, we show below that all physical observables, in particular the electromagnetic fields and the scattering amplitudes, do not rely on these choices and only depend on the physical boundary conditions imposed by Maxwell's equations.

Our quantization procedure can naturally be apply to random media. For such media the internal system Hamiltonian can be modelled using random matrix theory. The statistical properties of the system observables are then obtained by averaging over the pertinent ensemble. In addition by providing a separation of the inside/outside field in the case of overlapping resonances our quantization method provides a solid ground for the construction of a laser theory for multi-mode fields (see Chapter 5).

The outline of the chapter is as follow. In Sec. 3.1 the field quantization is described in terms of the exact eigenmodes of Maxwell's equations in the whole space. In Sec. 3.2 the system-and-bath Hamiltonian is derived using Feshbach's projector technique. Our derivation is valid for fields with arbitrary polarization. Finally, in Sec. 3.3 we demonstrate our method for a number of models frequently used for optical resonators. We compute their respective system-and-bath Hamiltonians, and show that the electromagnetic field and the scattering properties agree exactly with results obtained by direct solutions of the problem. Performing the computations for different sets of boundary conditions along the surface separating the resonator and channel region, we demonstrate that the physical observables are independent of that choice of boundary conditions.

The results presented in this chapter have been reported in Refs. [33, 97, 98].

3.1 Normal Modes

We consider the quantization of the electromagnetic field taking into account the three spatial dimensions and the complete vector character of the field. The space might be filled with a dielectric medium and we allow for the presence of material surfaces, e.g., mirrors, on which physical boundary conditions are imposed. The medium is characterized by a scalar dielectric constant $\epsilon(\boldsymbol{r})$[1] which depends on position and that we assumed to be real and frequency independent. We are meanly interested in resonator-like configurations suggested by particular geometrical arrangements of the material surfaces or by special behaviors of the dielectric constant, e.g., a piece of dielectric surrounded by free space. We thus assume that far from the region of space defining the cavity the electromagnetic field propagates freely, i.e., $\epsilon(\boldsymbol{r})$ becomes constant.

The electromagnetic field for the total system can be represented by a mode expansion involving the exact eigenmodes of Maxwell's equations which are defined throughout the whole space. This so-called modes-of-the-universe approach [42, 95, 50, 99] serves as a starting point for the derivation of the system-and-bath Hamiltonian in Sec. 3.2; we therefore summarize the main steps of this approach below.

It is convenient to formulate the quantization procedure in terms of the vector potential $\boldsymbol{A}$ and the scalar potential ϕ. We work in the Coulomb gauge which, in the absence of sources, corresponds to the choice $\phi = 0$ and the generalized transversality condition $\nabla \cdot [\epsilon(\boldsymbol{r})\boldsymbol{A}] = 0$. The magnetic and electric fields then follow from the potentials via the familiar relations

$$\boldsymbol{E} = -\frac{1}{c}\frac{\partial \boldsymbol{A}}{\partial t} \quad \text{and} \quad \boldsymbol{B} = \nabla \times \boldsymbol{A}. \tag{3.1}$$

The electromagnetic Hamiltonian of the problem is given by

$$H = \frac{1}{2}\int d\boldsymbol{r} \left[\frac{c^2 \boldsymbol{\Pi}(\boldsymbol{r},t)^2}{\epsilon(\boldsymbol{r})} + \big(\nabla \times \boldsymbol{A}(\boldsymbol{r},t)\big)^2 \right], \tag{3.2}$$

where $\boldsymbol{\Pi}(\boldsymbol{r},t) = \epsilon(\boldsymbol{r})\dot{\boldsymbol{A}}(\boldsymbol{r},t)/c^2$ is the canonical momentum field. The quantization of the fields may be achieved by imposing a suitable commutation relation between $\boldsymbol{A}(\boldsymbol{r},t)$ and $\boldsymbol{\Pi}(\boldsymbol{r},t)$. An alternative but equivalent procedure is to expand the fields in a complete set of mode functions and to impose canonical commutation relations for the expansion coefficients. We follow the second procedure here, and expand the vector potential in terms of the normal modes $\boldsymbol{f}_m(\omega,\boldsymbol{r})$, defined as solutions of the wave equation

$$\nabla \times \big(\nabla \times \boldsymbol{f}_m(\omega,\boldsymbol{r})\big) - \frac{\epsilon(\boldsymbol{r})\omega^2}{c^2}\boldsymbol{f}_m(\omega,\boldsymbol{r}) = \boldsymbol{0}. \tag{3.3}$$

[1]Generalization of the quantization theory for a real tensor dielectric function is straight forward.

The solutions automatically satisfy the transversality condition $\nabla \cdot [\epsilon(\boldsymbol{r})\boldsymbol{f}_m(\omega,\boldsymbol{r})] = 0$. The eigenmodes are labeled by the continuous frequency ω and a discrete index m that specifies the asymptotic boundary conditions far away from the resonator region (including the polarization). We consider asymptotic conditions corresponding to a scattering problem with incoming and outgoing waves. Then $\boldsymbol{f}_m(\omega,\boldsymbol{r})$ represents a solution with an incoming wave only in the single channel m and with outgoing waves in all open scattering channels. The definition of the channels depends on the problem at hand: For a dielectric coupled to free space, one may expand the asymptotic solutions in terms of angular momentum states. Then m corresponds to an angular momentum quantum number. On the other hand, for a cavity connected to external waveguides, m may represent a transverse mode index. The field expansions then take the form

$$\boldsymbol{A}(\boldsymbol{r},t) = c\sum_m \int_{\omega_m}^{\infty} \mathrm{d}\omega\; q_m(\omega,t)\boldsymbol{f}_m(\omega,\boldsymbol{r}), \tag{3.4a}$$

$$\boldsymbol{\Pi}(\boldsymbol{r},t) = \frac{1}{c}\sum_m \int_{\omega_m}^{\infty} \mathrm{d}\omega\; p_m(\omega,t)\boldsymbol{f}^{\dagger}_m(\omega,\boldsymbol{r}), \tag{3.4b}$$

where the expansion coefficients $q_m(\omega,t)$ and $p_m(\omega,t)$ are complex time dependent variables. The frequencies ω_m are the threshold frequency above which the m-channel becomes open. The wave functions $\boldsymbol{f}_m(\omega,\boldsymbol{r})$ have been allowed to be complex, because it is often convenient to use these rather than real ones, e.g., in scattering problems.

We follow reference [95] and stick to the usual internal product with respect to which the differential operator in Eq. (3.3) is not Hermitian. However the substitution

$$\boldsymbol{f}_m(\omega,\boldsymbol{r}) = \frac{1}{\sqrt{\epsilon(\boldsymbol{r})}}\boldsymbol{\phi}_m(\omega,\boldsymbol{r}) \tag{3.5}$$

transforms Eq. (3.3) into the eigenvalue problem

$$L\boldsymbol{\phi}_m(\omega,\boldsymbol{r}) \equiv \frac{1}{\sqrt{\epsilon(\boldsymbol{r})}}\nabla\times\left(\nabla\times\frac{\boldsymbol{\phi}_m(\omega,\boldsymbol{r})}{\sqrt{\epsilon(\boldsymbol{r})}}\right) = \frac{\omega^2}{c^2}\boldsymbol{\phi}_m(\omega,\boldsymbol{r}), \tag{3.6}$$

for the Hermitian differential operator L. Choosing an orthonormal set of basis functions $\boldsymbol{\phi}_m(\omega,\boldsymbol{r})$, it follows that the associated mode functions $\boldsymbol{f}_m(\omega,\boldsymbol{r})$ satisfy the orthonormality condition

$$\int \mathrm{d}\boldsymbol{r}\; \epsilon(\boldsymbol{r})\boldsymbol{f}^*_m(\omega,\boldsymbol{r})\cdot\boldsymbol{f}_{m'}(\omega',\boldsymbol{r}) = \delta_{mm'}\,\delta(\omega-\omega'). \tag{3.7}$$

The functions $\boldsymbol{\phi}_m(\omega)$ form a complete set in the subspace of L^2 functions defined by the transversality condition

$$\nabla\cdot\left[\sqrt{\epsilon(\boldsymbol{r})}\boldsymbol{\phi}_m(\omega,\boldsymbol{r})\right] = 0. \tag{3.8}$$

The associated mode functions $\boldsymbol{f}_m(\omega,\boldsymbol{r})$ form a complete set in the space of transverse functions [95, 99], with completeness relation given by

$$\sum_m \int_{\omega_m}^{\infty} \mathrm{d}\omega\; f_{mi}(\omega,\boldsymbol{r})f^*_{mj}(\omega,\boldsymbol{r}') = \delta^{(\epsilon)}_{ij}(\boldsymbol{r},\boldsymbol{r}'). \tag{3.9}$$

where $f_{mi}(\omega, \boldsymbol{r})$ are the vector components of $\boldsymbol{f}_m(\omega, \boldsymbol{r})$. In the space of transverse functions the generalized δ-function $\delta_{ij}^{(\epsilon)}(\boldsymbol{r}, \boldsymbol{r}')$ acts like the usual δ-function, $\delta_{ij}^{(\epsilon)}(\boldsymbol{r}, \boldsymbol{r}') = \delta_{ij}\delta(\boldsymbol{r} - \boldsymbol{r}')$; that is

$$\int \mathrm{d}\boldsymbol{r}' \; \epsilon(\boldsymbol{r}')\delta_{ij}^{(\epsilon)}(\boldsymbol{r}, \boldsymbol{r}') f_j(\boldsymbol{r}') = f_i(\boldsymbol{r}), \tag{3.10}$$

for $\boldsymbol{f}(\boldsymbol{r})$ belonging to the space of transverse functions (herein we adopt the convention of summation over repeated vector component indices). If a function $\boldsymbol{h}(\boldsymbol{r})$ does not belongs to this space then the action of $\delta_{ij}^{(\epsilon)}(\boldsymbol{r}, \boldsymbol{r}')$ on $\boldsymbol{h}(\boldsymbol{r})$ projects the function onto the space of transverse functions.

Inasmuch as the fields are real, the vector potential and its canonical momentum fulfill the relations $\boldsymbol{A} = \boldsymbol{A}^\dagger$ and $\boldsymbol{\Pi} = \boldsymbol{\Pi}^\dagger$. Together with Eq. (3.4), this implies

$$q_m(\omega) = \sum_{m'} \int_{\omega_{m'}}^{\infty} \mathrm{d}\omega' \; \mathcal{M}^\dagger_{mm'}(\omega, \omega') q^\dagger_{m'}(\omega'), \tag{3.11a}$$

$$p^\dagger_m(\omega) = \sum_{m'} \int_{\omega_{m'}}^{\infty} \mathrm{d}\omega' \; \mathcal{M}^\dagger_{mm'}(\omega, \omega') p_{m'}(\omega'), \tag{3.11b}$$

where $\mathcal{M}$ has the matrix elements

$$\mathcal{M}_{mm'}(\omega, \omega') = \int \mathrm{d}\boldsymbol{r} \; \epsilon(\boldsymbol{r}) \boldsymbol{f}_m(\omega, \boldsymbol{r}) \cdot \boldsymbol{f}_{m'}(\omega', \boldsymbol{r}). \tag{3.12}$$

We note that $\mathcal{M}$ is unitary and symmetric[2]. Moreover, $\mathcal{M}$ only couples degenerate modes, as modes with different frequencies are orthogonal, $\mathcal{M}(\omega, \omega') \sim \delta(\omega - \omega')$.

Substituting the field expansions (3.4) into the Hamiltonian (3.2), using Eq. (3.11) and the properties of $\mathcal{M}$, one obtains the Hamiltonian in terms of the variables q and p,

$$H = \frac{1}{2} \sum_m \int_{\omega_m}^{\infty} \mathrm{d}\omega \; \left[p^\dagger_m(\omega) p_m(\omega) + \omega^2 q^\dagger_m(\omega) q_m(\omega) \right]. \tag{3.13}$$

Quantization is now achieved by promoting the variables $q(\omega)$ and $p(\omega)$ to operators. The Heisenberg equations of motion for $q(\omega)$ and $p(\omega)$ lead to Maxwell's equations, provided we impose the equal time commutation relations

$$\begin{aligned} [q_m(\omega), q_{m'}(\omega')] &= [q_m(\omega), q^\dagger_{m'}(\omega')] = 0, \\ [p_m(\omega), p_{m'}(\omega')] &= [p_m(\omega), p^\dagger_{m'}(\omega')] = 0, \\ [q_m(\omega), p_{m'}(\omega')] &= \mathrm{i}\hbar \, \delta_{mn} \, \delta(\omega - \omega'). \end{aligned} \tag{3.14}$$

Further use of Eq. (3.11) gives the remaining commutation relation

$$[q_m(\omega), p^\dagger_{m'}(\omega')] = \mathrm{i}\hbar \mathcal{M}^\dagger_{mm'}(\omega, \omega'). \tag{3.15}$$

Combining the field expansions (3.4) with the completeness relation (3.9), it is easily seen that these commutation relations imply canonical commutation relations for the vector potential and the canonical momentum field.

[2]We use the convention $\mathcal{M}^\dagger_{mn}(\omega, \omega') = [\mathcal{M}_{nm}(\omega', \omega)]^*$.

The last step in the quantization procedure is to express the operators $q(\omega)$ and $p(\omega)$ in terms of creation and annihilation operators,

$$q_m(\omega) = \left(\frac{\hbar}{2\omega}\right)^{\frac{1}{2}} \left[A_m(\omega) + \sum_{m'} \int_{\omega_{m'}}^{\infty} \mathrm{d}\omega' \, \mathcal{M}^{\dagger}_{mm'}(\omega,\omega') A^{\dagger}_{m'}(\omega')\right], \tag{3.16a}$$

$$p_m(\omega) = \mathrm{i} \left(\frac{\hbar\omega}{2}\right)^{\frac{1}{2}} \left[A^{\dagger}_m(\omega) - \sum_{m'} \int_{\omega_{m'}}^{\infty} \mathrm{d}\omega' \, \mathcal{M}_{mm'}(\omega,\omega') A_{m'}(\omega')\right]. \tag{3.16b}$$

The latter obey the commutation relations

$$\begin{aligned} [A_m(\omega), A_{m'}(\omega')] &= 0, \\ [A_m(\omega), A^{\dagger}_{m'}(\omega')] &= \delta_{mm'} \, \delta(\omega - \omega'), \end{aligned} \tag{3.17}$$

obtained by inverting the relations (3.16) and making use of the commutation relations (3.14). In terms of the creation and annihilation operators the Hamiltonian takes the familiar form

$$H = \frac{1}{2} \sum_m \int_{\omega_m}^{\infty} \mathrm{d}\omega \, \hbar\omega \left[A^{\dagger}_m(\omega) A_m(\omega) + A_m(\omega) A^{\dagger}_m(\omega)\right], \tag{3.18}$$

describing a set of independent harmonic oscillators. Finally, substituting the representations (3.16) into Eqs. (3.4), one obtains the field expansions

$$\boldsymbol{A} = c \sum_m \int_{\omega_m}^{\infty} \mathrm{d}\omega \left(\frac{\hbar}{2\omega}\right)^{\frac{1}{2}} \left[A_m(\omega) \mathrm{e}^{-\mathrm{i}\omega t} \boldsymbol{f}_m(\omega, \boldsymbol{r}) + A_m(\omega)^{\dagger} \mathrm{e}^{\mathrm{i}\omega t} \boldsymbol{f}^*_m(\omega, \boldsymbol{r})\right] \tag{3.19a}$$

$$\boldsymbol{\Pi} = -\frac{\mathrm{i}}{c} \sum_m \int_{\omega_m}^{\infty} \mathrm{d}\omega \left(\frac{\hbar\omega}{2}\right)^{\frac{1}{2}} \epsilon(\boldsymbol{r}) \left[A_m(\omega) \mathrm{e}^{-\mathrm{i}\omega t} \boldsymbol{f}_m(\omega, \boldsymbol{r}) - A^*_m(\omega) \mathrm{e}^{\mathrm{i}\omega t} \boldsymbol{f}^*_m(\omega, \boldsymbol{r})\right]. \tag{3.19b}$$

In empty space, $\epsilon(\boldsymbol{r}) \equiv 1$, the fields expansions reduce to the standard mode expansion of the free electromagnetic field.

3.2 Cavity and Channel Fields

In this section we use the Feshbach projection technique [76] to provide an exact decomposition of the electromagnetic field into two components corresponding to two separated subsystems: the resonator and its exterior. The latter subsystem is usually referred to as the channel region in the scattering formalism; a notation that we shall adopt here. In quantum optics, under very general conditions, this subsystem plays the role of a reservoir. The main result of the section is the microscopic derivation of the field Hamiltonian which, under the proposed field decomposition, has the structure of a system-and-bath Hamiltonian accounting for arbitrarily large coupling between the two subsystems.

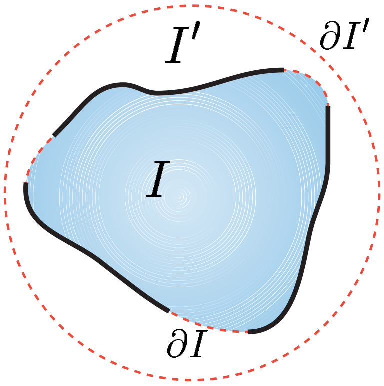

Figure 3.1: Sketch of a resonator-like configuration in two dimensions. The continuous lines represent mirrors that partially bound a region of space filled with a dielectric material (shaded region). I' and I are two possible choices of cavities for the problem. In both cases the separating surfaces are shown as dashed lines. $\partial I'$ defines a cavity with circular shape but with an intricate configuration of mirrors in its interior, while ∂I follows the boundary of the dielectric material, coinciding in some regions with the mirrors, and finally enclosing completely the dielectric material.

The starting point of the projection formalism is the inside/outside separation of the space into the two subsystems. This is accomplished by introducing a close surfaced that separates the internal or resonator region from the external or channel region (Fig. (3.1)). As mention before, this procedure entails certainly a degree of arbitrariness: First, the shape and size of the interface is merely restricted by the requirement that far from the resonator the field should propagate freely (this allow us to define asymptotic boundary conditions below). Second, the type of boundary conditions along the interface for the internal and external subsystems are only limited by the condition that the Hermiticity of the problem should be retained [96]. This arbitrariness is manifest in the representation obtained for the field expansions and in the explicit expression for the Hamiltonian. In spite of this, all physical observables can be shown to be independent of the choices made for the interface and boundary conditions. Explicit examples illustrating this fact are presented in Sec. 3.3.

3.2.1 Feshbach Projection

Formally, the separation of space in two regions is achieved using the projection operators [76]

$$\mathcal{Q} = \int_{r\in I} \mathrm{d}\boldsymbol{r}|\boldsymbol{r}\rangle\langle\boldsymbol{r}|, \qquad \mathcal{P} = \int_{r\notin I} \mathrm{d}\boldsymbol{r}|\boldsymbol{r}\rangle\langle\boldsymbol{r}|, \tag{3.20}$$

where $|\boldsymbol{r}\rangle$ denotes a standard position eigenket and I is the region of space occupied by the cavity (see Fig. (3.1)). The operators $\mathcal{Q}$ and $\mathcal{P}$ depend on the choice of I, but all physical observables turn out to be independent of this choice. One easily shows that $\mathcal{P}$ and $\mathcal{Q}$ are projection operators,

$$\mathcal{P} = \mathcal{P}^\dagger, \qquad \mathcal{P}^2 = \mathcal{P}; \tag{3.21a}$$
$$\mathcal{Q} = \mathcal{Q}^\dagger; \qquad \mathcal{Q}^2 = \mathcal{Q}. \tag{3.21b}$$

Moreover, they are orthogonal, $\mathcal{QP} = \mathcal{PQ} = 0$, and complete, $\mathcal{Q} + \mathcal{P} = 1$. Therefore, an arbitrary Hilbert space function $\boldsymbol{\psi}$ and the associated function $\boldsymbol{h} = \boldsymbol{\psi}/\sqrt{\epsilon}$ may be decomposed into their projections onto the resonator and channel space

$$\boldsymbol{\psi}(\boldsymbol{r}) = \chi_-(\boldsymbol{r})\boldsymbol{\mu}(\boldsymbol{r}) + \chi_+(\boldsymbol{r})\boldsymbol{\nu}(\boldsymbol{r}), \tag{3.22a}$$
$$\boldsymbol{h}(\boldsymbol{r}) = \chi_-(\boldsymbol{r})\boldsymbol{u}(\boldsymbol{r}) + \chi_+(\boldsymbol{r})\boldsymbol{v}(\boldsymbol{r}), \tag{3.22b}$$

where $\chi_\mp$ are the characteristic functions of the resonator and the channel region, respectively,

$$\chi_-(\boldsymbol{r}) = \int_{\boldsymbol{r}'\in I} \mathrm{d}\boldsymbol{r}'\delta(\boldsymbol{r}-\boldsymbol{r}'), \tag{3.23a}$$
$$\chi_+(\boldsymbol{r}) = 1 - \chi_-(\boldsymbol{r}). \tag{3.23b}$$

Acting on $\boldsymbol{\phi}$ with the differential operator L defined in Eq. (3.6), we obtain

$$L\boldsymbol{\psi} = \chi_-(\boldsymbol{r})L\,\boldsymbol{\mu}(\boldsymbol{r}) - \int_{\partial I}\mathrm{d}^2\boldsymbol{r}'K(\boldsymbol{r},\boldsymbol{r}')\boldsymbol{\mu}(\boldsymbol{r}') + \chi_+(\boldsymbol{r})L\,\boldsymbol{\nu}(\boldsymbol{r}) + \int_{\partial I}\mathrm{d}^2\boldsymbol{r}'K(\boldsymbol{r},\boldsymbol{r}')\boldsymbol{\nu}(\boldsymbol{r}'), \tag{3.24}$$

where $K(\boldsymbol{r},\boldsymbol{r}')$ is a singular differential operator defined at the boundary

$$K(\boldsymbol{r},\boldsymbol{r}')\boldsymbol{\mu}(\boldsymbol{r}')\Big|_{\boldsymbol{r},\boldsymbol{r}'\in\partial I} = \left[\frac{\delta(\boldsymbol{r}-\boldsymbol{r}')}{\sqrt{\epsilon(\boldsymbol{r})}}\mathbf{n}'\times\left(\nabla'\times\frac{\boldsymbol{\mu}(\boldsymbol{r}')}{\sqrt{\epsilon(\mathbf{r}')}}\right) + \frac{\nabla\delta(\mathbf{r}-\boldsymbol{r}')}{\sqrt{\epsilon(\boldsymbol{r})}}\times\left(\mathbf{n}'\times\frac{\boldsymbol{\mu}(\mathbf{r}')}{\sqrt{\epsilon(\boldsymbol{r}')}}\right)\right]\Bigg|_{\boldsymbol{r},\boldsymbol{r}'\in\partial I}. \tag{3.25}$$

Here ∇' denotes a derivative with respect to $\mathbf{r}'$, and $\mathbf{n}'$ is a unit vector normal to the boundary. The action of $K(\boldsymbol{r},\boldsymbol{r}')$ on $\boldsymbol{\nu}(\boldsymbol{r}')$ is defined in a similar fashion, with $\boldsymbol{\mu}(\boldsymbol{r}')$ replaced by $\boldsymbol{\nu}(\boldsymbol{r}')$.

The first (third) term on the right hand side of Eq. (3.24) contribute only inside (outside) the resonator. The second and fourth terms are boundary terms. They involve $\boldsymbol{\mu}$, $\boldsymbol{\nu}$, and their derivatives at the boundary; these functions must be evaluated in the limit where the boundary is approached from the cavity and the channel region, respectively. We note that the boundary terms generally gives rise to singular behavior. As a result, the action of L usually goes beyond the Hilbert space. The range of L within the Hilbert space is defined by the functions for which the singular terms vanish; this happens in particular for the eigenfunctions of L in Hilbert space.

We now want to decompose the operator L into a resonator, a channel, and a coupling contribution. However, it is not obvious how the decomposition can be carried out for the singular boundary terms. We therefore replace the boundary integrals by integrations along surfaces arbitrarily close to the boundary but located inside respectively outside the resonator region. There is still freedom in selecting which surface integral should belong to each of the subsystems. Different choices lead, in general, to different set of boundary conditions along the separating surface, only subject to the restrictions that the obtained decomposition of the operator L is self-adjoint. The freedom in choosing the boundary conditions is characteristic for the projector technique [76, 96]. For the sake of clarity and definiteness, in what follows we stick to one of these possible choices leading to a one particular set of boundary conditions. Other possibilities are study for specific examples in Sec. 3.3. Equation (3.24) then becomes

$$L\boldsymbol{\psi} = L_{\mathcal{QQ}}\boldsymbol{\mu} + L_{\mathcal{QP}}\boldsymbol{\nu} + L_{\mathcal{PQ}}\boldsymbol{\mu} + L_{\mathcal{PP}}\boldsymbol{\nu}, \tag{3.26}$$

where $L_{\mathcal{QQ}}$ and $L_{\mathcal{PP}}$ are the projections of L onto the resonator and channel space,

$$L_{\mathcal{QQ}}\boldsymbol{\mu} = \chi_-(\boldsymbol{r})\, L\boldsymbol{\mu}(\mathbf{r}) - \int_{\partial I_-} \mathrm{d}^2\boldsymbol{r}'_- \left[\frac{\delta(\boldsymbol{r}-\boldsymbol{r}'_-)}{\sqrt{\epsilon(\boldsymbol{r})}}\mathbf{n}' \times \left(\nabla' \times \frac{\boldsymbol{\mu}(\mathbf{r}'_-)}{\sqrt{\epsilon(\boldsymbol{r}'_-)}}\right)\right], \tag{3.27a}$$

$$L_{\mathcal{PP}}\boldsymbol{\nu} = \chi_+(\boldsymbol{r})\, L\boldsymbol{\nu}(\mathbf{r}) + \int_{\partial I_+} \mathrm{d}^2\boldsymbol{r}'_+ \left[\frac{\nabla\delta(\boldsymbol{r}-\boldsymbol{r}'_+)}{\sqrt{\epsilon(\boldsymbol{r})}} \times \left(\mathbf{n}' \times \frac{\boldsymbol{\nu}(\boldsymbol{r}'_+)}{\sqrt{\epsilon(\mathbf{r}'_+)}}\right)\right], \tag{3.27b}$$

and $L_{\mathcal{QP}}$ and $L_{\mathcal{PQ}}$ the coupling terms

$$L_{\mathcal{QP}}\boldsymbol{\nu} = +\int_{\partial I_-} \mathrm{d}^2\mathbf{r}'_- \left[\frac{\delta(\boldsymbol{r}-\boldsymbol{r}'_-)}{\sqrt{\epsilon(\boldsymbol{r})}}\mathbf{n}' \times \left(\nabla' \times \frac{\boldsymbol{\nu}(\boldsymbol{r}'_+)}{\sqrt{\epsilon(\boldsymbol{r}'_+)}}\right)\right], \tag{3.28a}$$

$$L_{\mathcal{PQ}}\boldsymbol{\mu} = -\int_{\partial I_+} \mathrm{d}^2\mathbf{r}'_+ \left[\frac{\nabla\delta(\boldsymbol{r}-\mathbf{r}'_+)}{\sqrt{\epsilon(\boldsymbol{r})}} \times \left(\mathbf{n}' \times \frac{\boldsymbol{\mu}(\mathbf{r}'_-)}{\sqrt{\epsilon(\boldsymbol{r}'_-)}}\right)\right]. \tag{3.28b}$$

The shorthands $\boldsymbol{r}'_\mp$ indicate that the integrals are to be evaluated in the limit where $\boldsymbol{r}'_-$ and $\boldsymbol{r}'_+$ approach the boundary from inside respectively outside the resonator. $L_{\mathcal{QQ}}$ and $L_{\mathcal{PP}}$ define Hermitian operators on the Hilbert space of functions of the resonator and the channel region, respectively. Moreover, $L_{\mathcal{QP}} = L^\dagger_{\mathcal{PQ}}$ showing that the decomposition (3.26) preserves the Hermiticity of L.

In particular, for the eigenfunctions of the operator L with the decomposition

$$|\boldsymbol{\phi}_m(\omega)\rangle = \mathcal{Q}|\boldsymbol{\phi}_m(\omega)\rangle + \mathcal{P}|\boldsymbol{\phi}_m(\omega)\rangle \equiv |\bar{\boldsymbol{\mu}}_m(\omega)\rangle + |\bar{\boldsymbol{\nu}}_m(\omega)\rangle\,, \tag{3.29}$$

substitution of Eq. (3.26) into the eigenmode equation (3.6) yields the two coupled equations:

$$\begin{pmatrix} L_{\mathcal{QQ}} & L_{\mathcal{QP}} \\ L_{\mathcal{PQ}} & L_{\mathcal{PP}} \end{pmatrix} \begin{pmatrix} \bar{\boldsymbol{\mu}}_m(\omega) \\ \bar{\boldsymbol{\nu}}_m(\omega) \end{pmatrix} = \frac{\omega^2}{c^2} \begin{pmatrix} \bar{\boldsymbol{\mu}}_m(\omega) \\ \bar{\boldsymbol{\nu}}_m(\omega) \end{pmatrix}. \tag{3.30}$$

The requirement that the singular terms on the left hand side vanish yields the two matching conditions

$$\mathbf{n} \times \big(\bar{\boldsymbol{u}}_m(\omega) - \bar{\boldsymbol{v}}_m(\omega)\big) = \mathbf{0}, \tag{3.31a}$$

$$\mathbf{n} \times \big(\nabla \times \bar{\boldsymbol{u}}_m(\omega) - \nabla \times \bar{\boldsymbol{v}}_m(\omega)\big) = \mathbf{0}, \tag{3.31b}$$

for all points along the boundary of the resonator region. The gauge condition $\nabla \cdot [\epsilon\boldsymbol{f}(\omega)] = 0$ and the requirement $\nabla \cdot \big(\nabla \times \boldsymbol{f}(\omega)\big) = 0$ along the boundary give the further matching conditions

$$\mathbf{n} \cdot \big(\epsilon\bar{\boldsymbol{u}}_m(\omega) - \epsilon\bar{\boldsymbol{v}}_m(\omega)\big) = 0, \tag{3.32a}$$

$$\mathbf{n} \cdot \big(\nabla \times \bar{\boldsymbol{u}}_m(\omega) - \nabla \times \bar{\boldsymbol{v}}_m(\omega)\big) = 0. \tag{3.32b}$$

The four matching conditions (3.31), (3.32) together with Eq. (3.1) realize the well-known [100] boundary conditions for the electromagnetic field at an interface in the absence of surface currents or surface charges and entail the continuity of the electromagnetic field on this surface.

3.2.2 Cavity and Channel Modes

The operators L_{QQ} and $L_{\mathcal{PP}}$ are self-adjoint operators in the Hilbert space of the resonator and the channel functions, respectively. The modes of the isolated resonator $|\boldsymbol{\mu}_\lambda\rangle$ are solutions of the eigenvalue equation

$$L_{QQ}|\boldsymbol{\mu}_\lambda\rangle = \left(\frac{\omega_\lambda}{c}\right)^2 |\boldsymbol{\mu}_\lambda\rangle. \tag{3.33}$$

From Eq. (3.27a), they satisfy

$$\nabla \times \big(\nabla \times \boldsymbol{u}_\lambda(\boldsymbol{r})\big) = \frac{\epsilon(\boldsymbol{r})\omega_\lambda^2}{c^2}\boldsymbol{u}_\lambda(\boldsymbol{r}). \tag{3.34}$$

with the boundary condition

$$\mathbf{n} \times \big(\nabla \times \boldsymbol{u}_\lambda(\boldsymbol{r})\big)\Big|_{\boldsymbol{r}\in\partial I} = \mathbf{0}, \tag{3.35}$$

obtained by demanding that the singular term in Eq. (3.27a) vanishes. Hence, the tangential component of $\nabla \times \boldsymbol{u}_\lambda$ vanishes at the boundary. No boundary condition for the normal component of $\nabla \times \boldsymbol{u}_\lambda$ is required as the three components of this vector are connected through the gauge condition. We note that the eigenmodes of the resonator form a discrete set.

In a similar fashion the eigenmodes of the channel region are solutions of the eigenvalue equation

$$L_{\mathcal{PP}}|\boldsymbol{\nu}_m(\omega)\rangle = \left(\frac{\omega}{c}\right)^2 |\boldsymbol{\nu}_m(\omega)\rangle. \tag{3.36}$$

Thus, from Eq. (3.27b) they satisfy the equation

$$\nabla \times \big(\nabla \times \boldsymbol{v}_m(\omega, \boldsymbol{r})\big) = \frac{\epsilon(\mathbf{r})\omega^2}{c^2}\boldsymbol{v}_m(\omega, \boldsymbol{r}), \tag{3.37}$$

together with the condition that the tangential component must vanish at the boundary,

$$\mathbf{n} \times \boldsymbol{v}_m(\omega, \boldsymbol{r})\Big|_{\boldsymbol{r}\in\partial I} = \mathbf{0}. \tag{3.38}$$

The channel modes form a continuum labeled by the frequency ω and the index m that specifies the asymptotic conditions at infinity. We note that the resonator modes $\boldsymbol{u}_\lambda$ have support only within the resonator and vanish in the channel region; vice versa the channel functions $\boldsymbol{v}_m(\omega)$ vanish inside the resonator and take nonzero values only within the channel region. The resonator and channel modes form complete and orthonormal basis sets for the resonator and channel region, respectively. As a result, the projectors $\mathcal{P}$ and $\mathcal{Q}$ can be represented in terms of these modes,

$$\mathcal{Q} = \sum_{\lambda} |\boldsymbol{\mu}_\lambda\rangle\langle\boldsymbol{\mu}_\lambda|, \tag{3.39a}$$

$$\mathcal{P} = \sum_{m} \int_{\omega_m}^{\infty} d\omega \; |\boldsymbol{\nu}_m(\omega)\rangle\langle\boldsymbol{\nu}_m(\omega)|. \tag{3.39b}$$

Together with the eigenmode equation (3.30) this reduces the eigenmode problem to the well–known problem [101, 102] of a discrete number of states coupled to a continuum.

We note that the boundary conditions (3.35) and (3.38) on the resonator and channel modes are a consequence of our separation of the singular terms in Eq. (3.24). As discussed before, this separation is by no means unique. For example, the substitution of $\delta(\boldsymbol{r}-\boldsymbol{r}')$ by $\delta(\mathbf{r}-\boldsymbol{r}_+{}')$ and of $\nabla\delta(\boldsymbol{r}-\mathbf{r}')$ by $\nabla\delta(\boldsymbol{r}-\boldsymbol{r}_-{}')$ in Eq. (3.25), leads to a new set of boundary conditions for which the conditions on the internal and external eigenmodes are just interchanged. Possible more general types of boundary conditions are discussed in Ref. [96].

It is worth emphasizing that neither the modes $\boldsymbol{\mu}_\lambda$ of the closed resonator nor the channel modes $\boldsymbol{\nu}_m(\omega)$ represent exact modes of the total system, as both of them depend on the choice made for the cavity boundary and the boundary conditions on it. The exact modes satisfy the matching conditions derived earlier but, in general, neither of the boundary conditions (3.35) or (3.38). Still the eigenmodes of the total system may be expanded in terms of the resonator and channel modes as these modes form complete basis sets in the respective regions. This fact is a consequence of the convergence in Hilbert space which *does not* imply point-wise convergence (at the boundary). Consequently, the matching conditions must not be imposed directly at the boundary but hold, as usual [100], in a limiting sense infinitesimally close to the boundary.

The eigenmode equation (3.30) in full space may now be solved by standard methods [101, 102, 103]. For the projection onto the channel space one has the Lippmann–Schwinger type solution

$$\mathcal{P}|\boldsymbol{\phi}_m(\omega)\rangle = |\boldsymbol{\nu}_m(\omega)\rangle + \frac{1}{\left(\frac{\omega}{c}\right)^2 - L_{\mathcal{PP}} + \mathrm{i}\epsilon} L_{\mathcal{PQ}}|\boldsymbol{\phi}_m(\omega)\rangle, \tag{3.40}$$

where the limit $\epsilon \to 0^+$ is implied. Substitution into the equation for the projection onto the resonator space yields

$$\mathcal{Q}|\boldsymbol{\phi}_m(\omega)\rangle = \frac{1}{\left(\frac{\omega}{c}\right)^2 - L_{\text{eff}}(\omega)} L_{\mathcal{QP}}|\boldsymbol{\nu}_m(\omega)\rangle, \tag{3.41}$$

where $L_{\text{eff}}(\omega)$ is the non–Hermitian operator

$$L_{\text{eff}}(\omega) \equiv L_{\mathcal{QQ}} + L_{\mathcal{QP}} \frac{1}{\left(\frac{\omega}{c}\right)^2 - L_{\mathcal{PP}} + \mathrm{i}\epsilon} L_{\mathcal{PQ}}. \tag{3.42}$$

The operator $L_{\mathrm{eff}}(\omega)$ is closely related to the effective Hamiltonian in open quantum systems [96]. To simplify notation, we introduce the retarded Green function of the resonator in the presence of the coupling to the channels

$$\mathcal{G}_{\mathcal{Q}\mathcal{Q}}(\omega) = \frac{1}{\left(\frac{\omega}{c}\right)^2 - L_{\mathrm{eff}}(\omega)}. \tag{3.43}$$

Combining Eqs. (3.40) and (3.41) we arrive at an expression for the eigenstates $|\boldsymbol{\phi}_m(\omega)\rangle$,

$$|\boldsymbol{\phi}_m(\omega)\rangle = \mathcal{G}_{\mathcal{Q}\mathcal{Q}}(\omega)L_{\mathcal{Q}\mathcal{P}}|\boldsymbol{\nu}_m(\omega)\rangle + \left[1 + \frac{1}{\left(\frac{\omega}{c}\right)^2 - L_{\mathcal{P}\mathcal{P}} + \mathrm{i}\epsilon} L_{\mathcal{P}\mathcal{Q}}\mathcal{G}_{\mathcal{Q}\mathcal{Q}}(\omega)L_{\mathcal{Q}\mathcal{P}}\right]|\boldsymbol{\nu}_m(\omega)\rangle. \tag{3.44}$$

Using the expansion (3.39), this yields an exact representation of the eigenstates in terms of the resonator and channel modes

$$|\boldsymbol{\phi}_m(\omega)\rangle = \sum_\lambda \alpha_{m\lambda}(\omega)|\boldsymbol{\mu}_\lambda\rangle + \sum_{m'} \int_{\omega_{m'}}^{\infty} \mathrm{d}\omega'\ \beta_{mm'}(\omega,\omega')|\boldsymbol{\nu}_{m'}(\omega')\rangle, \tag{3.45}$$

where the expansion coefficients are given by

$$\alpha_{m\lambda}(\omega) = \langle\boldsymbol{\mu}_\lambda|\mathcal{G}_{\mathcal{Q}\mathcal{Q}}(\omega)L_{\mathcal{Q}\mathcal{P}}|\boldsymbol{\nu}_m(\omega)\rangle, \tag{3.46a}$$

$$\beta_{mm'}(\omega,\omega') = \langle\boldsymbol{\nu}_{m'}(\omega')|\left[1 + \frac{1}{\left(\frac{\omega}{c}\right)^2 - L_{\mathcal{P}\mathcal{P}} + \mathrm{i}\epsilon} L_{\mathcal{P}\mathcal{Q}}\mathcal{G}_{\mathcal{Q}\mathcal{Q}}(\omega)L_{\mathcal{Q}\mathcal{P}}\right]|\boldsymbol{\nu}_m(\omega)\rangle. \tag{3.46b}$$

The normal modes $\boldsymbol{f}_m(\omega)$ of the electromagnetic field are recovered from $\boldsymbol{\phi}_m(\omega)$ using Eqs. (3.5) and (3.22):

$$\boldsymbol{f}_m(\omega,\boldsymbol{r}) = \sum_\lambda \alpha_{m\lambda}(\omega)\boldsymbol{u}_\lambda(\boldsymbol{r}) + \sum_{m'} \int_{\omega_{m'}}^{\infty} \mathrm{d}\omega'\ \beta_{mm'}(\omega,\omega')\boldsymbol{v}_{m'}(\omega',\boldsymbol{r}). \tag{3.47}$$

3.2.3 Hamiltonian and Field Expansions

The decomposition of the electromagnetic field modes into a resonator and a channel contribution suggests a quantization scheme different from the modes-of-the-universe approach discussed in Sec. 3.1. Here we carry out the field quantization on the basis of the resonator and channel modes. Our starting point is the expansion of the vector potential and the canonical momentum in terms of these modes; combining Eqs. (3.4) and (3.47) this expansion takes the form

$$\boldsymbol{A}(\boldsymbol{r},t) = c\sum_\lambda Q_\lambda \boldsymbol{u}_\lambda(\boldsymbol{r}) + c\sum_{m'} \int_{\omega_{m'}}^{\infty} \mathrm{d}\omega\ Q_{m'}(\omega)\boldsymbol{v}_{m'}(\omega,\boldsymbol{r}), \tag{3.48a}$$

$$\boldsymbol{\Pi}(\boldsymbol{r},t) = \frac{\epsilon(\boldsymbol{r})}{c}\left[\sum_\lambda P_\lambda \boldsymbol{u}^*_\lambda(\boldsymbol{r}) + \sum_{m'} \int_{\omega_{m'}}^{\infty} \mathrm{d}\omega\ P_{m'}(\omega)\boldsymbol{v}^*_{m'}(\omega,\boldsymbol{r})\right], \tag{3.48b}$$

where we have defined the position operators

$$Q_\lambda = \sum_m \int_{\omega_m}^{\infty} \mathrm{d}\omega \; q_m(\omega)\alpha_{m\lambda}(\omega), \tag{3.49a}$$

$$Q_m(\omega) = \sum_{m'} \int_{\omega_{m'}}^{\infty} \mathrm{d}\omega' \; q_{m'}(\omega')\beta_{m'm}(\omega', \omega), \tag{3.49b}$$

and the momentum operators

$$P_\lambda = \sum_m \int_{\omega_m}^{\infty} \mathrm{d}\omega \; p_m(\omega)\alpha^*_{m\lambda}(\omega), \tag{3.50a}$$

$$P_m(\omega) = \sum_{m'} \int_{\omega_{m'}}^{\infty} \mathrm{d}\omega' \; p_{m'}(\omega')\beta^*_{m'm}(\omega', \omega). \tag{3.50b}$$

The Q_λ and P_λ are time–dependent operators that represent complex amplitudes associated with the resonator field. Likewise, the operators $Q_m(\omega)$ and $P_m(\omega)$ are amplitudes describing the channel field. The reality condition on $\boldsymbol{A}$ and $\boldsymbol{\Pi}$ implies the following relations between the cavity operators and their adjoints

$$Q_\lambda = \sum_{\lambda'} \mathcal{N}^\dagger_{\lambda\lambda'} Q^\dagger_{\lambda'} \tag{3.51a}$$

$$P^\dagger_\lambda = \sum_{\lambda'} \mathcal{N}^\dagger_{\lambda\lambda'} P_{\lambda'}. \tag{3.51b}$$

Likewise, the channel operators are connected with their adjoints via the relations

$$Q_m(\omega) = \sum_{m'} \int_{\omega_{m'}}^{\infty} \mathrm{d}\omega' \; \mathcal{N}^\dagger_{mm'}(\omega, \omega') Q^\dagger_{m'}(\omega'), \tag{3.52a}$$

$$P^\dagger_m(\omega) = \sum_{m'} \int_{\omega_{m'}}^{\infty} \mathrm{d}\omega' \; \mathcal{N}^\dagger_{mm'}(\omega, \omega') P_{m'}(\omega'). \tag{3.52b}$$

The matrix elements

$$\mathcal{N}_{\lambda\lambda'} = \int \mathrm{d}\boldsymbol{r} \; \epsilon(\boldsymbol{r})\boldsymbol{u}_\lambda(\boldsymbol{r}) \cdot \boldsymbol{u}_{\lambda'}(\boldsymbol{r}), \tag{3.53a}$$

$$\mathcal{N}_{mm'}(\omega, \omega') = \int \mathrm{d}\boldsymbol{r} \; \epsilon(\boldsymbol{r})\boldsymbol{v}_m(\omega, \boldsymbol{r}) \cdot \boldsymbol{v}_{m'}(\omega', \boldsymbol{r}). \tag{3.53b}$$

are the expansion coefficients of the mode functions $\boldsymbol{u}_\lambda$ ($\boldsymbol{v}_m(\omega)$) in terms of the complex conjugate functions $\boldsymbol{u}^*_\lambda$ ($\boldsymbol{v}^*_m(\omega)$). The matrix $\mathcal{N}$ is the projection of the matrix $\mathcal{M}$ defined in Eq. (3.12), onto the cavity and channel space, so it is unitary, symmetric and only couples degenerate modes. The (equal–time) commutation relations of the various operators are discussed in Appendix 3.A. The calculation shows that operators associated with different subsystems commute. Moreover, for each subsystem Q and P behave like the fundamental operators for position and momentum, respectively.

To discuss the dynamical evolution of the resonator and channel operators, we must express the field Hamiltonian in terms of these operators. We use the representation (3.49) and (3.50) along with the completeness relation $\mathcal{Q}+\mathcal{P}=1$ to invert the relation between the operators for the total system and the operator for the two subsystems

$$q_m(\omega) = \sum_\lambda \alpha^*_{m\lambda}(\omega) Q_\lambda + \sum_{m'} \int_{\omega_{m'}}^{\infty} \mathrm{d}\omega' \, \beta^*_{mm'}(\omega,\omega') Q_{m'}(\omega'), \tag{3.54a}$$

$$p_m(\omega) = \sum_\lambda \alpha_{m\lambda}(\omega) P_\lambda + \sum_{m'} \int_{\omega_{m'}}^{\infty} \mathrm{d}\omega' \, \beta_{mm'}(\omega,\omega') P_{m'}(\omega'). \tag{3.54b}$$

Substitution into Eq. (3.13) yields the desired expression for the field Hamiltonian. Using relations between the expansion coefficients α and β, that follow from the completeness and orthogonality of the modes functions (see Appendix 3.B), we can write the result in the form

$$\begin{aligned} H = \frac{1}{2}\sum_\lambda \left[P^\dagger_\lambda P_\lambda + \omega^2_\lambda Q^\dagger_\lambda Q_\lambda\right] + \frac{1}{2}\sum_m \int_{\omega_m}^{\infty} \mathrm{d}\omega \left[P^\dagger_m(\omega) P_m(\omega) + \omega^2 Q^\dagger_m(\omega) Q_m(\omega)\right] \\ + \sum_\lambda \sum_m \int_{\omega_m}^{\infty} \mathrm{d}\omega \, W_{\lambda m}(\omega) Q^\dagger_\lambda Q_m(\omega), \end{aligned} \tag{3.55}$$

with the coupling amplitudes

$$W_{\lambda m}(\omega) = c^2 \langle \boldsymbol{\mu}_\lambda | L | \boldsymbol{\nu}_m(\omega)\rangle. \tag{3.56}$$

The first two terms clearly describe two independent sets of harmonic oscillators associated with the two subsystems. The third term shows that the operators of the subsystems do not simply oscillate as they would if the subsystems were completely isolated from each other, since this term couple the motion of the resonator and channel operators. The coupling reflects the fact that the boundary of the dielectric is not completely reflecting; thus radiation may leak through the boundary to the external radiation field.

The operators Q and P have a standard representation in terms of creation and annihilation operators,

$$Q_\lambda = \left(\frac{\hbar}{2\omega_\lambda}\right)^{\frac{1}{2}} \left[a_\lambda + \sum_{\lambda'} \mathcal{N}^\dagger_{\lambda\lambda'} a^\dagger_{\lambda'}\right], \tag{3.57a}$$

$$P_\lambda = \mathrm{i}\left(\frac{\hbar\omega_\lambda}{2}\right)^{\frac{1}{2}} \left[a^\dagger_\lambda - \sum_{\lambda'} \mathcal{N}_{\lambda\lambda'} a_{\lambda'}\right]. \tag{3.57b}$$

The operators a_λ and $a_\lambda^\dagger$ obey the canonical commutation relations

$$[a_\lambda, a_{\lambda'}^\dagger] = \delta_{\lambda\lambda'}, \qquad [a_\lambda, a_{\lambda'}] = 0. \tag{3.58}$$

In a similar fashion one derives the representation of the channel operators $Q_m(\omega)$ and $P_m(\omega)$ in terms of a continuous set of creation and annihilation operators $b_m^\dagger(\omega)$ and $b_m(\omega)$. Substituting these representations into the Hamiltonian (3.55) and using the symmetry and unitarity of the overlap matrices, one arrives at the Hamiltonian

$$\begin{aligned} H = \sum_\lambda \hbar\omega_\lambda\, a_\lambda^\dagger a_\lambda + \sum_m \int_{\omega_m}^{\infty} \mathrm{d}\omega\ \hbar\omega\, b_m^\dagger(\omega) b_m(\omega) \\ + \hbar \sum_\lambda \sum_m \int_{\omega_m}^{\infty} \mathrm{d}\omega \big[\mathcal{W}_{\lambda m}(\omega)\, a_\lambda^\dagger b_m(\omega) + \mathcal{V}_{\lambda m}(\omega)\, a_\lambda b_m(\omega) + \text{H.c.}\big], \end{aligned} \tag{3.59}$$

where we have omitted an irrelevant zero point contribution. The coupling matrix elements are given by

$$\mathcal{W}_{\lambda m}(\omega) = \frac{c^2}{2\sqrt{\omega_\lambda \omega}} \langle \boldsymbol{\mu}_\lambda | L_{\mathcal{QP}} | \boldsymbol{\nu}_m(\omega)\rangle, \tag{3.60a}$$

$$\mathcal{V}_{\lambda m}(\omega) = \frac{c^2}{2\sqrt{\omega_\lambda \omega}} \langle \boldsymbol{\mu}_\lambda^* | L_{\mathcal{QP}} | \boldsymbol{\nu}_m(\omega)\rangle. \tag{3.60b}$$

The notation $\langle \boldsymbol{\mu}_\lambda^* |$ means $\langle \boldsymbol{\mu}_\lambda^* | \boldsymbol{r}\rangle \equiv \boldsymbol{\mu}(\boldsymbol{r})$. In case the system is time reversal invariant the wavefunctions may be chosen real, the amplitudes $\mathcal{W}$ and $\mathcal{V}$ then become real and identical, $\mathcal{W} = \mathcal{V}$. Finally, substituting the representation (3.57) into Eq. (3.48) we find the expansion of the intra-cavity field

$$\boldsymbol{A}(\boldsymbol{r}, t) = c \sum_\lambda \left(\frac{\hbar}{2\omega_\lambda}\right)^{1/2} [a_\lambda \boldsymbol{u}_\lambda(\boldsymbol{r}) + a_\lambda^\dagger \boldsymbol{u}_\lambda^*(\boldsymbol{r})], \tag{3.61a}$$

$$\boldsymbol{\Pi}(\boldsymbol{r}, t) = -\frac{\mathrm{i}}{c} \sum_\lambda \left(\frac{\hbar\omega_\lambda}{2}\right)^{1/2} \epsilon(\boldsymbol{r}) [a_\lambda \boldsymbol{u}_\lambda(\boldsymbol{r}) - a_\lambda^\dagger \boldsymbol{u}_\lambda^*(\boldsymbol{r})]. \tag{3.61b}$$

The field expansions of the open resonator reduce precisely to the standard expressions known from closed resonators. However, the field dynamics is *fundamentally* different, as shown in the following chapter.

The Hamiltonian (3.59) and the field expansions (3.61) are the key results of the quantization procedure. Although system-and-bath Hamiltonias similar to one above, are frequently encountered in phenomenological approaches to open quantum systems [37, 38, 39], our result differs from them in a fundamental aspect: we provide explicit expressions for the coupling amplitudes between the resonator and the bath subsystems. We notice that in the Hamiltonian (3.59) the resonator modes are coupled to the external radiation field via both resonant ($a^\dagger b$, $b^\dagger a$) and non-resonant (ab, $a^\dagger b^\dagger$) terms. In most cases of interest the mode widths are smaller than the relevant frequencies, then the rotating-wave approximation can be made, which amounts to keeping only the resonant terms in the Hamiltonian. In this approximation, the Hamiltonian reduces to the well-known system-and-bath Hamiltonian [37, 38, 39] of quantum optics. The non-resonant terms become important only in the case of overdamping, which appears of not much interest in optics. It has been argued before [104, 105, 106] that the system-and-bath Hamiltonian can provide only an *approximate* description of open optical cavities provided they are of very high quality, i.e., when the modes widths are much smaller than both the typical internal oscillation frequencies and the spacing between internal frequencies $\Delta\omega$. Our derivation shows that such pessimism is inappropriate: the system-and-bath Hamiltonian (3.59) describes in an *exact* manner isolated modes, spectrally overlapping modes (when the widths are larger than the mode spacing $\Delta\omega$), as well as the extreme case of overdamped modes (when the mode frequencies ω_λ are overwhelmed by large escape rates).

When applied to chaotic cavities or in the presence of disordered dielectrics our quantization method naturally accommodates for an statistical description of the field properties. In that case the isolated cavity Hamiltonian may be represented by a proper ensemble of random matrices. Then the internal modes $\boldsymbol{u}_\lambda$ share the statistics of the eigenvectors of the random matrices and the eigenfrequencies ω_λ display level repulsion.

To conclude this section we notice that the cavity resonances, i.e., the complex frequencies that determine the cavity response to external excitations in the presence of the coupling to the outside world, are also found within the projection formalism. Formally the resonances are defined as the poles of the resolvent operator $\mathcal{G}(\omega)$ projected onto the cavity space and analytically continued in the second Reimannian sheet [103]. Such a projection is given by Eq. (3.43), from which the resonances follows as the solutions of the eigenvalue problem

$$L_{\text{eff}}(\omega)|\xi_i(\omega)\rangle = \sigma_i^2(\omega)|\xi_i(\omega)\rangle. \tag{3.62}$$

Since $L_{\text{eff}}(\omega)$ depends parametrically on ω, both its right eigenstates $|\xi_i(\omega)\rangle$ and the complex eigenvalues $\sigma_i(\omega)$ generally depend on ω as well. The states $|\xi_i(\omega)\rangle$ correspond to the Kapur–Peierls states [107, 41] of scattering theory. Combining equations (3.43) and (3.62) the cavity resonances are found as the solutions of the fixed point equation $c\sigma_i(\omega) = \omega$. We emphasize that this resonance condition is independent of the inside/outside separation and the choice of boundary condition made within the system-and-bath description.

3.3 Applications to Open Optical Resonators

In the previous section we focused on the general quantization of the electromagnetic field using the Feshbach projection formalism. The main result was the system-and-bath Hamiltonian (3.59). In this section we explicitly demonstrate the method for a number of models frequently used for optical resonators. Specifically, we consider the three types of cavities shown in Fig. 3.2: (a) A one-dimensional dielectric slab with (positive) refractive index n bounded on one side by a perfectly reflecting mirror, (b) a one-dimensional cavity defined by a perfectly reflecting mirror on one side and a thin semi-transparent mirror on the other side, and (c) a two-dimensional dielectric disk with refractive index n. The dielectrics are embedded in empty space. The normal

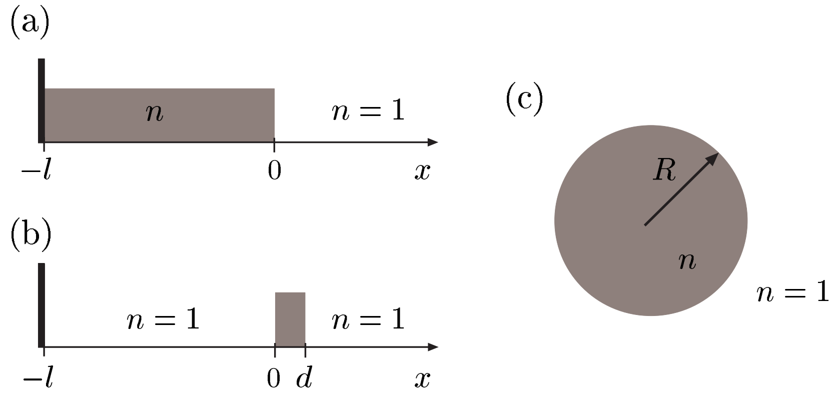

Figure 3.2: Open optical cavities: (a) A one–dimensional dielectric slab of length l with (positive) refractive index n bounded on one side ($x = -l$) by a perfectly reflecting mirror. (b) A one–dimensional cavity bounded by a perfectly reflecting mirror at ($x = -l$) and a thin semi–transparent mirror of width $d \ll l$ at ($x = 0$). (c) A two–dimensional dielectric disk with refractive index n.

modes of all three systems in question as well as their scattering properties can be computed exactly. Likewise, exact expressions can be obtained for the electromagnetic fields both within the cavities and in the external region. This makes all three models an ideal testing ground for our system-and-bath description. Such a test is particularly important to illustrate how in the projection formalism all physical observables do not relay in the choice of the separating surface and boundary conditions, but only on the physical boundary conditions imposed by Maxwell's equations. For each of the examples considered we compute their respective system-and-bath Hamiltonian, and show that the electromagnetic fields and the scattering properties agree exactly with results obtained by direct solutions of the quantization problem. In addition, the cavity resonances are found for all the systems and shown to be independent of the choice of boundary condition made on the fictitious boundary separating system and bath.

3.3.1 One Dimensional Dielectric Cavity

Our first example is the one dimensional dielectric cavity depicted in Fig. 3.2(a) [43]. The dielectric with refractive index n is nonabsorbing and nondispersive. It is bounded by a perfectly reflecting mirror at $x = -l$ while there is no mirror at the other end of the dielectric at $x = 0$. The free space outside the cavity runs from $x = 0$ to infinity, and light propagates freely there, $n = 1$. We assume the electromagnetic field to be linearly polarized with the electric field vector pointing in the z–direction. Cavity field excitations will decay due to leakage into the empty half-space. The dielectric function of the total system including the cavity and the attached half-space is given by

$$\epsilon(x) = n^2\Theta(-x) + \Theta(x), \tag{3.63}$$

where the Heaviside–function $\Theta(x)$ is equal to one for positive x and vanishes for negative x. The normal modes of Maxwell's equations for this problem are given in Eq. (3.D.1). To solve the problem within the projection formalism, we separate system and bath at $x = 0$. The cavity thus runs from $x = -l$ to $x = 0$, and the channel region from $x = 0$ to ∞. The boundary conditions at the interface are only restricted by the requirement that they lead to a Hermitian eigenvalue problem. Below we address two different such boundary conditions: In the first case we set Neumann boundary conditions for the cavity; Hermiticity [96] then imposes Dirichlet conditions for the channel problem. In the second case we consider the inverse situation with Dirichlet boundary condition for the cavity and Neumann conditions outside.

Cavity with von–Neumann Boundary Conditions

The inside/outside decomposition of the differential operator L follows from Eq. (3.24),

$$L_{\mathcal{QQ}}\mu(x) = -\frac{1}{n^2}\frac{\mathrm{d}^2}{\mathrm{d}x^2}\mu(x) + \frac{\delta(x-0_-)}{n^2}\frac{\mathrm{d}}{\mathrm{d}x'}\mu(x')\bigg|_{x'=0_-}, \tag{3.64a}$$

$$L_{\mathcal{PP}}\nu(x) = -\frac{\mathrm{d}^2}{\mathrm{d}x^2}\nu(x) - \delta'(x-0_+)\nu(0_+), \tag{3.64b}$$

$$L_{\mathcal{PQ}}\mu(x) = \frac{\delta'(x-0_+)}{n}\mu(0_-), \tag{3.64c}$$

$$L_{\mathcal{QP}}\nu(x) = -\frac{\delta(x-0_-)}{n}\frac{\mathrm{d}}{\mathrm{d}x'}\nu(x')\bigg|_{x'=0_+}. \tag{3.64d}$$

The shorthands $0_\mp$ indicate the limits where the interface at $x = 0$ is approached from inside respectively outside the resonator. The singular terms guarantee the matching conditions for the electromagnetic field at the interface. In addition, these terms ensure the Hermiticity of $L_{\mathcal{QQ}}$ and $L_{\mathcal{PP}}$. The range of the operators in equations (3.64a) and (3.64b) within Hilbert space is given by the functions for which the singular term vanishes.

The eigenmodes $\mu_\lambda(x)$ of the closed cavity are the solutions of the eigenvalue problem $L_{\mathcal{QQ}}\mu_\lambda(x) = k_\lambda^2\mu_\lambda(x)$ with $k_\lambda = \omega_\lambda/c$. From Eq. (3.64a), they satisfy the equation

$$\frac{\mathrm{d}^2}{\mathrm{d}x^2}\mu_\lambda(x) + n^2k_\lambda^2\mu_\lambda(x) = 0, \tag{3.65}$$

subject to the boundary conditions

$$\mu_\lambda(-l) = 0, \tag{3.66a}$$

$$\frac{\mathrm{d}}{\mathrm{d}x}\mu_\lambda(x)\bigg|_{x=0_-} = 0. \tag{3.66b}$$

The first condition is imposed by the perfectly reflecting mirror at $x = -l$, and the second follows from the requirement that the singular boundary term applied to μ_λ must vanish. The normalized solutions of the eigenvalue problem form the discrete set

$$\mu_\lambda(x) = \sqrt{\frac{2}{l}}\sin(nk_\lambda(x+l)), \tag{3.67}$$

with wave numbers $k_\lambda = (2\lambda + 1)\pi/2nl$ ($\lambda = 0, 1, 2, \ldots$). In the channel region, the eigenvalue problem reads

$$\frac{\mathrm{d}^2}{\mathrm{d}x^2}\nu(k, x) + k^2\nu(k, x) = 0; \quad (k = \omega/c), \tag{3.68}$$

with Dirichlet conditions at the resonator surface,

$$\nu(k, 0_+) = 0. \tag{3.69}$$

This determines a continuous set of δ–normalized channel modes,

$$\nu(k, x) = \sqrt{\frac{2}{\pi}}\sin(kx). \tag{3.70}$$

Since both the cavity and channel modes are real valued functions, the coupling amplitudes $\mathcal{W}$ and $\mathcal{V}$ become real and identical, $\mathcal{W} = \mathcal{V}$. Combining equations (3.60a), (3.64d) with the mode functions (3.67) and (3.70), we obtain

$$\mathcal{W}_\lambda(k) = \mathcal{V}_\lambda(k) = \frac{(-1)^{\lambda+1}}{n}\sqrt{\frac{k}{\pi k_\lambda l}}. \tag{3.71}$$

The result for the internal frequencies $\omega_\lambda = ck_\lambda$, together with the coupling amplitudes (3.71), and the mode functions (3.67) and (3.70), completely specify the system-and-bath Hamiltonian and the electric and magnetic field.

We now turn to an illustration of our results. To compare the exact scattering states with their representation in terms of cavity and channel modes, we combine equations (3.A.10a), (3.A.10b) with the results (3.D.1), (3.67), and (3.70). This yields the expansion coefficients

$$\alpha_\lambda(k) = \frac{(-1)^{\lambda+1} I_k k\cos(nkl)}{n\sqrt{\pi l}(k^2 - k_\lambda^2)}, \tag{3.72}$$

$$\beta(k, k') = \frac{1}{2\pi}\left[\mathcal{P}\left(\frac{2k'(1 + S_k)}{k'^2 - k^2}\right) - \mathrm{i}\pi(1 - S_k)\delta(k' - k)\right]. \tag{3.73}$$

The symbol $\mathcal{P}$ denotes the principal value. The scattering matrix S_k and the amplitude I_k are given, respectively, by equations (3.D.2) and (3.D.3). Figure 3.3 shows the real part of the scattering wave function with wavenumber $kl = 18$. We compare the exact result (solid gray line) with the system-and-bath expansion (dashed line). In the resonator region we only included 11 cavity modes with wavenumber centered around $kl = 18$. The agreement is very good; deviations are only visible close to $x = 0$, i.e., near the boundary separating system and bath. It has been argued before [104] that cavity or channel expansions must fail close to the boundary; so a remark concerning the status of such expansions is in order here: The inclusion of all cavity and all channel modes yields an exact point–to–point representation of the scattering function and its derivative, everywhere *except* for the point $x = 0$. This representation does not converge uniformly but it is exact in the L^2 sense. Therefore the system-and-bath expansion is an exact representation of the scattering state in the underlying Hilbert space.

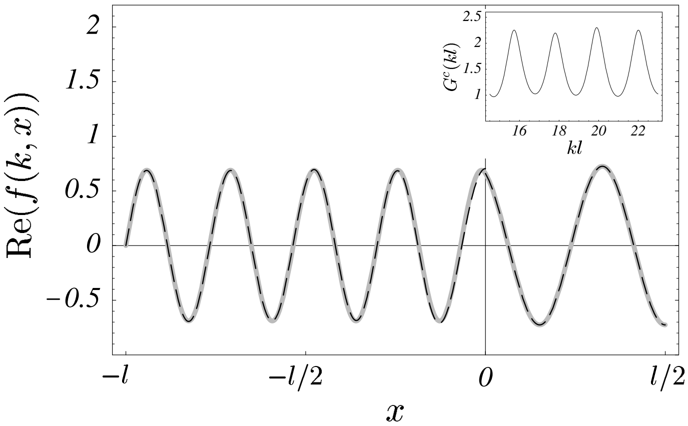

Figure 3.3: Real part of the scattering wave function corresponding to $kl = 18$, computed for a one dimensional dielectric cavity with refractive index $n = 1.5$. The solid line is the exact solution, the dashed line the expansion in terms of the resonator and channels modes. Only 11 cavity modes with $k_\lambda l$ around $kl = 18$ were included. The inset shows the cavity gain factor as function of kl for a range around $kl = 18$.

To determine the cavity resonances we solve the eigenvalue problem for the non-Hermitian operator $L_{\text{eff}}(k)$. Explicit calculation (Appendix 3.E) shows that $L_{\text{eff}}(k)$ acts on an arbitrary resonator state $\mu(x)$ according to

$$L_{\text{eff}}(k)\mu(x) = -\frac{1}{n^2}\frac{\mathrm{d}^2}{\mathrm{d}x^2}\mu(x) + \frac{\delta(x-0_-)}{n^2}\left[\frac{\mathrm{d}}{\mathrm{d}x'}\mu(x')\bigg|_{x'=0_-} - \mathrm{i}k\mu(0_-)\right]. \tag{3.74}$$

Due to the singular term, the action of $L_{\text{eff}}(k)$ generally goes beyond Hilbert space. The range of $L_{\text{eff}}(k)$ within Hilbert space is defined by the wave functions for which the singular term vanishes. It follows that the right eigenstates $\xi_j(k,x)$ of $L_{\text{eff}}(k)$ are solutions of the Helmholtz equation

$$\frac{\mathrm{d}^2}{\mathrm{d}x^2}\xi_j(k,x) + n^2\sigma_j^2(k)\xi_j(k,x) = 0, \tag{3.75}$$

that obey the boundary conditions

$$\xi_j(k,-l) = 0, \tag{3.76a}$$

$$\frac{\mathrm{d}}{\mathrm{d}x'}\xi_j(k,x')\bigg|_{x'=0_-} = \mathrm{i}k\xi_j(k,0_-). \tag{3.76b}$$

The first condition results from the perfect mirror at $x = -l$ while the second defines the so–called Siegert boundary condition. It accounts for the leakage out of the cavity: In the channel region that boundary condition implies a purely outgoing wave. For a fixed value of k, one finds the discrete set of solutions

$$\xi_j(k,x) = A_j(k)\sin(n\sigma_j(k)(x+l)), \tag{3.77}$$

with some normalization factors $A_j(k)$. Substituting the solutions into Eq. (3.76b) we obtain the secular equation for the eigenvalues,

$$\sigma_j(k) = \frac{\mathrm{i}}{n} k \tan(n\sigma_j(k)l). \tag{3.78}$$

The fixed point equation $k = \sigma_j(k)$ determines the cavity resonances. Analytical continuation of Eq. (3.78) into the complex plane then yields the resonance condition

$$\tan(nkl) + \mathrm{i}n = 0, \tag{3.79}$$

which has solutions only for complex k. The resonances can be found analytically and are given by

$$k_j = \frac{1}{nl} \begin{cases} \dfrac{(2j+1)\pi}{2} + \dfrac{\mathrm{i}}{2} \ln(|r|)\,; \quad j = 0, 1, \ldots \quad (n > 1), \\ j\pi + \dfrac{\mathrm{i}}{2} \ln(|r|)\,; \quad j = 1, 2, \ldots \quad (n < 1), \end{cases} \tag{3.80}$$

where $r = (n-1)/(n+1)$ is the reflection amplitude at the dielectric surface. Comparison with the direct calculation (cf. Eq. (3.D.2)) shows that the resonances coincide with the poles of the scattering–matrix. All resonances have the same width and are located along a straight line in the lower half of the complex plane. The resonance spacing, i.e., the difference in real parts of two successive resonances, is constant, $\Delta k = \pi/nl$. The resonances start to overlap when the modulus of the reflection amplitude becomes smaller than $|r| = \exp(-\pi)$.

We finally evaluate the cavity gain factor. The free–space local density of states is $\rho_0(k, x) = \sqrt{\frac{2}{\pi}} \sin^2(k(x + l))$. Integration over the cavity volume yields

$$\int_{-l}^{0} \mathrm{d}x\, \rho_0(k, x) = \frac{l}{\pi} \left[1 - \frac{\sin(2kl)}{2kl}\right]. \tag{3.81}$$

The integrated cavity density of states follows from equations (3.C.6) and (3.72) by means of the Poisson sum rule,

$$\begin{aligned} \int_{-l}^{0} \mathrm{d}x\, \rho(k, x) &= \frac{|I_k|^2 k^2 \cos^2(nkl)}{\pi l n^2} \sum_{\lambda=0}^{+\infty} \frac{1}{(k^2 - k_\lambda^2)^2} \\ &= \frac{l|I_k|^2}{4\pi} \left[1 - \frac{\sin(2nkl)}{2nkl}\right]. \end{aligned} \tag{3.82}$$

Combining these results with Eq. (3.D.3) for I_k, we obtain the cavity gain factor

$$G^c(k) = \frac{n^2 \left[1 - \frac{\sin(2nkl)}{2nkl}\right]}{\left[n^2 \cos^2(nkl) + \sin^2(nkl)\right] \left[1 - \frac{\sin(2kl)}{2kl}\right]}. \tag{3.83}$$

The inset in Fig. 3.3 shows the cavity gain factor over a range of kl. The peaks are equally spaced and have approximately the same high and width as expected from Eq. (3.80).

Cavity with Dirichlet Boundary Conditions

It is interesting to carry out the system-and-bath quantization in a basis other than that considered in the previous section. To that end we reconsider the dielectric resonator of Fig. 3.2(a) but perform the system-and-bath quantization with *interchanged* boundary conditions at the resonator/channel interface: The resonator modes are now required to satisfy Dirichlet boundary conditions at $x = 0$ while Neumann conditions hold for the channel modes. The differential operators corresponding to this choice have the form

$$L_{\mathcal{QQ}}\mu(x) = -\frac{1}{n^2}\frac{\mathrm{d}^2}{\mathrm{d}x^2}\mu(x) + \frac{\delta'(x-0_-)}{n^2}\mu(0_-)\,, \tag{3.84a}$$

$$L_{\mathcal{PP}}\nu(x) = -\frac{\mathrm{d}^2}{\mathrm{d}x^2}\nu(x) - \delta(x-0_+)\frac{\mathrm{d}}{\mathrm{d}x'}\nu(x')\bigg|_{x'=0_+}\,, \tag{3.84b}$$

$$L_{\mathcal{PQ}}\mu(x) = \frac{\delta(x-0_+)}{n}\frac{\mathrm{d}}{\mathrm{d}x'}\mu(x')\bigg|_{x'=0_-}\,, \tag{3.84c}$$

$$L_{\mathcal{QP}}\nu(x) = -\frac{\delta'(x-0_-)}{n}\nu(0_+). \tag{3.84d}$$

The closed cavity eigenmodes of $L_{\mathcal{QQ}}$ solve the Helmholtz equation and satisfy Dirichlet boundary conditions both at $x = l$ and $x = 0_-$. The second of these conditions follows from the requirement that the application of $L_{\mathcal{QQ}}$ on any eigenmode must yield a vanishing singular contribution. The eigenmodes form the discrete set of functions

$$\mu_\lambda(x) = \sqrt{\frac{2}{l}}\sin(nk_\lambda(x+l)), \tag{3.85}$$

with eigenvalues $k_\lambda = \pi\lambda/nl$ ($\lambda = 1, 2, \dots$). In a similar fashion one finds the continuous set of channel modes

$$\nu(k,x) = \sqrt{\frac{2}{\pi}}\cos(kx), \tag{3.86}$$

that satisfy Neumann boundary conditions at $x = 0_+$. Substituting the mode functions into the definitions (3.60) we obtain the coupling amplitudes

$$\mathcal{W}_{\lambda k} = \mathcal{V}_{\lambda k} = (-1)^\lambda\sqrt{\frac{k_\lambda}{\pi k l}}. \tag{3.87}$$

We note that the cavity eigenfrequencies and the coupling amplitudes obtained with the present set of boundary conditions differ from the results obtained in the previous section. Consequently, two different system-and-bath Hamiltonians are obtained in the two cases. However, as we show below both Hamiltonians provide an equivalent, and exact, description of the field dynamics.

Expanding the modes-of-the-universe $f(k,x)$ in terms of resonator and channel modes, we find the expansions coefficients

$$\alpha_\lambda(k) = \frac{(-1)^\lambda I_k k_\lambda \sin(nkl)}{n\sqrt{\pi}l(k^2-k_\lambda^2)}, \tag{3.88}$$

$$\beta(k,k') = \frac{\mathrm{i}}{2\pi}\left[\mathcal{P}\left(\frac{2k(1-S_k)}{k'^2-k^2}\right) - \mathrm{i}\pi(1+S_k)\delta(k'-k)\right], \tag{3.89}$$

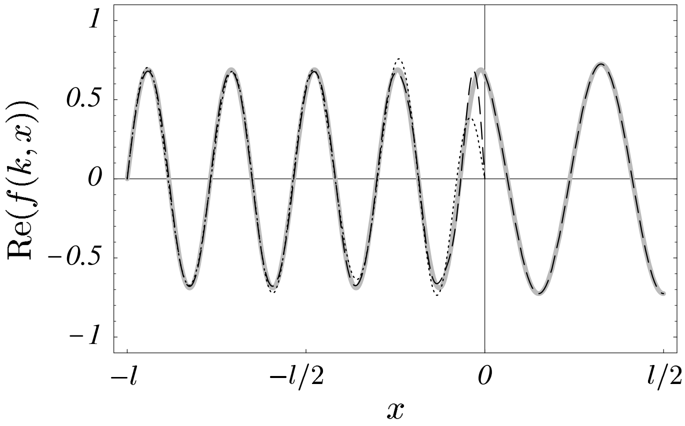

Figure 3.4: Real part of the scattering wave function for a one dimensional dielectric cavity with the same parameters as in Fig. 3.3. The solid gray curve is the exact solution. The system-and-bath expansion (dotted, dashed line) is based on 11, respectively, 25 cavity modes satisfying Dirichlet boundary conditions at $x = 0$. The dashed line for $x > 0$ is the representation in terms of channel modes.

with S_k and I_k defined, respectively, by equations (3.D.2) and (3.D.3). In Fig. 3.4 we compare the exact scattering wave function (3.D.1) (solid gray line) with the mode expansion using coefficients (3.88) and (3.89). Perfect agreement is found in the channel region $x > 0$. In the cavity region there is slow convergence close to $x = 0$, due to the Dirichlet boundary conditions at $x = 0_-$. The slower convergence visible in Fig. 3.4 must be compared with the faster convergence found for the other set of boundary conditions (Fig. 3.3). It indicates that, in spite of the freedom inherent in the projection formalism for the choice of boundary conditions, certain boundary conditions are better suited for the problem yielding good approximations with less terms in the mode expansions.

We may now evaluate the system resonances and the cavity gain factor. With the present boundary conditions the operator $L_{\text{eff}}(k)$ reduces to (Appendix 3.E)

$$L_{\text{eff}}(k)\mu(x) = -\frac{1}{n^2}\frac{\mathrm{d}^2}{\mathrm{d}x^2}\mu(x) + \frac{\delta'(x-0_-)}{n^2}\left[\mu(0_-) + \frac{\mathrm{i}}{k}\frac{d}{\mathrm{d}x'}\mu(x')\bigg|_{x'=0_-}\right]. \tag{3.90}$$

It is illustrative to compare this with the result (3.74) that holds for interchanged resonator/channel boundary conditions. Both results differ in their singular terms. However, upon projection onto the Hilbert space the same operator is recovered as the singular contributions vanish. In both cases the resulting boundary condition at the resonator/channel–interface is the Siegert condition (3.76b).

The integrated cavity density of states follows upon combination of equations (3.C.6) and (3.88), with the result

$$\int_{-l}^{0} \mathrm{d}x\, \rho(k,x) = \frac{l|I_k|^2}{4\pi}\left[1 - \frac{\sin(2nkl)}{2nkl}\right]. \tag{3.91}$$

It agrees with the result (3.82) obtained for the other set of boundary conditions. This demonstrates that the physical observables are indeed independent of the choice of boundary conditions.

3.3.2 One Dimensional Cavity with a Semitransparent Mirror

The model of Lay and Loudon [46] is a one dimensional cavity defined by a totally reflecting mirror at one end and a semitransparent mirror at the other end (Fig. 3.2(b)). The electric field is linearly polarized in the z–direction. Radiation can leak out through the semitransparent mirror modeled by a dielectric slab of width d and refractive index n. The limit $d \to 0$ and $n \to \infty$ with $n^2 d = \eta$ fixed is taken at the end of the calculation; here η is a factor characterizing the mirror transparency. In this limit, the frequency dependent mirror reflexion and transmission amplitudes are given by

$$r(k) = \frac{\mathrm{i}k\eta}{2 - \mathrm{i}k\eta}, \qquad t(k) = \frac{2}{2 - \mathrm{i}k\eta}. \tag{3.92}$$

They obey the common relations for symmetric mirrors, $|r|^2 + |t|^2 = 1$ and $rt^* + r^*t = 0$.

The exact eigenmodes of Maxwell's equations for this problem are given in Eq. (3.D.4). Within the projection formalism there are two natural ways of a resonator/channel separation: Either one assumes the mirror to be part of the cavity or the mirror is part of the channel region. Here, we stick to the latter choice. Accordingly, the cavity runs from $x = -l$ to $x = 0$ and the channel region from $x = 0$ to ∞. The alternative definition with the mirror being part of the cavity can easily be shown to lead to the same physical results. We choose Dirichlet conditions for the resonator boundary at $x = 0_-$, which implies von Neumann conditions for the outside problem. The differential operators corresponding to these definitions are

$$L_{\mathcal{QQ}}\mu(x) = -\frac{\mathrm{d}^2}{\mathrm{d}x^2}\mu(x) + \delta'(x - 0_-)\mu(0_-), \tag{3.93a}$$

$$L_{\mathcal{PP}}\nu(x) = -\frac{1}{n(x)}\frac{\mathrm{d}^2}{\mathrm{d}x^2}\left(\frac{\nu(x)}{n(x)}\right) - \frac{\delta(x - 0_+)}{n(x)}\frac{\mathrm{d}}{\mathrm{d}x'}\left(\frac{\nu(x')}{n(x')}\right)\bigg|_{x'=0_+}, \tag{3.93b}$$

$$L_{\mathcal{PQ}}\mu(x) = \frac{\delta(x - 0_+)}{n(x)}\frac{\mathrm{d}}{\mathrm{d}x'}\mu(x')\bigg|_{x'=0_-}, \tag{3.93c}$$

$$L_{\mathcal{QP}}\nu(x) = -\delta'(x - 0_-)\frac{\nu(0_+)}{n(0_+)}, \tag{3.93d}$$

where $n(x)$ is the refractive index in the channel region,

$$n(x) = \begin{cases} n & (0_+ \le x \le d), \\ 1 & (d < x). \end{cases} \tag{3.94}$$

The eigenvalue problem defined by $L_{\mathcal{QQ}}$ reduces to that of the dielectric resonator of the first example in Sec. 3.3.1 in the case when the dielectric function equals 1. Adopting our earlier results in that limiting case we find the closed cavity eigenmodes

$$\mu_\lambda(x) = \sqrt{\frac{2}{l}}\sin(k_\lambda(x + l)), \tag{3.95}$$

with the eigenvalues $k_\lambda = \pi\lambda/l$ ($\lambda = 1, 2, \dots$). The channel modes are the solutions of the Helmholtz equation

$$\frac{\mathrm{d}^2}{\mathrm{d}x^2}\nu(k,x) + n^2(x)k^2\nu(k,x) = 0, \tag{3.96}$$

with Neumann boundary conditions at $x = 0_+$. In addition, they must satisfy the two conditions

$$\frac{1}{n}\nu(k,d_-) = \nu(k,d_+), \tag{3.97}$$

$$\frac{1}{n}\frac{\mathrm{d}}{\mathrm{d}x}\nu(k,x)\bigg|_{x=d_-} = \frac{\mathrm{d}}{\mathrm{d}x}\nu(k,x)\bigg|_{x=d_+}, \tag{3.98}$$

imposed by the continuity of the electric and magnetic field at the right end of the semitransparent mirror. The shorthands $d_\pm$ indicate the limit where d is approached from the left (d_-) or from the right (d_+). Solving for $\nu(k,x)$ and taking the limit $d \to 0$, $n \to \infty$ with $n^2 d = \eta$, one obtains the following continuous set of channel modes,

$$\nu(k,x) = \frac{1}{\sqrt{2\pi}}\left(\mathrm{e}^{-\mathrm{i}kx} + S_c(k)\mathrm{e}^{\mathrm{i}kx}\right), \quad S_c(k) = \frac{\mathrm{i} - \eta k}{\mathrm{i} + \eta k}. \tag{3.99}$$

The coupling amplitudes follow upon substituting the wavefunctions (3.95) and (3.99) into the definitions (3.60a) and (3.60b). The result is

$$\mathcal{W}_\lambda(k) = \mathcal{V}_\lambda(k) = \frac{(-1)^\lambda}{1 - \mathrm{i}\eta k}\sqrt{\frac{k_\lambda}{\pi k l}}. \tag{3.100}$$

Finally, the representation of the exact modes $f(k,x)$ in terms of the system and bath modes yields the expansion coefficients

$$\alpha_\lambda(k) = \frac{(-1)^\lambda I_k k_\lambda \sin(nkl)}{\sqrt{\pi l}(k^2 - k_\lambda^2)}, \tag{3.101}$$

$$\beta(k,k') = \frac{\mathrm{i}}{2\pi}\left[\mathcal{P}\left(\frac{1 - S_c^*(k')S_k}{k' - k} + \frac{S_c^*(k') - S_k}{k' + k}\right) - \mathrm{i}\pi(1 + S_c^*(k)S_k)\delta(k' - k)\right], \tag{3.102}$$

where S_k and I_k are given by Eq. (3.D.5) and Eq. (3.D.6), respectively. Figure 3.5 shows the real part of the scattering wave function with $kl = 28.9$. The exact solution (3.D.4) (solid gray line) is compared with the mode expansion (dashed line) using the expansion coefficients (3.101) and (3.102). The first 35 cavity modes were included. The deviations from the exact scattering wave function visible near $x = 0$ can be made arbitrary small by including more terms in the mode expansion.

In order to find the resonances one must solve the eigenvalue equation for $L_{\mathrm{eff}}(k)$. The real space representation of $L_{\mathrm{eff}}(k)$ for our choice of boundary conditions follows upon combination of equations (3.42) and (3.93a) (see Appendix 3.E), with the result

$$L_{\mathrm{eff}}(k)\mu(x) = -\frac{\mathrm{d}^2}{\mathrm{d}x^2}\mu(x) + \delta'(x - 0_-)\left[\mu(0_-) - \frac{1}{k(\mathrm{i} + \eta k)}\frac{\mathrm{d}}{\mathrm{d}x'}\mu(x')\bigg|_{x'=0_-}\right], \tag{3.103}$$

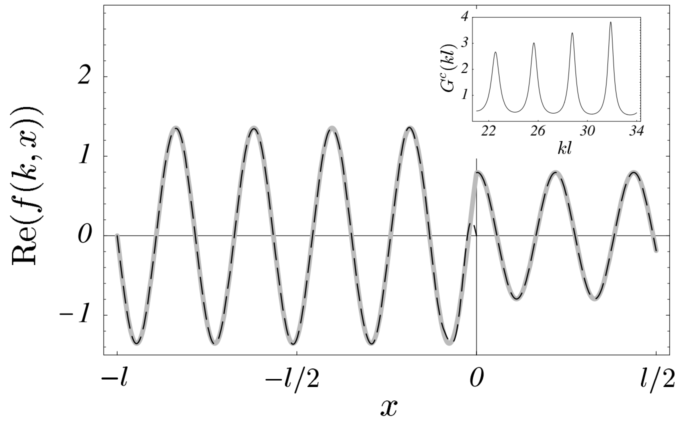

Figure 3.5: Real part of the scattering wave function with $kl = 28.9$ for a one dimensional optical cavity with a perfectly reflecting mirror at $x = -l$ and a semitransparent mirror at $x = 0$. The mirror transparency is characterized by $\eta = 0.0453$ corresponding to the reflexion coefficient $|r(kl = 28.9)|^2 = 0.3$. The solid line is the exact solution, the dashed line represents the mode expansion truncated to the first 35 modes in the cavity region. Inset: Cavity gain factor as function of kl for a range around $kl = 28$.

where $\mu(x)$ is an arbitrary resonator function. The range of $L_{\text{eff}}(k)$ within Hilbert space is defined by the resonator functions for which the singular term on the right hand side vanishes. In particular, this holds for the right eigenstates $\xi_j(k,x)$. It follows that these states satisfy the boundary condition

$$\xi_j(k,x) = \frac{1}{k(\mathrm{i}+\eta k)} \frac{\mathrm{d}}{\mathrm{d}x} \xi_j(k,0_-)\bigg|_{x=0_-}, \tag{3.104}$$

at the semitransparent mirror. There is a discrete set of solutions,

$$\xi_j(k,x) = A_j(k) \sin(\sigma_j(k)(x+l)), \tag{3.105}$$

where $A_j(k)$ is a normalization constant. Substitution into Eq. (3.104) yields the equation for the eigenvalues $\sigma_j(k)$,

$$\sigma_j(k) \cot(\sigma_j(k) l) = k(\mathrm{i} + k\eta). \tag{3.106}$$

After analytical continuation of the fixed point equation $k = \sigma_j(k)$ into the complex plane we obtain the resonance condition

$$\mathrm{i} + \eta k - \cot(kl) = 0\,, \tag{3.107}$$

that coincides with the equation for the poles of the S-matrix (cf. Eq. (3.D.5)).

To quantify the resonant response of the cavity to external excitations we compute the integrated local density of states, again using the Poisson sum rule,

$$\begin{aligned}\int_{-l}^{0} \mathrm{d}x\, \rho(k,x) &= \frac{l|I_k|^2 \sin^2(kl)}{l^2\pi} \sum_{\lambda=1}^{+\infty} \frac{k_\lambda^2}{(k^2-k_\lambda^2)^2}, \\ &= \frac{l|I_k|^2}{4\pi} \left[1 - \frac{\sin(2kl)}{2kl}\right].\end{aligned} \tag{3.108}$$

Combination with the free–space density of states (3.81) gives the cavity gain factor

$$G^c(k) = \frac{1}{\left[1 - \eta k \sin(2kl) + (\eta k)^2 \sin^2(nkl)\right]}. \tag{3.109}$$

With increasing kl sharper resonances are found in the cavity gain factor (see Fig. 3.5 (inset)). The reason is the reduction of the mirror transmission for large kl that, in turn, enhances the lifetime of the cavity resonances.

3.3.3 Dielectric Disk

In this section we demonstrate our quantization technique for resonators of spatial dimension larger than one. Specifically, we consider a two–dimensional circular dielectric of radius R and refractive index n (Fig. 3.2(c)). The resonator is embedded in free space. We restrict ourselves to TM modes with the electric field polarized in the z–direction. It is convenient to use polar coordinates $\boldsymbol{r} = (r, \phi)$ below. The dielectric function then reads

$$\epsilon(r) = n^2 \Theta(R - r) + \Theta(r - R). \tag{3.110}$$

The scattering problem at the resonator can be solved exactly. The normal modes of Maxwell's equations are summarized in Eq. (3.D.7).

To apply our quantization technique we separate system and bath along the boundary of the dielectric: The dielectric disk ($r \le R_-$) is taken as the cavity, while the free space ($r \ge R_+$) becomes the channel region. For the cavity we assume Dirichlet boundary conditions at $r = R_-$, which implies Neumann conditions at $r = R_+$ for the channel problem. The differential operator resulting from this choice reads

$$L_{\mathcal{QQ}}\mu(r,\phi) = -\frac{1}{n^2}\nabla^2\mu(r,\phi) + \frac{\partial}{\partial r}\left(\frac{1}{r}\delta(r - R_-)\right)\frac{R_-}{n^2}\mu(R_-,\phi), \tag{3.111a}$$

$$L_{\mathcal{PP}}\nu(r,\phi) = -\nabla^2\nu(r,\phi) - \delta(r - R_+)\frac{\partial}{\partial r'}\nu(r',\phi)\bigg|_{r'=R_+}, \tag{3.111b}$$

$$L_{\mathcal{PQ}}\mu(r,\phi) = \frac{\delta(r - R_+)}{n}\frac{\partial}{\partial r'}\mu(r',\phi)\bigg|_{r'=R_-}, \tag{3.111c}$$

$$L_{\mathcal{QP}}\nu(r,\phi) = -\frac{\partial}{\partial r}\left(\frac{1}{r}\delta(r - R_-)\right)\frac{R_-}{n}\nu(R_+,\phi). \tag{3.111d}$$

Due to the rotational symmetry we can choose the eigenstates to be angular momentum eigenstates.

The eigenmodes $\mu_{m\lambda}$ of the closed cavity are labeled by the angular momentum number m and the radial quantum number λ. They solve the Helmholtz equation

$$\nabla^2\mu_{m\lambda}(r,\phi) = -n^2 k_{m\lambda}^2 \mu_{m\lambda}(r,\phi), \tag{3.112}$$

and satisfy the Dirichlet condition $\mu_{m\lambda}(R_-,\phi) = 0$. The normalized eigenstates are given in terms of Bessel functions of the first kind,

$$\mu_{m\lambda}(r,\phi) = \frac{\mathrm{e}^{im\phi} J_m(nk_{m\lambda} r)}{\sqrt{\pi} R J_{m+1}(x_{m\lambda})}, \tag{3.113}$$

with $m = 0, \pm 1, \pm 2, \dots$ and $\lambda = 0, 1, 2, \dots$. The eigenvalues are $k_{m\lambda} = x_{m\lambda}/nR$ where $x_{m\lambda}$ denotes the λ-th zero of $J_m(r)$. In a similar fashion, one determines the eigenstates in the channel region. They can be written in terms of Hankel functions,

$$\nu_m(k, r, \phi) = \sqrt{\frac{k}{8\pi}} \mathrm{e}^{\mathrm{i}m\phi} (H_m^{(2)}(kr) + S_m(k) H_m^{(1)}(kr)), \tag{3.114}$$

with the diagonal element of the scattering matrix

$$S_m(k) = -\frac{H_m'^{(2)}(kR)}{H_m'^{(1)}(kR)}. \tag{3.115}$$

The channel states obey the Neumann condition $\frac{\partial}{\partial r}\nu_m(k, r, \phi)\big|_{r=R_+} = 0$.

In addition to the internal frequencies $\omega_{m\lambda} = ck_{m\lambda}$ we need the coupling amplitudes $\mathcal{W}$ and $\mathcal{V}$ to fully determine the system-and-bath Hamiltonian. Combination of Eq. (3.111d) with the mode functions (3.113), (3.114) and the definitions (3.60a) and (3.60b) yields after a short calculation

$$\mathcal{W}_{m\lambda,n}(k) = \frac{-\mathrm{i}\sqrt{2k_{m\lambda}}}{\pi k R H_m'^{(1)}(kR)}\, \delta_{m,n}, \tag{3.116a}$$

$$\mathcal{V}_{m\lambda,n}(k) = \frac{-\mathrm{i}\sqrt{2k_{m\lambda}}}{\pi k R H_m'^{(1)}(kR)}\, \delta_{m,-n}. \tag{3.116b}$$

We note that the resonant amplitude $\mathcal{W}$ couples only cavity and channel modes with the same angular momentum, while the antiresonant amplitude $\mathcal{V}$ couples modes with opposite angular momentum. This feature guarantees angular momentum conservation: The resonant terms $\mathcal{W}_{\lambda m} a_m^\dagger b_m$ and $\mathcal{W}_{\lambda m}^* a_m b_m^\dagger$ account for the creation of a photon with angular momentum m and the simultaneous annihilation of a second photon with the same angular momentum. By contrast, the antiresonant terms, $\mathcal{V}_{\lambda m} a_{m\lambda} b_{-m}$ and $\mathcal{V}_{\lambda m}^* a_{m\lambda}^\dagger b_{-m}^\dagger$ describe the simultaneous annihilation or creation of two photons with opposite value of angular momentum. In both cases, the total angular momentum is conserved.

We now turn to the electromagnetic field and the cavity resonances. In the cavity region the exact scattering states $f_m(k)$ can be represented in terms of the cavity modes $u_{m\lambda}$, with the expansion coefficients

$$\alpha_{m\lambda,n}(k) = \sqrt{\frac{k}{2}} \frac{k_{m\lambda} I_{mk} J_m(nkR)}{n(k^2 - k_{m\lambda}^2)} \delta_{m,n}, \tag{3.117}$$

where I_{mk} is given by Eq. (3.D.9). It suffices to compare the radial component of the scattering wave functions. In Fig. 3.6 we show the real part of that component for angular momentum $m = 13$ and $kR = 10.5$. The solid gray line is the exact result (3.D.7) while the dotted and dashed lines represent the system-and-bath expansion using the first 11 and 25 cavity modes, respectively.

The cavity resonances are obtained by solving the eigenvalue problem for $L_{\mathrm{eff}}(k)$. The calculation is presented in Appendix 3.E and yields the resonance condition

$$J_m(nkR) H_m'^{(1)}(kR) - n J_m'(nkR) H_m^{(1)}(kR) = 0, \tag{3.118}$$

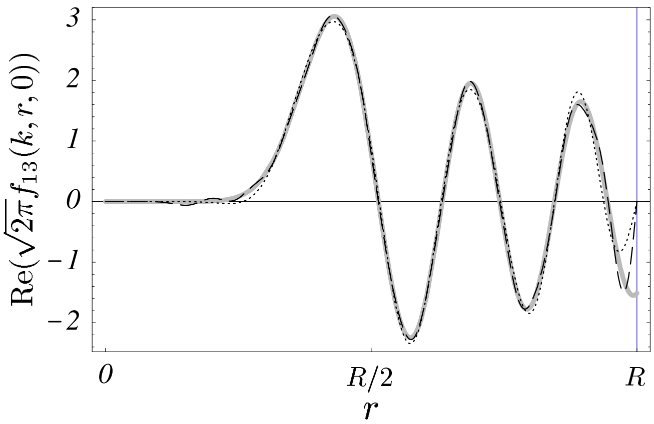

Figure 3.6: Real part of the radial component of the scattering wave function with angular momentum $m = 13$ and $kR = 10.5$ inside a dielectric disk with radius R and index of refraction $n = 3.3$. The solid gray curve is the exact result. The dotted (dashed) line follows from the mode expansion taking into account the first 11 (25) cavity modes.

which is equivalent to the equation that determines the poles of the S-matrix (cf. Eq. (3.D.8)).

Substitution of Eq. (3.117) into Eq. (3.C.6) yields the integrated local density of states inside the dielectric disk (Appendix 3.F),

$$\int_{\text{disk}} d\boldsymbol{r}\rho(k, \boldsymbol{r}) = \sum_{m=-\infty}^{+\infty} \frac{kR^2|I_{mk}|^2}{8n^2} \left(J_m^2(nkR) - J_{m+1}(nkR)J_{m-1}(nkR)\right). \tag{3.119}$$

Together with the free–space local density of states $\rho_0(k) = k/2\pi$, we obtain the cavity gain factor

$$G^c(k) = \sum_m \frac{4\left(J_m^2(nkR) - J_{m+1}(nkR)J_{m-1}(nkR)\right)}{(\pi nkR)^2 \left|J_m(nkR)H_m^{\prime(1)}(kR) - nJ_m'(nkR)H_m^{(1)}(kR)\right|^2}, \tag{3.120}$$

where we used the explicit expression (3.D.9) for the mode amplitude I_{mk}. The cavity gain factor displays a set of very sharp resonances (see Fig. 3.7), corresponding to states with angular momentum $kR < m < nkR$, superimposed over a smooth background due to broad resonances with $m < kR$ [108].

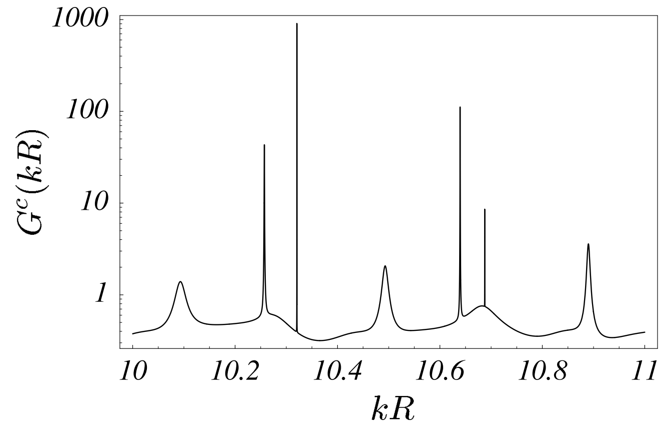

Figure 3.7: Cavity gain factor as function of kR for a dielectric disk with radius R and index of refraction $n = 3.3$. The sharp resonances correspond to states with angular momentum $10 < m < 18$, very sharp resonances with $m \gg 18$ are not resolved.

3.A Commutation Relations for Cavity and Channel Operators

In this appendix we compute the (equal–time) commutation relations for the cavity and channels position and momentum operators. One finds that the cavity operators obey the commutation relations

$$[Q_\lambda, Q_{\lambda'}] = [Q_\lambda, Q^\dagger_{\lambda'}] = 0, \tag{3.A.1}$$

$$[P_\lambda, P_{\lambda'}] = [P_\lambda, P^\dagger_{\lambda'}] = 0, \tag{3.A.2}$$

$$[Q_\lambda, P_{\lambda'}] = \mathrm{i}\hbar\, \delta_{\lambda\lambda'}\,, \tag{3.A.3}$$

$$[Q_\lambda, P^\dagger_{\lambda'}] = \mathrm{i}\hbar \mathcal{N}^*_{\lambda\lambda'}\,, \tag{3.A.4}$$

while for the channel operators the following commutation relations hold

$$[Q_m(\omega), Q_n(\omega')] = [Q_m(\omega), Q^\dagger_n(\omega')] = 0, \tag{3.A.5}$$

$$[P_m(\omega), P_n(\omega')] = [P_m(\omega), P^\dagger_n(\omega')] = 0, \tag{3.A.6}$$

$$[Q_m(\omega), P_n(\omega')] = \mathrm{i}\hbar\, \delta_{mn}\, \delta(\omega - \omega'), \tag{3.A.7}$$

$$[Q_m(\omega), P^\dagger_n(\omega')] = \mathrm{i}\hbar \mathcal{N}^*_{nm}(\omega', \omega), \tag{3.A.8}$$

and in addition the cavity operators commute with all channel operators. This shows that for each subsystem the operators Q and P behave like the basic operators of position an momentum, respectively.

The equal–time commutation relations follow easily from the commutation relations (3.14) for the operators of the total system and the completeness of the modes $|\boldsymbol{\phi}_m(\omega)\rangle$. As an example we show that $[Q_\lambda, P_m(\omega)] = 0$. Using the definitions (3.49a), (3.50b) of Q_λ and $P_m(\omega)$, we obtain

$$\begin{aligned}
[Q_\lambda, P_m(\omega)] &= \sum_{m'm''} \int\limits_{\omega_{m'}}^{\infty} \mathrm{d}\omega' \int\limits_{\omega_{m''}}^{\infty} \mathrm{d}\omega''\ \alpha_{m'\lambda}(\omega')\beta^*_{m''m}(\omega'', \omega)[q_{m'}(\omega'), p_{m''}(\omega'')] \\
&= i\hbar \sum_{m'} \int\limits_{\omega_{m'}}^{\infty} d\omega'\ \alpha_{m'\lambda}(\omega')\beta^*_{m'm}(\omega', \omega),
\end{aligned} \tag{3.A.9}$$

where we used the commutation relation (3.14). According to Eq. (3.46), the coefficients α and β can be written as

$$\alpha_{m'\lambda}(\omega') = \langle \boldsymbol{\mu}_\lambda | \boldsymbol{\phi}_{m'}(\omega')\rangle, \tag{3.A.10a}$$

$$\beta_{m'm}(\omega', \omega) = \langle \boldsymbol{\nu}_m(\omega) | \boldsymbol{\phi}_{m'}(\omega')\rangle. \tag{3.A.10b}$$

Substitution into the right hand side of Eq. (3.A.9) yields

$$\begin{aligned}
\sum_{m'} \int\limits_{\omega_{m'}}^{\infty} \mathrm{d}\omega'\ \alpha_{m'\lambda}(\omega')\beta^*_{m'm}(\omega', \omega) &= \sum_{m'} \int\limits_{\omega_{m'}}^{\infty} \mathrm{d}\omega'\ \langle \boldsymbol{\mu}_\lambda | \boldsymbol{\phi}_{m'}(\omega')\rangle \langle \boldsymbol{\phi}_{m'}(\omega') | \boldsymbol{\nu}_m(\omega)\rangle \\
&= \langle \boldsymbol{\mu}_\lambda | \boldsymbol{\nu}_m(\omega)\rangle,
\end{aligned} \tag{3.A.11}$$

which vanishes due to the orthogonality between resonator and channel modes. The calculation of all remaining commutators reduces to Eq. (3.A.11) or to one of the expressions

$$\sum_m \int_{\omega_m}^{\infty} \mathrm{d}\omega \; \alpha_{m\lambda}(\omega)\alpha^*_{m\lambda'}(\omega) = \delta_{\lambda\lambda'}, \tag{3.A.12}$$

$$\sum_n \int_{\omega_n}^{\infty} \mathrm{d}\omega'' \; \beta_{nm}(\omega'', \omega)\beta^*_{nm'}(\omega''\omega') = \delta_{mm'}\delta(\omega - \omega'), \tag{3.A.13}$$

obtained in a similar fashion as Eq. (3.A.11).

3.B The Hamiltonian

Here we show how the Hamiltonian (3.55) is derived from the Hamiltonian (3.13) that involves operators associated with the eigenmodes of the total system. We separately treat the two contributions to the Hamiltonian (3.13) involving integrals over momentum and position operators, respectively. We start with the contribution

$$T = \frac{1}{2}\sum_m \int_{\omega_m}^{\infty} \mathrm{d}\omega \; p^\dagger_m(\omega)p_m(\omega). \tag{3.B.1}$$

Substitution of the representation (3.54) for $p_m(\omega)$ reduces the right hand side to three integrals which can be done using Eqs. (3.A.11)–(3.A.13). The result has the form

$$T = \frac{1}{2}\sum_\lambda P^\dagger_\lambda P_\lambda + \frac{1}{2}\sum_m \int_{\omega_m}^{\infty} \mathrm{d}\omega \; P^\dagger_m(\omega)P_m(\omega). \tag{3.B.2}$$

The second contribution

$$V = \frac{1}{2}\sum_m \int_{\omega_m}^{\infty} \mathrm{d}\omega \; \omega^2 q^\dagger_m(\omega)q_m(\omega) \tag{3.B.3}$$

is more difficult to compute due to the presence of the term ω^2 in the integral over frequency. Substituting the representation (3.54) for $q_m(\omega)$ into Eq. (3.B.3), we obtain

$$\begin{aligned} V = \frac{1}{2}\sum_{\lambda\lambda'} V^{(1)}_{\lambda\lambda'} Q^\dagger_\lambda Q_{\lambda'} + \frac{1}{2}\sum_{m'm''} \int_{\omega_{m'}}^{\infty} \mathrm{d}\omega' \int_{\omega_{m''}}^{\infty} \mathrm{d}\omega'' \; V^{(2)}_{m'm''}(\omega', \omega'')Q^\dagger_{m'}(\omega')Q_{m''}(\omega'') \\ + \frac{1}{2}\sum_{m'}\sum_\lambda \int_{\omega_{m'}}^{\infty} \mathrm{d}\omega' \left(V^{(3)}_{m'\lambda}(\omega')Q^\dagger_\lambda Q_{m'}(\omega') + \text{H.c.} \right), \end{aligned} \tag{3.B.4}$$

where $V^{(1)}$, $V^{(2)}$, and $V^{(3)}$ are integrals over the coefficients α and β,

$$V^{(1)}_{\lambda\lambda'} = \sum_m \int\limits_{\omega_m}^{\infty} \mathrm{d}\omega\ \omega^2 \alpha_{m\lambda}(\omega)\alpha^*_{m\lambda'}(\omega), \tag{3.B.5}$$

$$V^{(2)}_{m'm''}(\omega',\omega'') = \sum_m \int\limits_{\omega_m}^{\infty} \mathrm{d}\omega\ \omega^2 \beta_{m'm}(\omega',\omega)\beta^*_{m''m}(\omega'',\omega), \tag{3.B.6}$$

$$V^{(3)}_{m'\lambda}(\omega') = \sum_m \int\limits_{\omega_m}^{\infty} \mathrm{d}\omega\ \omega^2 \alpha_{m\lambda}(\omega)\beta^*_{m'm}(\omega',\omega). \tag{3.B.7}$$

We compute these integrals using relations that follow from the eigenmode equation (3.30). Projecting this equation onto the cavity states $\langle \boldsymbol{\mu}_\lambda|$ and the channel states $\langle \boldsymbol{\nu}_m(\omega)|$, we obtain the set of coupled equations

$$\left(\omega^2 - \omega_\lambda^2\right) \alpha_{m\lambda}(\omega) = \sum_n \int\limits_{\omega_n}^{\infty} \mathrm{d}\omega'\ W_{\lambda n}(\omega')\beta_{mn}(\omega,\omega'), \tag{3.B.8a}$$

$$\left(\omega^2 - \omega'^2\right) \beta_{mn}(\omega,\omega') = \sum_\lambda W^*_{\lambda n}(\omega')\alpha_{m\lambda}(\omega). \tag{3.B.8b}$$

We used the definition (3.56) of $W_{\lambda m}(\omega)$ and the definitions (3.A.10) of α and β. As an example we evaluate the integral $V^{(1)}$. We multiply both sides of Eq. (3.B.8a) by $\alpha^*_{\lambda' m}(\omega)$ and then sum over m and integrate over ω. This yields

$$\begin{aligned} V^{(1)}_{\lambda\lambda'} = \omega_\lambda^2 \sum_m \int\limits_{\omega_m}^{\infty} \mathrm{d}\omega\ \alpha^*_{m\lambda'}(\omega)\alpha_{m\lambda}(\omega) \\ + \sum_{m'} \int\limits_{\omega_{m'}}^{\infty} \mathrm{d}\omega'\ W_{\lambda m'}(\omega') \left[\sum_m \int\limits_{\omega_m}^{\infty} \mathrm{d}\omega\ \alpha^*_{m\lambda'}(\omega)\beta_{mm'}(\omega,\omega') \right]. \end{aligned} \tag{3.B.9}$$

The term in the square brackets vanishes according to Eq. (3.A.11). The remaining term on the right hand side can be simplified using Eq. (3.A.10a). Equation (3.B.9) then reduces to

$$\begin{aligned} V^{(1)}_{\lambda\lambda'} &= \omega_\lambda^2 \sum_m \int\limits_{\omega_m}^{\infty} \mathrm{d}\omega\ \langle \boldsymbol{\mu}_\lambda | \boldsymbol{\phi}_m(\omega)\rangle \langle \boldsymbol{\phi}_m(\omega)|\boldsymbol{\mu}_{\lambda'}\rangle \\ &= \omega_\lambda^2\, \delta_{\lambda\lambda'}. \end{aligned} \tag{3.B.10}$$

In a similar fashion we obtain for $V^{(2)}$ and $V^{(3)}$

$$V^{(2)}_{m'm''}(\omega',\omega'') = \omega'\, \delta_{m'm''}\, \delta(\omega' - \omega''), \tag{3.B.11}$$

$$V^{(3)}_{m'\lambda}(\omega') = W_{\lambda m'}(\omega'). \tag{3.B.12}$$

Combining results the second contribution to the Hamiltonian takes the form

$$V = \frac{1}{2}\sum_{\lambda}\omega_{\lambda}^{2}Q_{\lambda}^{\dagger}Q_{\lambda} + \frac{1}{2}\sum_{m}\int_{\omega_m}^{\infty}\mathrm{d}\omega\,\omega^{2}Q_{m}^{\dagger}(\omega)Q_{m}(\omega) + \sum_{m}\sum_{\lambda}\int_{\omega_m}^{\infty}\mathrm{d}\omega\,W_{\lambda m}(\omega)Q_{\lambda}^{\dagger}Q_{m}(\omega). \tag{3.B.13}$$

Where for the last term we used

$$\sum_{m}\sum_{\lambda}\int_{\omega_m}^{\infty}\mathrm{d}\omega\,W_{\lambda m}(\omega)Q_{\lambda}^{\dagger}Q_{m}(\omega) = \sum_{m}\sum_{\lambda}\int_{\omega_m}^{\infty}\mathrm{d}\omega\,W_{\lambda m}^{*}(\omega)Q_{\lambda}Q_{m}^{\dagger}(\omega). \tag{3.B.14}$$

This last identity is obtained using relations (3.51a), (3.52a) for the position operators, and the alternative definition of the coupling amplitude

$$W_{\lambda m}(\omega) = \sum_{\lambda'}\sum_{n}\int_{\omega_n}^{\infty}\mathrm{d}\omega'\,\mathcal{N}_{\lambda\lambda'}\mathcal{N}_{mn}^{\dagger}(\omega,\omega')W_{\lambda' m}^{*}. \tag{3.B.15}$$

The sum of the contributions (3.B.2) and (3.B.13) yields the Hamiltonian (3.55).

3.C Local Density of States Inside an Open Resonator

For the electromagnetic field in the presence of a dielectric medium the local density of states at at point $\boldsymbol{r}$ is defined in terms of the Wiener–Khintchine theorem [78],

$$\rho(\omega,\boldsymbol{r}) = \frac{1}{\pi\hbar\omega}\int_{-\infty}^{+\infty}\mathrm{d}\tau\,\mathrm{e}^{\mathrm{i}\omega\tau}\epsilon(\boldsymbol{r})\langle\boldsymbol{E}^{(+)}(\boldsymbol{r},t)\boldsymbol{E}^{(-)}(\boldsymbol{r},t-\tau)\rangle_{\mathrm{vac}}. \tag{3.C.1}$$

Here $\epsilon(\boldsymbol{r})$ is the real and frequency independent dielectric constant, $\langle\ldots\rangle_{\mathrm{vac}}$ denotes the quantum average over the vacuum state, and $(\pm)$ refers to the positive and negative component of the electric field. Substituting the field representation in terms of the normal modes of Maxwell's equations (see Eq. (3.3)),

$$\boldsymbol{E}^{(+)}(\boldsymbol{r},t) = \sum_{m}\int\mathrm{d}\omega\left(\frac{\hbar\omega}{2}\right)^{\frac{1}{2}}A_{m}(\omega)\mathrm{e}^{-\mathrm{i}\omega t}\boldsymbol{f}_{m}(\omega,\boldsymbol{r}), \tag{3.C.2}$$

and taking into account that $\langle A_m(\omega)A_{m'}^{\dagger}(\omega')\rangle_{\mathrm{vac}} = \delta_{mm'}\delta(\omega-\omega')$, equation (3.C.1) reduces to

$$\rho(\omega,\boldsymbol{r}) = \sum_{m}\epsilon(\boldsymbol{r})|\boldsymbol{f}_{m}(\omega,\boldsymbol{r})|^{2}. \tag{3.C.3}$$

In the case of open cavities one is mainly interested in the local density of states at points $\boldsymbol{r}$ inside the resonator. It is then useful to use the projection formalism to express the local density of states inside the cavity; utilizing the mode expansion (3.47), Eq. (3.C.3) may be rewritten as

$$\rho(\omega,\boldsymbol{r}) = \sum_m \sum_{\lambda\lambda'} \epsilon(\boldsymbol{r})\alpha_{\lambda m}(\omega)\alpha^*_{\lambda' m}(\omega)\boldsymbol{u}_\lambda(\boldsymbol{r})\cdot\boldsymbol{u}^*_{\lambda'}(\boldsymbol{r}), \tag{3.C.4}$$

for $\boldsymbol{r}$ inside the cavity. Here $\boldsymbol{u}_\lambda(\boldsymbol{r})$ are the mode functions of the cavity.

The change in the local density of states introduced by the cavity are quantitatively studied using the cavity gain factor

$$G^c(\omega) = \frac{\int_{\boldsymbol{r}\in I} \mathrm{d}\boldsymbol{r}\,\rho(\omega,\boldsymbol{r})}{\int_{\boldsymbol{r}\in I} \mathrm{d}\boldsymbol{r}\,\rho_0(\omega,\boldsymbol{r})}\,, \tag{3.C.5}$$

that is closely related to the dwell time of scattered radiation inside the resonator [109]. Here, $\rho(\omega,\boldsymbol{r})$ is the local density of states inside the cavity and $\rho_0(\omega,\boldsymbol{r})$ the free space local density of states in the absence of the cavity. In addition, we note that the integrated local density of states can be expressed in terms of the expansions coefficients (3.46a) as

$$\int_{\boldsymbol{r}\in I} \mathrm{d}\boldsymbol{r}\,\rho(\omega,\boldsymbol{r}) = \sum_m \sum_\lambda |\alpha_{m\lambda}(\omega)|^2. \tag{3.C.6}$$

3.D Exact Modes of Maxwell's Equations

In this appendix we summarize the normal modes of Maxwell's equations for the three systems treated in Sec. 3.3; for a more detailed derivation we refer to references [43, 46, 108]. The modes–of–the–universe are taken to be scattering states with an incoming wave in only one scattering channel. In the two dimensional example, this channel is labeled by the angular momentum number m. The scattering states are normalized according to Eq. (3.7).

One Dimensional Dielectric Cavity

For the dielectric cavity of Fig. 3.2(a) the scattering states are given by

$$f(k,x) = \frac{1}{\sqrt{2\pi}} \begin{cases} \dfrac{I_k}{n}\sin(nk(x+l)) & (-l<x<0), \\ \exp(-\mathrm{i}kx) + S_k\exp(\mathrm{i}kx) & (0<x). \end{cases} \tag{3.D.1}$$

They satisfy the boundary condition $f(k,-l)=0$, imposed by the completely reflecting mirror at $x=-l$, and are continuous with continuous derivative for any value of $x>-l$. The single-channel scattering matrix and the mode strength amplitude are given, respectively, by

$$S_k = -\frac{n+\mathrm{i}\tan(nkl)}{n-\mathrm{i}\tan(nkl)}, \tag{3.D.2}$$

$$I_k = -\frac{2\mathrm{i}n}{n\cos(nkl)-\mathrm{i}\sin(nkl)}\,. \tag{3.D.3}$$

Cavity with Semitransparent Mirror

The scattering states for the one dimensional cavity with the semitransparent mirror (Fig. 3.2(b)) have the form

$$f(k,x) = \frac{1}{\sqrt{2\pi}} \begin{cases} I_k \sin(k(x+l)) & (-l < x < 0), \\ \exp(-\mathrm{i}kx) + S_k \exp(\mathrm{i}kx) & (0 < x), \end{cases} \tag{3.D.4}$$

where the scattering matrix S_k and the mode strength amplitude I_k are given by

$$S_k = \frac{\mathrm{i} - \eta k + \cot(kl)}{\mathrm{i} + \eta k - \cot(kl)}, \tag{3.D.5}$$

$$I_k = \frac{2\mathrm{i}}{(\mathrm{i} + k\eta)\sin(kl) - \cos(kl)}. \tag{3.D.6}$$

Here η specifies the mirror transparency. The modes satisfy $f(k,-l) = 0$ at the perfectly reflecting mirror and are continuous everywhere else. At the semitransparent mirror their derivative has a discontinuity proportional to the mode amplitude, $f'(k,0_+) - f'(k,0_-) = -\eta k^2 f(k,0)$, where the prime denotes differentiation with respect to the position.

Dielectric Disk

The exact eigenstates for a two dimensional dielectric disk of radius R and refractive index n embedded in empty space read

$$f_m(k,r,\phi) = \sqrt{\frac{k}{8\pi}} \mathrm{e}^{-\mathrm{i}m\phi} \begin{cases} I_{mk} J_m(nkr) & (0 < r < R), \\ H_m^{(2)}(kr) + S_{mk} H_m^{(1)}(kr) & (R < r), \end{cases} \tag{3.D.7}$$

where m labels angular momentum. The channel with index m is open when k exceeds the channel threshold $k_m = m/nR$. Due to rotational symmetry angular momentum is conserved, and the scattering matrix is diagonal in the angular momentum basis

$$S_{mk} = -\frac{H_m'^{(2)}(kR) - n[J_m'(nkR)/J_m(nkR)]H_m^{(2)}(kR)}{H_m'^{(1)}(kR) - n[J_m'(nkR)/J_m(nkR)]H_m^{(1)}(kR)}. \tag{3.D.8}$$

The mode strength amplitude takes the form

$$I_{mk} = \frac{4\mathrm{i}}{\pi kR\Big(J_m(nkR)H_m'^{(1)}(kR) - nJ_m'(nkR)H_m^{(1)}(kR)\Big)}. \tag{3.D.9}$$

3.E External Green Functions

Here we evaluate the action of the non–Hermitian differential operator $L_{\mathrm{eff}}(k)$ on an arbitrary cavity state. According to Eq. (3.42) $L_{\mathrm{eff}}(k)$ is the sum of two operators.

The first contribution $L_{\mathcal{QQ}}$ has already been computed in equations (3.64a), (3.84a), (3.93a) and (3.111a). The second contribution has the form

$$L_{\mathcal{QP}}\mathcal{G}_{\text{ch}}(k)L_{\mathcal{PQ}}\mu(r,\phi) = L_{\mathcal{QP}}\sum_m \int_{k_m}^{\infty}\mathrm{d}k'\,\frac{|\boldsymbol{\nu}_m(k')\rangle\langle\boldsymbol{\nu}_m(k')|}{k^2-k'^2+\mathrm{i}\epsilon}L_{\mathcal{PQ}}\mu(r,\phi), \tag{3.E.1}$$

where $\mathcal{G}_{\text{ch}}$ stands for the retarded Green function of the isolated channel region and on the right hand side we used the completeness of the channel modes with the help of Eq. (3.36). Below we compute this contribution for the cavities of interest.

One Dimensional Channel

For a one dimensional semi-infinite channel $x \geq 0$ with Dirichlet boundary conditions at $x = 0_+$ we find the retarded Green function from the solutions (3.70) by contour integration,

$$\begin{aligned}\mathcal{G}_{\text{ch}}(k,x,x') &= \frac{2}{\pi}\int_0^{\infty}\mathrm{d}k'\frac{\sin(k'x)\sin(k'x')}{k^2-k'^2+\mathrm{i}\epsilon}\\ &= \frac{\mathrm{i}}{2k}\big(\mathrm{e}^{\mathrm{i}k|x+x'|}-\mathrm{e}^{-\mathrm{i}k|x-x'|}\big).\end{aligned} \tag{3.E.2}$$

Combination with the definitions (3.64c) and (3.64d) yields the real space representation of $L_{\text{eff}}(k)$. The relevant derivatives have to be done with care as the limits $x \to 0$ and $x' \to 0$ must be taken independently. The result takes the form

$$L_{\mathcal{QP}}\mathcal{G}_{\text{ch}}(k)L_{\mathcal{PQ}}\mu(x) = -\frac{\mathrm{i}k\delta(x-0_-)}{n^2}\mu(0_-). \tag{3.E.3}$$

Together with equation (3.64a) we arrive at the result (3.74) for $L_{\text{eff}}(k)$.

In a similar fashion we evaluate the retarded Green function for the isolated channel problem with Neumann conditions at $x = 0_+$. Using the solutions (3.86) we obtain in this case

$$\begin{aligned}\mathcal{G}_{\text{ch}}(k,x,x') &= \frac{2}{\pi}\int_0^{\infty}\mathrm{d}k'\frac{\cos(k'x)\cos(k'x')}{k^2-k'^2+\mathrm{i}\epsilon}\\ &= -\frac{\mathrm{i}}{2k}\big(\mathrm{e}^{\mathrm{i}k|x+x'|}+\mathrm{e}^{-\mathrm{i}k|x-x'|}\big).\end{aligned} \tag{3.E.4}$$

Combination with the real space representation (3.84c) and (3.84d) of $L_{\mathcal{PQ}}$ and $L_{\mathcal{QP}}$, respectively, yields

$$L_{\mathcal{QP}}\mathcal{G}_{\text{ch}}(k)L_{\mathcal{PQ}}\mu(x) = \frac{\mathrm{i}\,\delta'(x-0_-)}{n^2k}\,\frac{\mathrm{d}}{\mathrm{d}x'}\mu(x')\bigg|_{x'=0_-}. \tag{3.E.5}$$

Combinations of equations (3.42), (3.84a), and (3.E.5) yields $L_{\text{eff}}(k)$ given in equation (3.90).

Channel with Semitransparent Mirror

The semitransparent mirror has width d and refractive index n. In the limit $d \to 0$, $n \to \infty$ with $n^2 d = \eta$ fixed, the retarded Green function can be expressed in terms of an integral over products of the scattering states (3.99),

$$\mathcal{G}_{\text{ch}}(k, x, x') = \frac{1}{2\pi} \int_{-\infty}^{\infty} \mathrm{d}k' \frac{\mathrm{e}^{\mathrm{i}k'(x-x')} + S_c(k')\mathrm{e}^{\mathrm{i}k'(x+x')}}{k^2 - k'^2 + \mathrm{i}\epsilon} . \tag{3.E.6}$$

The integral can be done by contour integration. Using the unitarity of $S_c(k)$ and taking into account that $S_c(k)$ is analytic in the upper half of the complex plane, Eq. (3.E.6) reduces to

$$\mathcal{G}_{\text{ch}}(k, x, x') = -\frac{\mathrm{i}}{2k}\left(\mathrm{e}^{\mathrm{i}k|x-x'|} + S_c(k)\mathrm{e}^{\mathrm{i}k|x+x'|}\right) . \tag{3.E.7}$$

Combination with the definitions (3.93c) and (3.93d) yields

$$L_{\mathcal{QP}}\mathcal{G}_{\text{ch}}(k)L_{\mathcal{PQ}}\mu(x) = -\frac{\delta'(x - 0_-)}{k(\mathrm{i} + \eta k)} \frac{\mathrm{d}}{\mathrm{d}x'}\mu(x')\bigg|_{x'=0_-} . \tag{3.E.8}$$

Equations (3.93a), (3.E.8) along with Eq. (3.42) yield Eq. (3.103).

Angular Momentum Channels

The retarded Green function for the two–dimensional Helmholtz equation with Neumann boundary conditions along a disk of radius R, has the form

$$\begin{aligned}&\mathcal{G}_{\text{ch}}(k, r', \phi', r, \phi) = \\ &\quad -\frac{\mathrm{i}}{2\pi}\sum_{-\infty}^{+\infty} \mathrm{e}^{im(\phi-\phi')} \frac{H_m^{(1)}(kr_>)}{H_m'^{(1)}(kR)} \left(H_m^{(2)}(kr_<)H_m'^{(1)}(kR) - H_m'^{(2)}(kR)H_m^{(1)}(kr_<)\right),\end{aligned} \tag{3.E.9}$$

where $r_<$ ($r_>$) stands for the smaller (larger) of r and r'. Substitution of the definitions (3.111c) and (3.111d) yields

$$\begin{aligned}L_{\mathcal{QP}}\mathcal{G}_{\text{ch}}(k)L_{\mathcal{PQ}}\mu(r, \phi) = &-\frac{R}{2n^2\pi}\frac{\partial}{\partial r}\left(\frac{1}{r}\delta(r - R_-)\right) \\ &\times \sum_{m=-\infty}^{+\infty} \int_0^{2\pi} \mathrm{d}\phi' \, \mathrm{e}^{\mathrm{i}m(\phi-\phi')} \frac{H_m^{(1)}(kR)}{kH_m'^{(1)}(kR)} \frac{\partial}{\partial r''}\mu(r'', \phi')\bigg|_{r''=R_-} .\end{aligned} \tag{3.E.10}$$

Combination with equations (3.42) and (3.111a) shows that $L_{\text{eff}}(k)$ acts on an arbitrary resonator state $\mu(r, \phi)$ like

$$\begin{aligned}L_{\text{eff}}(k)\mu(r, \phi) = &-\frac{1}{n^2}\nabla^2\mu(r, \phi) + \frac{R}{n^2}\frac{\partial}{\partial r}\left(\frac{1}{r}\delta(r - R_-)\right)\Bigg[\mu(R_-, \phi) \\ &-\frac{1}{2\pi}\sum_{m=-\infty}^{+\infty} \int_0^{2\pi} d\phi' \, \mathrm{e}^{\mathrm{i}m(\phi-\phi')} \frac{H_m^{(1)}(kR)}{kH_m'^{(1)}(kR)} \frac{\partial}{\partial r''}\mu(r'', \phi')\bigg|_{r''=R_-}\Bigg] .\end{aligned} \tag{3.E.11}$$

Conservation of angular momentum and the requirement that the singular terms must vanishes for the right eigenstates $\xi_{mj}(k,r,\phi)$ yield the boundary condition

$$\xi_{mj}(k,R_-,\phi) = \frac{H_m^{(1)}(kR)}{kH_m'^{(1)}(kR)}\frac{\partial}{\partial r''}\xi_{mj}(k,r'',\phi)\bigg|_{r''=R_-}. \tag{3.E.12}$$

There is a discrete set of solutions

$$\xi_{mj}(k,r,\phi) = A_{mj}(k)\mathrm{e}^{\mathrm{i}m\phi}J_m(n\sigma_{mj}(k)r), \tag{3.E.13}$$

with normalization constants $A_{mj}(k)$. Substitution into Eq. (3.E.12) yields the equation for the eigenvalues

$$kJ_m(n\sigma_{mj}(k)R)H_m'^{(1)}(kR) - n\sigma_{mj}(k)J_m'(n\sigma_{mj}(k)R)H_m^{(1)}(kR) = 0. \tag{3.E.14}$$

Combination with the fixed point equation $k = \sigma_{mj}(k)$ finally gives the resonance condition (3.118).

3.F Local Density of States Inside a Dielectric Disk

Here we determine the density of states inside a dielectric disk with radius R and refractive index n. We start from equation (3.C.6). Using the coefficients (3.117), we obtain

$$\int\limits_{\text{disk}} \mathrm{d}\boldsymbol{r}\rho(k,\boldsymbol{r}) = \sum_{m=-\infty}^{+\infty}\frac{k|I_{mk}|^2}{2n^2}J_m^2(nkR)\sum_{\lambda=1}^{\infty}\frac{k_{m\lambda}^2}{(k^2-k_{m\lambda}^2)^2}. \tag{3.F.1}$$

We concentrate on the evaluation of the last sum on the right hand side. It can be written as a derivative

$$\sum_{\lambda=1}^{\infty}\frac{k_{m\lambda}^2}{(k^2-k_{m\lambda}^2)^2} = -\frac{1}{2}\frac{\partial}{\partial\alpha}\sum_{\lambda=1}^{\infty}\frac{1}{(k^2-\alpha^2k_{m\lambda}^2)}\bigg|_{\alpha=1}. \tag{3.F.2}$$

The right hand side can be simplified by noticing that $nRk_{m\lambda} = x_{m\lambda}$ is the λ-th zero of the Bessel function $J_m(x)$. Thus the sum can be identify as the trace of the Green function for the radial part of the Helmholtz equation in a dielectric disk with Dirichlet conditions on the disk perimeter. Eq. (3.F.2) becomes

$$\sum_{\lambda=1}^{\infty}\frac{k_{m\lambda}^2}{(k^2-k_{m\lambda}^2)^2} = -\frac{1}{2}\frac{\partial}{\partial\alpha}\int\limits_0^R \mathrm{d}r\, r\mathcal{G}_{\text{disk}}(k/\alpha,r,r)\bigg|_{\alpha=1}. \tag{3.F.3}$$

The disk Green function can be found by standard methods [100] and is given by

$$\begin{aligned}\mathcal{G}_{\text{disk}}(k/\alpha,r',r) = {}& \frac{\mathrm{i}\pi}{4J_m(nkR/\alpha)}J_m(nkr_</\alpha)\\ &\times\left(J_m(nkR/\alpha)Y_m(nkr_>/\alpha) - Y_m(nkR/\alpha)J_m(nkr_>/\alpha)\right),\end{aligned} \tag{3.F.4}$$

where Y_m is a Bessel function of the second kind and $r_<$ ($r_>$) the smaller (larger) of r and r'. The problem then reduces to the evaluation of the integral in Eq. (3.F.3). Using the relations

$$\int_0^R \mathrm{d}r\, r J_m^2(kr) = \frac{R^2}{2}\left(J_m^2(kR) - J_{m+1}(kR)J_{m-1}(kR)\right), \tag{3.F.5}$$

$$\begin{aligned}\int_0^R \mathrm{d}r\, r J_m(kr)Y_m(kr) = \frac{R^2}{2}\Big(&J_m(kR)Y_m(kR) \\ &- \frac{1}{2}J_{m+1}(kR)Y_{m-1}(kR) - \frac{1}{2}J_{m-1}(kR)Y_{m+1}(kR)\Big),\end{aligned} \tag{3.F.6}$$

we find after some straightforward manipulations the result

$$\int_0^R \mathrm{d}r\, r\mathcal{G}_{\mathrm{disk}}(k/\alpha, r, r) = \frac{\alpha R J_m'(kR/\alpha)}{2kJ_m(kR/\alpha)}. \tag{3.F.7}$$

Substitution into Eq. (3.F.3) yields

$$\sum_{\lambda=1}^{\infty} \frac{k_{m\lambda}^2}{(k^2 - k_{m\lambda}^2)^2} = \frac{R^2}{4J_m^2(nkR)}\left(J_m^2(nkR) - J_{m+1}(nkR)J_{m-1}(nkR)\right). \tag{3.F.8}$$

After replacement into Eq. (3.F.1), one arrives at the integrated density of states (3.119).

Chapter 4

Multi-Mode Field Dynamics in Optical Resonators

Perhaps the most studied model of damping in quantum mechanics is that of a single harmonic oscillator linearly coupled to a continuum of harmonic oscillators [10, 77, 39]. This exactly solvable model describes the damping and noise for a *single-mode* field inside an open optical resonator due to the interaction with the external field. In the textbooks the dynamics of the single-mode field is usually regarded only in the weak coupling limit [10, 77, 39], yet the quantum properties of this field for arbitrary damping strength and arbitrary heat-bath temperature are known [110, 111, 112]. Less understood are the damping and noise properties of *multi-mode* fields in optical resonators. Until quite recently investigations on this subject were hampered by the lack of a quantization method that could properly described the field leakage in cavities with overlapping resonances. In the preceding chapter such a field quantization method was implemented and an exact quantum representation of the electromagnetic fields and the Hamiltonian systems was obtained. Based on these results, we consider in this chapter the dynamics of multi-mode fields in optical cavities.

Our starting point is the system-and-bath Hamiltonian (3.59), which corresponds to a discrete set of harmonic oscillators linearly coupled to the same single continuum (or even several continua distinguished by the "channel" index). The Hamiltonian (3.59) is then a straight forward generalization of the single-mode model; however the dynamics that it generates is of a very different nature. Due to the coupling to one and the same bath, the cavity modes does not evolve independently in time but become coupled through both damping and noise; the emerging correlations among the resonator modes are thus seen to be responsible for the excess noise characteristic of multi-mode fields. Still the equations of motion for the field operators are linear (since the Hamiltonian is a bilinear form of the field operators) and can be integrated exactly (up to a frequency integral that depends on the density of states of the system at hand). Explicit expressions for the cavity and channel field operators are given in Appendix 4.A; they are the generalization of the single-mode solution in [110, 111, 112] to multi-mode fields coupled to a continuum.

Measurements on optical resonators are typically done with detectors located in the external region outside the cavity. The detector therefore measures the external field, and an input–output theory is required to relate the time evolution of the external field to the dynamics of the system of interest. In this chapter we implement the input–output formalism of Gardiner and Collet [88, 39, 77] for multi-mode fields in resonators with overlapping resonances. We establish the input–output relation using the exact field equations of motion; thus the results apply even in the case of field overdamping. We then use the input–output relation to derive the system S matrix. In particular, we will address the case of chaotic scattering, i.e., the case when the propagation of light in the cavity becomes chaotic due to random fluctuations of the refractive index or due to scattering at irregular shaped mirrors. As an application of our input–output theory we consider a linear amplifier and show that our theory reduces to the scattering theory of Beenakker and coworkers [68, 69, 70] for light propagation in random media. Additionally, the input–output relation sets the ground for the introduction of Langevin equations to describe the cavity field dynamics.

The main result of this chapter is the derivation of stochastic equations for the field dynamics in resonators with overlapping resonances. Restricting our analysis to optical fields, we can employ the rotating wave approximation and a Markov approximation for the system memory. Equations of motion for the cavity field are then obtained both within the Heisenberg picture (in terms of quantum Langevin equations) and within the Schrödinger picture (employing a master equation for the reduced density operator of the cavity modes) which include explicit expressions for all damping and noise forces. We show that the resulting stochastic equations correctly describe isolated as well as spectrally overlapping resonances. Corrections would only be important if the resonance widths were to become comparable to the resonance frequencies themselves, a regime not encountered in optical resonators. Our derivation clarifies the status of previously proposed stochastic equations [61, 113, 114, 115, 116, 62, 34] which were not derived from a rigorously quantized electromagnetic field.

In the last section of the chapter we address a representation of the cavity electromagnetic field in terms of nonorthogonal modes. Such modes correspond to the "true" resonances of the open cavity, and arise naturally in our derivation of the stochastic equations. It is shown that the deterministic part of the time evolution of the field is generated by a non-Hermitian operator $\mathcal{H}$ whose complex eigenvalues are the cavity resonances and whose eigenvectors represent the cavity resonance modes. The field dynamics in this representation takes a simpler form than within the orthogonal mode representation, however one has to pay the price that the operators related to the nonorthogonal modes are no longer standard creation and annihilation operators.

In Sec. 4.1 we consider the exact field dynamics in open resonators and derive the system S matrix. We then introduce the rotating wave approximation and the Markov approximation in Sec. 4.2 to derive the Langevin equations of motion. The results are applied to linear amplifiers. The master equation is derived in Sec. 4.3 and the equivalent Fokker–Plank equation in Sec. 4.4. The equivalence between the Langevin and master equation is demonstrated. We conclude with Sec. 4.5 were the field dynamics is represented in terms of nonorthogonal modes.

Some of the results in this chapter have been reported in Refs. [97, 117].

4.1 Exact Dynamics

In this section we present an exact input–output relation for multi-mode fields in open cavities. The relation is for arbitrary values of the outcoupling amplitudes and holds independently of the nature of the cavity field dynamics (whether linear or nonlinear). When the dynamics is linear, the input–output relation is employed to derive the S matrix of the system.

4.1.1 Equations of Motion

To start with, we concentrate on the intracavity field dynamics. The equations of motion for the cavity operators are obtained by first formally integrating the equations of motion for the channel operators and then substituting the solution into the equations for the resonator operators; the time evolution of the intracavity field is thus seen to depend on the channel field only through its initial state. Using Hamiltonian (3.59), the Heisenberg equations of motion for the internal and external annihilation operators a_λ and $b_m(\omega)$, respectively, are

$$\dot{a}_\lambda(t) = -\mathrm{i}\omega_\lambda a_\lambda(t) - \mathrm{i}\sum_m \int_{\omega_m}^{\infty} \mathrm{d}\omega \, \left[\mathcal{W}_{\lambda m}(\omega) b_m(\omega,t) + \mathcal{V}^*_{\lambda m}(\omega) b^\dagger_m(\omega,t)\right], \tag{4.1}$$

$$\dot{b}_m(\omega,t) = -\mathrm{i}\omega b_m(\omega) - \mathrm{i}\sum_\lambda \left[\mathcal{W}^*_{\lambda m}(\omega) a_\lambda(t) + \mathcal{V}^*_{\lambda m}(\omega) a^\dagger_\lambda(t)\right]. \tag{4.2}$$

Due to the presence of the antiresonant terms in the system Hamiltonian the equations of motion for the creation and annihilation operators are coupled. For an initial time $t_0 < t$, formal integration of the equations of motion for the channel operators yields

$$b_m(\omega,t) = \mathrm{e}^{-\mathrm{i}\omega(t-t_0)} b_m(\omega,t_0) - \mathrm{i}\sum_\lambda \int_{t_0}^{t} \mathrm{d}t' \, \mathrm{e}^{-\mathrm{i}\omega(t-t')} \left[\mathcal{W}^*_{\lambda m}(\omega) a_\lambda(t') + \mathcal{V}^*_{\lambda m}(\omega) a^\dagger_\lambda(t')\right], \tag{4.3}$$

where $b_m(\omega,t_0)$ denotes the operator $b_m(\omega)$ at time t_0. In an analogous fashion, one can express $b_m(\omega,t)$ in terms of the operators at the final time $t_1 > t$,

$$b_m(\omega,t) = \mathrm{e}^{-\mathrm{i}\omega(t-t_1)} b_m(\omega,t_1) + \mathrm{i}\sum_\lambda \int_{t}^{t_1} \mathrm{d}t' \, \mathrm{e}^{-\mathrm{i}\omega(t-t')} \left[\mathcal{W}^*_{\lambda m}(\omega) a_\lambda(t') + \mathcal{V}^*_{\lambda m}(\omega) a^\dagger_\lambda(t')\right]. \tag{4.4}$$

Although in this section we are only interested in the time evolution of the cavity field for times $t > t_0$, Eq. (4.4) is necessary to establish the input–output relation for the system below. Substituting Eq. (4.3) into Eq. (4.1), and after some straightforward manipulations for which the identities

$$\mathcal{V}^*_{\lambda m}(\omega) = \sum_n \int_{\omega_n}^{\infty} \mathrm{d}\omega' \mathcal{N}^\dagger_{mn}(\omega,\omega') \mathcal{W}_{\lambda n}(\omega') = \sum_{\lambda'} \mathcal{N}^\dagger_{\lambda\lambda'} \mathcal{W}^*_{\lambda' m}(\omega) \tag{4.5}$$

are required, the equations of motion for the cavity annihilation operators can be written as

$$\dot{a}_\lambda(t) = -\mathrm{i}\omega_\lambda a_\lambda(t) - \sum_{\lambda''} \int_{t_0}^{t} \mathrm{d}t' \tilde{C}_{\lambda\lambda'}(t-t') \Big[a_{\lambda'}(t') + \sum_{\lambda'} \mathcal{N}^\dagger_{\lambda'\lambda''} a^\dagger_{\lambda''}(t') \Big] + \tilde{F}_\lambda(t). \quad (4.6)$$

where the effects of the channel field on the dynamics of the cavity operators are encoded in the operators $\tilde{F}(t)$ and the matrix $\tilde{C}(t)$. The operators $\tilde{F}(t)$ are defined by

$$\tilde{F}_\lambda(t) = \\ -\mathrm{i} \sum_m \int_{\omega_m}^{\infty} \mathrm{d}\omega\, \mathcal{W}_{\lambda m}(\omega) \Big[\mathrm{e}^{-\mathrm{i}\omega(t-t_0)} b_m(\omega, t_0) + \mathrm{e}^{\mathrm{i}\omega(t-t_0)} \sum_n \int_{\omega_n}^{\infty} \mathrm{d}\omega' \mathcal{N}^\dagger_{mn}(\omega, \omega') b^\dagger_n(\omega', t_0) \Big], \quad (4.7)$$

and we notice that the channel operators enter only through their values at the initial time t_0. For appropriated states of the external system, $\tilde{F}(t)$ may be interpreted as noise forces. The matrix elements

$$\tilde{C}_{\lambda\lambda'}(t) = -2\mathrm{i} \sum_m \int_{\omega_m}^{\infty} \mathrm{d}\omega\, \mathcal{W}_{\lambda m}(\omega) \mathcal{W}^*_{\lambda' m}(\omega) \sin(\omega t), \quad (4.8)$$

on the other hand, are the channel response functions [112] $\tilde{C}_{\lambda\lambda'}(t) = \big\langle [\tilde{F}_\lambda(t), \tilde{F}^\dagger_{\lambda'}(0)] \big\rangle$, where $\langle \ldots \rangle$ denotes the quantum average over the initial channel state. The matrix $\tilde{C}$ introduces the response time of the channel field as a relevant time scale in the dynamics of the cavity field. In order to treat the channel field as a bath this time scale must be smaller than the damping time for the cavity operators; this condition is always accomplished provided the coupling is weak enough [39].

The equations of motion (4.6) hold for an arbitrary strength of the coupling between the resonator and the channel field and are suitable to describe even the case of overdamped resonator dynamics, but they are far from being simple. Due to the time integral on the right hand side the dynamics is not Markovian; the state of the cavity field at one instant does not suffice to determine the future state of the field. Simplifications may occur in the optical domain, which is the most relevant regime for this thesis. There the oscillation frequencies are typically much larger than the field damping rates, and Eq. (4.6) can be simplified by means of the *rotating wave approximation*, which amounts to neglecting the fast oscillating counter-rotating terms. This approximation provides a description of the field in a narrow bandwidth (small compared to the frequencies themselves) around a central frequency of interest (see Sec. 4.2).

4.1.2 Input–Output Relation

The time evolution of the external field is related to the dynamics of the internal field by the input–output relation [39, 88, 77]. The starting point of the input–output theory are the equations of motion (4.1) and (4.2) for the intracavity and channel field modes. Formal integration of the equations for the channel operators, both for an initial and a final condition, yields Eqs. (4.3) and (4.4). Subtracting the former from the latter and integrating the result over frequency we arrive at the input–output relation in the time domain

$$b_m^{\text{out}}(t) - b_m^{\text{in}}(t) = -\frac{\mathrm{i}}{2\pi}\sum_\lambda \int_{\omega_m}^{\infty} \mathrm{d}\omega \int_{t_0}^{t_1} \mathrm{d}t'\, \mathrm{e}^{-\mathrm{i}\omega(t-t')}\big[\mathcal{W}_{\lambda m}^*(\omega) a_\lambda(t') + \mathcal{V}_{\lambda m}^*(\omega) a_\lambda^\dagger(t')\big]. \quad (4.9)$$

Equation (4.9) relates the cavity operators in the time interval $t_0 < t < t_1$ to the external input and output field operators

$$b_m^{\text{in}}(t) \equiv \frac{1}{2\pi}\int_{\omega_m}^{\infty} \mathrm{d}\omega\, \mathrm{e}^{-\mathrm{i}\omega(t-t_0)} b_m(\omega, t_0), \quad (4.10\text{a})$$

$$b_m^{\text{out}}(t) \equiv \frac{1}{2\pi}\int_{\omega_m}^{\infty} \mathrm{d}\omega\, \mathrm{e}^{-\mathrm{i}\omega(t-t_1)} b_m(\omega, t_1). \quad (4.10\text{b})$$

In analogy with the scattering formalism, we are eventually interested in the limits $t_0 \to -\infty$ and $t_1 \to \infty$. Using the identity (4.5) the input–output relation can be written as

$$b_m^{\text{out}}(t) - b_m^{\text{in}}(t) = -\frac{\mathrm{i}}{2\pi}\sum_\lambda \int_{\omega_m}^{\infty} \mathrm{d}\omega \int_{t_0}^{t_1} \mathrm{d}t'\, \mathrm{e}^{-\mathrm{i}\omega(t-t')}\mathcal{W}_{\lambda m}^*(\omega)\Big[a_\lambda(t') + \sum_{\lambda'} \mathcal{N}_{\lambda\lambda'}^\dagger a_{\lambda'}^\dagger(t')\Big], \quad (4.11\text{a})$$

$$= -\frac{\mathrm{i}}{2\pi}\sum_\lambda \int_{\omega_m}^{\infty} \mathrm{d}\omega \int_{t_0}^{t_1} \mathrm{d}t'\, \mathrm{e}^{-\mathrm{i}\omega(t-t')}\frac{1}{\sqrt{2\hbar\omega}} W_{\lambda m}^*(\omega) Q_\lambda(t'), \quad (4.11\text{b})$$

where we used definition (3.57a) to obtain the last line. That input and output annihilation operators in Eq. (4.11a) are related through a linear combination of cavity creation and annihilation operators is consequence of the exact field dynamics which mixes creation and annihilation operators. More precisely, Eq. (4.11b) shows that the resonator field dynamics couples the exterior bath to the position operators Q_λ defined in Eq. (3.55). Fourier transformation of Eq. (4.11b) yields the input–output relation in the frequency domain. In the asymptotic limit $t_0 \to -\infty$ and $t_1 \to \infty$ the result takes the form

$$b^{\text{out}}(\omega) - b^{\text{in}}(\omega) = -\frac{\mathrm{i}}{\sqrt{2\hbar\omega}} W^\dagger(\omega) Q_{\text{cav}}(\omega), \quad (4.12)$$

where we combined the input and output operators at frequency ω to M–component vectors. The coupling amplitudes $W_{\lambda m}$ form an $N \times M$ coupling matrix W, and the cavity position operators an N–component vector. The finite number N of cavity modes is artificial, and will eventually be taken to infinity. We note that the input and output operators are simply related to the channel mode operators at time t_0 and t_1, respectively, $b^{\mathrm{in}}(\omega) = \mathrm{e}^{i\omega t_0} b(\omega, t_0)$ and $b^{\mathrm{out}}(\omega) = \mathrm{e}^{i\omega t_1} b(\omega, t_1)$.

It is a remarkable feature of the input–output relations (4.9) and (4.12) that no assumption whatsoever was made concerning the nature of the dynamics of the intracavity field. The relations hold, not only for empty cavities but also in the case when the internal field is coupled to other systems, e.g., an ensemble of intracavity atoms, leading to a nonlinear dynamics. However, in the simple case of a linear cavity dynamics simplifications occur that will be addressed in the following section.

4.1.3 S Matrix

For linear systems one can eliminate the cavity modes from the equations of motion to derive a linear relation between the input and output field. Here we consider the empty cavity described by Hamiltonian (3.59). Fourier transformation of the exact result for the cavity position operator (4.A.2) yields $Q_\lambda(\omega)$. Since the initial state has been specified in the remote past $t_0 \to -\infty$, only the oscillatory terms are kept. The result is

$$Q_{\mathrm{cav}}(\omega) = \frac{\pi}{c^2} \sqrt{\frac{2\hbar}{\omega}} \mathcal{G}_{QQ}(\omega) W(\omega) b^{\mathrm{in}}(\omega). \tag{4.13}$$

Here $\mathcal{G}_{QQ}(\omega)$ is the $N \times N$ matrix representation of the projected resolvent (3.43), the matrix elements of its inverse (cf. Eq. (3.43)) are

$$\mathcal{G}^{-1}_{QQ}(\omega)_{\lambda\lambda'} = \frac{1}{c^2} \left[\left(\omega^2 - \omega_\lambda^2\right)\delta_{\lambda\lambda'} + \mathcal{P} \int\limits_{\omega_m}^{\infty} d\omega' \frac{\left[W(\omega')W^\dagger(\omega')\right]_{\lambda\lambda'}}{\omega'^2 - \omega^2} + \frac{i\pi}{2\omega} \left[W(\omega)W^\dagger(\omega)\right]_{\lambda\lambda'} \right]. \tag{4.14}$$

Combining Eqs. (4.12) and (4.13) one can eliminate the cavity operators from the input–output relation. This yields a linear relation between the incoming and outgoing field,

$$b^{\mathrm{out}}(\omega) = S(\omega) b^{\mathrm{in}}(\omega) \tag{4.15}$$

where $S(\omega)$ is the $M \times M$ scattering matrix,

$$S(\omega) = \mathbb{1} - \frac{\mathrm{i}\pi}{\omega c^2} W^\dagger(\omega) \mathcal{G}_{QQ}(\omega) W(\omega). \tag{4.16}$$

This representation of the S-matrix for optical systems can be shown to be equivalent to the representation used in nuclear and condense matter physics [118, 119, 102] where the S matrix is parameterized by the energy. The later is recovered from Eq. (4.16) by replacing $(\omega/c)^2 \to E$. Equation (4.16) is a generalization of the usual Breit–Wigner result for a single resonance to the scattering in the presence of N resonances. Using the commutation relations $[b_n(\omega), b_m^\dagger(\omega')] = \delta_{nm}\, \delta(\omega - \omega')$ for both $b = b^{\mathrm{in}}$ and $b = b^{\mathrm{out}}$, one can easily show that S is unitary, $SS^\dagger = S^\dagger S = \mathbb{1}$. The S matrix describes scattering both in the limit of isolated resonances and in the regime of overlapping resonances. In the context of quantum optics, the regime of isolated resonances corresponds to the weak-damping or almost closed cavity regime, where all matrix elements of $WW^\dagger/\omega^2$ are much smaller than the mean frequency separation of the resonator modes. The opposite regime of overlapping resonances is realized when the damping rates exceed the mean frequency spacing.

According to Eqs. (4.15) and (4.16) the field dynamics is governed by the *resonances* of the open cavity. The resonances are the complex poles of the S matrix which coincide with the poles of $\mathcal{G}_{QQ}(\omega)$. They are the solutions of the equation $\det\left[\omega^2 - c^2 L_{\mathrm{eff}}(\omega)\right] = 0$; from Eq. (4.14) one can see that they represent the complex eigenvalues of the internal field dynamics in the presence of damping inflicted by the coupling to the external radiation field. We note that the resonances determine the field dynamics even though the underlying field quantization is formulated in terms of closed–cavity eigenmodes (with boundary conditions as discussed in Sec. 3.2.2).

Equation (4.16) has found widespread application in the random matrix theory of scattering [119, 102]. It is the starting point for the so-called Hamiltonian approach to chaotic scattering. This approach assumes that the Hamiltonian of a closed chaotic resonator can be represented by a random matrix drawn from a Gaussian ensemble of random matrix theory. The eigenvalues of the internal Hamiltonian show level repulsion and universal statistical properties. The statistics of the scattering matrix is derived from the distribution of the internal Hamiltonian using Eq. (4.16). An alternative approach to chaotic scattering is the random S matrix approach in which one directly models the statistical properties of S without introduction of a Hamiltonian. Based on the latter approach, Beenakker and coworkers [68, 69, 120, 121, 71] recently computed the noise properties of disordered and chaotic optical resonators. The Hamiltonian and the S matrix approach to chaotic scattering are known to be equivalent. However, the Hamiltonian approach has the advantage that one can include the interaction with an atomic medium on a microscopic level. An example is given in Sec.5.2 where we study the spontaneous emission of an atom inside an open resonator.

4.2 Langevin Equations in the Optical Domain

We now turn to a description of the field dynamics in the optical regime. The equations of motion for the cavity mode operators simplify considerable under two, not completely independent, approximations often valid in this regime: the *rotating wave approximation* and *the Markov approximation*. The rotating wave approximation describes the system dynamics in a spectral bandwidth which is small compared with the typical oscillation frequencies but that still contains a large number of cavity resonances. In this spectral band one then assumes the cavity field damping rates Γ to be smaller than the field oscillation frequencies. The rotating wave approximation amounts to neglecting the fast oscillating terms on the scale of $1/\Gamma$ in the field equations of motion. Our implementation of the rotating wave approximation covers the case of spectrally-overlapping cavity modes, generalizing the standard approach for a single resonator mode [39, 77] with weak outcoupling. In a resonator with overlapping resonances the mode spectral broadening is comparable to the mean frequency spacing $\Delta\omega$ of the internal cavity resonances. Therefore oscillatory terms with frequencies of the order of $\Delta\omega$ must be kept in the equations of motion leading to an effective coupling among the modes through the damping. In the rotating wave approximation the system-and-bath Hamiltonian takes the form

$$H_{\mathrm{SB}} = \sum_{\lambda} \hbar\omega_{\lambda}\, a_{\lambda}^{\dagger} a_{\lambda} + \sum_{m} \int \mathrm{d}\omega\, \hbar\omega\, b_{m}^{\dagger}(\omega) b_{m}(\omega) + \hbar \sum_{\lambda}\sum_{m} \int \mathrm{d}\omega \left[\mathcal{W}_{\lambda m}(\omega)\, a_{\lambda}^{\dagger} b_{m}(\omega) + \mathrm{H.c.} \right], \quad (4.17)$$

which is obtained from the Hamiltonian (3.59) by neglecting the fast oscillating antiresonant terms $\mathcal{V}_{\lambda m}(\omega) a_{\lambda} b_{m}(\omega) + \mathcal{V}_{\lambda m}^{*}(\omega) a_{\lambda}^{\dagger} b_{m}^{\dagger}(\omega)$ and extending the range of the frequency integrals from $-\infty$ to $+\infty$. This extension is consistent with the rotating wave approximation and necessary for the Markov approximation [39]. Keeping the fast oscillating terms introduces corrections to the dynamics of the order $\Gamma/\bar{\omega}$ and $\Delta/\bar{\omega}$, where $\bar{\omega}$ is a typical frequency in the bandwidth we are interested (see Appendix 4.B). The Markov approximation assumes a separation of time scales between the typical life times of the cavity modes and the "bath correlations times" (like the thermal time $\tau_{\mathrm{bath}}^{\mathrm{th}} = \hbar/k_B T$) such that the former are much in excess of the later, $1/\Gamma \gg \tau_{\mathrm{bath}}$. This approximation simplifies the equations of motion in a twofold way: First, the coupling amplitudes $\mathcal{W}_{\lambda m}$ can be taken to be frequency independent over the spectral bandwidth[1]. Second, on the same spectral range, the number of photons in the bath may be assumed independent of the frequency. Together, both approximations lead to a set of Langevin equations with white noise that describe the resonator field dynamics for times $t > \tau_{\mathrm{bath}}$.

4.2.1 Derivation of the Langevin Equations

The Heisenberg equations of motion in the rotating wave approximation are obtained using the Hamiltonian (4.17) [2],

$$\dot{a}_{\lambda} = -\mathrm{i}\omega_{\lambda} a_{\lambda} - \mathrm{i} \sum_{m} \int \mathrm{d}\omega\, \mathcal{W}_{\lambda m}(\omega) b_{m}(\omega), \quad (4.18a)$$

$$\dot{b}_{m}(\omega) = -\mathrm{i}\omega b_{m}(\omega) - \mathrm{i} \sum_{\lambda} \mathcal{W}_{\lambda m}^{*}(\omega) a_{\lambda}. \quad (4.18b)$$

They coincide with Eqs. (4.1) and (4.2) if the counter rotating terms are set equal to zero, $\mathcal{V}_{\lambda m}(\omega) = 0$. By following the same reasoning than in Sec. 4.1.1 one arrives at the equations of motion for the cavity annihilation operators

$$\dot{a}_{\lambda}(t) = -\mathrm{i}\omega_{\lambda} a_{\lambda}(t) - \sum_{\lambda'} \int_{t_0}^{t} \mathrm{d}t' C_{\lambda\lambda'}(t-t') a_{\lambda'}(t') + F_{\lambda}(t). \quad (4.19)$$

[1] This assumption implies that the frequencies in the spectral range considered are far from the threshold frequencies for the opening of further channels, see, e.g., Ref. [122]

[2] The Heisenberg equations of motions are linear in the cavity and channel operators and can therefore be solved exactly. The results are given in the Appendix 4.A. We notice that the Langevin equations obtained in this section could also be obtained by starting from the exact solution (4.A.6) of the equations of motion and then implementing the necessary approximations at that level, as done in [110] for the single-mode coupled to a continuum model. For multi-mode fields however such a path turns out to be much more involved than directly dealing with the equations of motion.

The noise force operators $F(t)$ and the bath response matrix $C(t)$ are defined, respectively, by

$$F_\lambda(t) = -\mathrm{i}\sum_m \int \mathrm{d}\omega\, \mathcal{W}_{\lambda m}(\omega) \mathrm{e}^{-\mathrm{i}\omega(t-t_0)} b_m(\omega, t_0), \tag{4.20}$$

$$C_{\lambda\lambda'}(t) = \frac{1}{\pi}\int \mathrm{d}\omega\, \Gamma_{\lambda\lambda'}(\omega)\mathrm{e}^{-\mathrm{i}\omega t}, \tag{4.21}$$

and the damping matrix $\Gamma_{\lambda\lambda'}(\omega)$ is given by

$$\Gamma_{\lambda\lambda'}(\omega) = \pi\big[\mathcal{W}(\omega)\mathcal{W}^\dagger(\omega)\big]_{\lambda\lambda'}. \tag{4.22}$$

We now introduce a set of slowly changing variables by the transformation

$$a_\lambda(t) = \mathrm{e}^{-\mathrm{i}\omega_\lambda t}\bar{a}_\lambda(t). \tag{4.23}$$

Since it has been assumed that the mode oscillation frequencies are much larger than the mode damping rates the dominant term in (4.19) is $-\mathrm{i}\omega_\lambda a_\lambda(t)$; therefore $\bar{a}_\lambda(t)$ must change slowly with time. In particular $\bar{a}_\lambda(t)$ does not vary much on the time scale of τ_{bath} in which the bath response matrix $C(t)$ decays to zero. The equations of motion for the slowly varying variables are obtained substituting Eq. (4.23) in Eq. (4.19) and replacing $\bar{a}_\lambda(t')$ with $\bar{a}_\lambda(t)$,

$$\dot{\bar{a}}_\lambda(t) = -\sum_{\lambda'} C_{\lambda\lambda'}(\omega_{\lambda'})\mathrm{e}^{\mathrm{i}(\omega_\lambda-\omega_{\lambda'})t}\bar{a}_{\lambda'}(t) + \mathrm{e}^{\mathrm{i}\omega_\lambda t}F_\lambda(t). \tag{4.24}$$

Here $C(\omega)$ is given by

$$\begin{aligned} C_{\lambda\lambda'}(\omega_{\lambda'}) &= \int_{-\infty}^{t} \mathrm{d}t' C_{\lambda\lambda'}(t-t')\mathrm{e}^{\mathrm{i}\omega_{\lambda'}(t-t')} \\ &= -\frac{\mathrm{i}}{\pi}\mathcal{P}\int d\omega \frac{\Gamma_{\lambda\lambda'}(\omega)}{\omega-\omega_{\lambda'}} + \Gamma_{\lambda\lambda'}(\omega_{\lambda'}), \end{aligned} \tag{4.25}$$

and we set $t_0 \to -\infty$ because $C(t)$ is assumed to decay on the time scale of the order of τ_{bath} while we are interested in times $t - t_0 > \tau_{\mathrm{bath}}$. After moving back to the original variables, the equations of motion in the rotating wave approximation become

$$\dot{a}_\lambda(t) = -\mathrm{i}\omega_\lambda a_\lambda(t) - \sum_{\lambda'} C_{\lambda\lambda'}(\omega_{\lambda'})a_{\lambda'}(t) + F_\lambda(t). \tag{4.26}$$

Equations (4.26) generalize the Langevin equations for spectrally isolated modes [39, 77] to the case of overlapping modes. We note that the resulting equations differ from the independent oscillator equations of standard laser theory [11] in two respects: First, the mode operators a_λ are coupled due to the damping by the matrix $C(\omega)$. Second, generically the noise force operators F_λ are correlated, $\langle F_\lambda(t), F^\dagger_{\lambda'}(t')\rangle \neq \delta_{\lambda\lambda'}$, as different modes coupled to the same external channels ($\langle \ldots \rangle$ denotes the quantum average over the channel field at t_0). The mode coupling by both damping and noise can be understood as a consequence of the fluctuation–dissipation theorem.

The deviations from the independent oscillator dynamics may be understood in the limiting case of weak damping. This is the regime where all matrix elements of Γ are much smaller than the resonator mode spacing $\Delta\omega$. This regime is realized, e.g., in dielectrics that strongly confine light due to a large mismatch in the refractive index. To leading order in $\Gamma/\Delta\omega$ only diagonal elements contribute to the damping matrix, and Eq. (4.26) reduces to the standard equation of motion for independent oscillators. This shows that the independent–oscillator dynamics is a limiting case of the true mode dynamics in the regime of weak damping.

In obtaining the Langevin equation (4.26) no reference was made to the statistic of the noise force $F(t)$. For arbitrary baths Eq. (4.26) may lead to non-Markovian dynamics for averaged system observables. The dynamics simplifies if the Markov approximation is employed. In that limit the frequency dependence of the coupling amplitudes $\mathcal{W}$ can be dropped over the spectral range in consideration, and the cavity mode operators a_λ obeys the equation

$$\dot{a}_\lambda(t) = -\mathrm{i}\omega_\lambda a_\lambda(t) - \sum_{\lambda'} \Gamma_{\lambda\lambda'} a_{\lambda'}(t) + F_\lambda(t), \tag{4.27}$$

where the small frequency shift in $C_{\lambda\lambda'}$, which is rarely needed in practice, has been neglected. In the same limit one arrives at white noise with $\langle F_\lambda(t)\rangle = 0$, and the correlation functions

$$\langle F_\lambda^\dagger(t) F_{\lambda'}(t')\rangle = 2\Gamma_{\lambda'\lambda}\, n_{\mathrm{th}}\, \delta(t-t'), \tag{4.28a}$$

$$\langle F_\lambda(t) F_{\lambda'}^\dagger(t')\rangle = 2\Gamma_{\lambda\lambda'}(1+n_{\mathrm{th}})\, \delta(t-t')\,. \tag{4.28b}$$

The second two-time correlation functions follows from the first and the commutation relations for the channel operators b_m. The remaining second moments vanish, $\langle F_\lambda(t) F_{\lambda'}(t')\rangle = 0 = \langle F_\lambda^\dagger(t) F_{\lambda'}^\dagger(t')\rangle$, and higher-order moments follow from the ones of orders 1 and 2 according to Gaussian statistics. The thermal number of photons $n_{\mathrm{th}} = [\exp(\hbar\bar{\omega}/kT)-1]^{-1}$ appearing in the second moments must be taken as frequency independent throughout the spectral range under consideration. Previously, Bardroff and Stenholm [114] proposed a similar set of Langevin equations for the cavity field coupled to a bath of atoms. Their equations are recovered from ours in the limit $kT \ll \hbar\bar{\omega}$.

We note that the deterministic part of the field dynamics in Eq. (4.27) is generated by the *non-Hermitian* matrix

$$\mathcal{H}_{\lambda\lambda'} = \hbar\omega_\lambda \delta_{\lambda\lambda'} - \mathrm{i}\hbar\Gamma_{\lambda\lambda'}\,. \tag{4.29}$$

Its Hermitian part corresponds to the dynamics of the closed system describing the reversible dynamics, while its anti-Hermitian part accounts for the irreversible dynamics due to the openness of the system. For some applications it will prove helpful to rewrite the above Langevin equation in the eigenbasis of the operator $\mathcal{H}$. That basis is formed by the resonant modes of the cavity and their eigenvalues correspond to the cavity resonances. As a "penalty" for that change of representation one has to work with non-standard commutation relations for the operators associated with the eigenvectors of $\mathcal{H}$ (see Sec. 4.5).

At this point a remark concerning the field dynamics inside chaotic optical resonators is at hand. According to the universality hypothesis of chaotic scattering, the internal Hamiltonian of chaotic resonators can be represented by a random matrix from the Gaussian orthogonal ensemble of random-matrix theory [85]. The eigenvalues ω_λ display level repulsion and universal statistical properties. However, from Eqs. (4.27) and (4.29), the mode dynamics of open chaotic resonators is not only determined by the eigenvalues of the internal Hamiltonian but also by the coupling strength to the external radiation field: The spectrum of such resonators is governed by a non–Hermitian random matrix. We thus encounter an interesting connection between the spectral properties of chaotic optical resonators and non–Hermitian random matrices [123, 122, 124].

4.2.2 Inputs and Outputs

Here we address the input–output theory within the rotating wave approximation. Following a similar procedure as the one used in Sec. 4.1.2 one could re-derive the input–output relation from the equations of motion generated by the Hamiltonian (4.17). The result, however, is seen to follow immediately from Eq. (4.11a) upon neglecting the fast oscillating terms proportional to the cavity creation operators $a_\lambda^\dagger$ and extending the frequency integration range from $-\infty$ to $+\infty$. Then, for $t_0 < t < t_1$, the input and output field operators are related to the resonator operators by

$$b_m^{\mathrm{out}}(t) - b_m^{\mathrm{in}}(t) = -\frac{\mathrm{i}}{2\pi}\sum_\lambda \int \mathrm{d}\omega \int_{t_0}^{t_1} \mathrm{d}t' \, \mathrm{e}^{-\mathrm{i}\omega(t-t')} \mathcal{W}_{\lambda m}^*(\omega) a_\lambda(t'). \tag{4.30}$$

We note that the input and output fields do not change in the rotating wave approximation and are still given by Eq. (4.10). In the frequency domain, the input–output relation is obtained by Fourier transformation of Eq. (4.30),

$$b^{\mathrm{out}}(\omega) - b^{\mathrm{in}}(\omega) = -\mathrm{i}\mathcal{W}^\dagger(\omega) a(\omega), \tag{4.31}$$

where the asymptotic limit $t_0 \to -\infty$ and $t_1 \to \infty$ is implied and, as in Eq. (4.12), we used a vector notation for the operators $b^{\mathrm{in/out}}(\omega)$ and $a(\omega)$, and the coupling matrix $\mathcal{W}(\omega)$.

4.2.3 Linear Systems

The S matrix for a linear system simplifies in the rotating wave approximation. Here we derive the S matrix for an empty cavity and then address the more general case of a cavity filled with a linear absorbing and/or amplifying medium.

S Matrix

In Appendix 4.A the equations of motion for the electromagnetic field in the rotating wave approximation are solve exactly. Here we are only interested in the asymptotic limit $t_0 \to -\infty$ and $t_1 \to +\infty$. Therefore, for a_λ in Eq. (4.A.6a), only the oscillatory terms proportional to the input field must be kept. After Fourier transformation one finds the relation between the cavity modes operators and the input operators

$$a(\omega) = 2\pi D^{-1}(\omega)\mathcal{W}(\omega)b^{\text{in}}(\omega), \tag{4.32}$$

where D is the $N \times N$ matrix with matrix elements

$$D_{\lambda\lambda'}(\omega) = (\omega - \omega_\lambda)\delta_{\lambda\lambda'} + \mathcal{P}\int d\omega' \frac{\Gamma_{\lambda\lambda'}(\omega')}{\omega' - \omega} + i\pi\Gamma_{\lambda\lambda'}(\omega). \tag{4.33}$$

We now substitute Eq. (4.32) into Eq. (4.31) and eliminate the resonator operators from the input–output relation. This yields a linear relation between the incoming and outgoing field,

$$b^{\text{out}}(\omega) = S(\omega)b^{\text{in}}(\omega), \tag{4.34}$$

involving the $M \times M$ scattering matrix in the rotating wave approximation,

$$S(\omega) = \mathbb{1} - 2\pi\mathrm{i}\mathcal{W}^\dagger(\omega)D^{-1}(\omega)\mathcal{W}(\omega). \tag{4.35}$$

The operator $D^{-1}(\omega)$ corresponds to the rotating wave approximation of the projected system resolvent (cf. Eq. (4.16)). We notice that if in addition the Markov approximation is performed, and the frequency dependence of the coupling amplitudes is neglected, Eq. (4.33) reduces to

$$D(\omega) = \omega - \mathcal{H}/\hbar \tag{4.36}$$

where $\mathcal{H}$ is the non-Hermitian operator defined in Eq. (4.29). Hence, in this approximation, $D^{-1}(\omega)$ corresponds to the resolvent of a system whose dynamics is described by the effective Hamiltonian $\mathcal{H}$.

As we mentioned before, in open cavities the field dynamics is governed by the complex poles of the S matrix which correspond to the cavity *resonances*. In the rotating wave approximation they coincide with the poles of $D^{-1}(\omega)$ and are obtained by solving the equation $\det[D(\omega)] = 0$. In Sec. 4.1.3 we showed that in the exact dynamics the system resonances coincide with the poles of the projected resolvent $\mathcal{G}_{QQ}(\omega)$. It is then illustrative to write down the relation between $\mathcal{G}_{QQ}(\omega)$ and $D(\omega)$. Considering Eq. (4.14) in the rotating wave approximation one obtains,

$$\mathcal{G}^{-1}_{QQ}(\omega)_{\lambda\lambda'} \simeq \frac{2\omega}{c^2}D(\omega)_{\lambda\lambda'}, \tag{4.37}$$

which shows that in this approximation the zeros of $D(\omega)$ coincide with the poles $\mathcal{G}_{QQ}(\omega)$. Furthermore, the approximated S matrix (4.35) follows from the exact S matrix (4.16) upon replacing $\mathcal{G}_{QQ}$ by $(c^2/2\omega)D^{-1}$. The importance of this result can be underline if we make the Markov approximation. Then, the eigenvalues of the non-Hermitian operator $\mathcal{H}$ correspond to the system resonances, and hence the associated right (left) eigenvectors are the "true" cavity modes, corresponding to solutions of the Maxwell's equations with outgoing (incoming) boundary conditions. Although these modes no longer form an orthogonal basis they can still be used to represent the cavity field. Such expansion is discussed in Sec. 4.5.

Linear Absorbing or Amplifying Medium

The presence of an absorbing or amplifying medium within the cavity leads to additional noise and modifies the input–output relation. Phenomenologically, the interaction with linear media can be modeled [39, 68, 69] by coupling the cavity modes to additional baths. An absorbing medium is described by a thermal bath of harmonic oscillators while an amplifying medium may be represented by a bath of inverted harmonic oscillators at a negative temperature $-T$. The total Hamiltonian is then given by

$$H = H_{\mathrm{SB}} + H_{\mathrm{abs}} + H_{\mathrm{amp}}, \tag{4.38}$$

where H_{SB} is the system–and–bath Hamiltonian (4.17), while H_{abs} and H_{amp} represent the absorbing and amplifying bath,

$$H_{\mathrm{abs}} = \sum_l \int d\omega\, \hbar\omega\, c_l^\dagger(\omega) c_l(\omega) + \hbar \sum_\lambda \sum_l \int d\omega \left[\kappa_{\lambda l}(\omega)\, a_\lambda^\dagger c_l(\omega) + \text{H.c.}\right], \tag{4.39a}$$

$$H_{\mathrm{amp}} = -\sum_k \int d\omega\, \hbar\omega\, d_k^\dagger(\omega) d_k(\omega) + \hbar \sum_\lambda \sum_k \int d\omega \left[\sigma_{\lambda k}(\omega)\, a_\lambda^\dagger d_k(\omega) + \text{ H.c. }\right], \tag{4.39b}$$

with coupling amplitudes $\kappa_{\lambda l}$ and $\sigma_{\lambda k}$. The operators c_l, $c_l^\dagger$ obey the canonical commutation relations

$$[c_l(\omega), c_{l'}^\dagger(\omega')] = \delta_{ll'}\, \delta(\omega - \omega'), \tag{4.40}$$

and account for thermal emission within the absorbing medium. The operators d_k and $d_{k'}^\dagger$ represent the amplifying medium and have the commutation relations [39]

$$[d_k(\omega), d_{k'}^\dagger(\omega')] = -\delta_{kk'}\, \delta(\omega - \omega'). \tag{4.41}$$

As the Hamiltonian (4.38) gives rise to linear equations of motion, we can compute the cavity output field using Fourier transformation. The calculation proceeds along the lines of the calculation presented in Sec. 4.1. The result is

$$b^{\mathrm{out}}(\omega) = S(\omega) b^{\mathrm{in}}(\omega) + U(\omega) c^{\mathrm{in}}(\omega) + V(\omega) d^{\mathrm{in}}(\omega), \tag{4.42}$$

where c^{in} and d^{in} represent the input noise of the absorbing and amplifying bath. Both are integrals over bath operators at the initial time t_0,

$$c_l^{\mathrm{in}}(t) \equiv \frac{1}{2\pi} \int d\omega\, \mathrm{e}^{-\mathrm{i}\omega(t-t_0)} c_l(\omega, t_0), \tag{4.43a}$$

$$d_k^{\mathrm{in}}(t) \equiv \frac{1}{2\pi} \int d\omega\, \mathrm{e}^{-\mathrm{i}\omega(t-t_0)} d_k(\omega, t_0). \tag{4.43b}$$

The S matrix has the again the form (4.35) and the matrices U and V are given by

$$U(\omega) = -2\pi\mathrm{i}\mathcal{W}^\dagger(\omega) D^{-1}(\omega) \mathcal{K}(\omega), \tag{4.44a}$$

$$V(\omega) = -2\pi\mathrm{i}\mathcal{W}^\dagger(\omega) D^{-1}(\omega) \Sigma(\omega), \tag{4.44b}$$

where the $N \times L$ matrix $\mathcal{K}$ and the $N \times K$ matrix Σ comprise the coupling amplitudes $\kappa_{\lambda l}$ and $\sigma_{\lambda k}$, respectively. In the presence of the absorbing and amplifying baths, the elements of the $N \times N$ matrix $D(\omega)$ have the form

$$D_{\lambda\lambda'}(\omega) = (\omega - \omega_\lambda)\delta_{\lambda\lambda'} + \mathcal{P}\int d\omega' \frac{\Delta_{\lambda\lambda'}(\omega')}{\omega' - \omega} + \mathrm{i}\pi\Delta_{\lambda\lambda'}(\omega), \tag{4.45}$$

where Δ is the matrix

$$\Delta(\omega) = \mathcal{W}(\omega)\mathcal{W}^\dagger(\omega) + \mathcal{K}(\omega)\mathcal{K}^\dagger(\omega) - \Sigma(\omega)\Sigma^\dagger(\omega). \tag{4.46}$$

Using Eq. (4.42) and the commutation relations for the output and input noise operators, one obtains the relation

$$UU^\dagger - VV^\dagger = \mathbb{1} - SS^\dagger, \tag{4.47}$$

that was first derived by Beenakker [68, 69] using a scattering approach to field quantization. We note that the matrix $\mathbb{1} - SS^\dagger$ is positive definite in an absorbing medium ($V = 0$) and negative definite in an amplifying medium ($U = 0$). The relations (4.42) and (4.47) are important as they relate the intensity of the output field to the amplitudes of the input field and the scattering matrix of the cavity. The statistical properties of the scattering matrix are known from random matrix theory. This allows [68, 69] to compute moments or even the full distribution of the output field intensity from linear random media.

4.3 Master Equation

In this section we address the resonator dynamics within the Schrödinger picture. We use the reduce density operator $\rho(\omega)$ to represent the cavity field and derive a master equation to describe its time evolution. We assume a time scale separation between the damping time of the resonator field and the response time of the bath, $1/\Gamma \ll \tau_{\mathrm{bath}}$, which allow us to make the Markov approximation to the Nakajima–Zwanzig equation [125], and simplifies the derivation of the master equation.

4.3.1 Derivation of the Master Equation

We consider the cavity field dynamics in the rotating wave approximation. Our starting point is the system-and-bath Hamiltonian (4.17), which we now write in terms of three contributions,

$$H_{\mathrm{SB}} = H_{\mathrm{S}} + H_{\mathrm{B}} + H_{\mathrm{Int}}, \tag{4.48}$$

where H_{S} and H_{B} are the isolated cavity and bath Hamiltonian, respectively, and H_{Int} describes the interaction between the two subsystems; the explicit form of the respective terms follow straightforwardly from Eq. (4.17).

The time evolution of the reduce density operator $\rho(t)$ of the cavity field is given by the Nakajima–Zwanzig equation [125]. This equation is obtained from the Liouville–von Neumann equation $\dot{\rho}_{\mathrm{tot}}(t) = -\mathrm{i}[H_{\mathrm{SB}}, \rho_{\mathrm{tot}}]/\hbar$ for the density operator of the full electromagnetic field by projecting the dynamics onto the cavity space, and tracing over the degrees of freedom of the outside field using a reference bath state ρ_{B}. In the Markov approximation, and taking as the reference state for the bath the canonical density operator $\rho_{\mathrm{B}} = \mathrm{e}^{-H_{\mathrm{B}}/kT} / \operatorname{Tr}_{\mathrm{B}}\{\mathrm{e}^{-H_{\mathrm{B}}/kT}\}$, the master equation for the reduce density operator is

$$\dot{\rho}(t) = \Lambda\rho(t), \tag{4.49}$$

with the time evolution generator operator

$$\Lambda = -\frac{\mathrm{i}}{\hbar}[H_{\mathrm{S}}, \,\cdot\,] + \int_0^{+\infty} \mathrm{d}t' K(t'). \tag{4.50}$$

Here the integral kernel operator reads

$$K(t')\rho(t) = \frac{1}{\hbar^2} \operatorname{Tr}_{\mathrm{B}}\big\{[H_{\mathrm{Int}}(t), [H_{\mathrm{Int}}(t'), \rho_{\mathrm{B}} \otimes \rho(t)]]\big\}, \tag{4.51}$$

where $\operatorname{Tr}_{\mathrm{B}}\{\,\cdot\,\}$ stands for the trace over the bath degrees of freedom, and the time dependent interaction Hamiltonian $H_{\mathrm{int}}(t)$ is given by

$$H_{\mathrm{Int}}(t) = \exp\Big(-\frac{\mathrm{i}}{\hbar}(H_{\mathrm{S}} + H_{\mathrm{B}})t\Big) H_{\mathrm{Int}} \exp\Big(\frac{\mathrm{i}}{\hbar}(H_{\mathrm{S}} + H_{\mathrm{B}})t\Big). \tag{4.52}$$

The evaluation of (4.49) using Eqs. (4.50)–(4.52) is a lengthy but simple exercise. The final result is derived in Appendix 4.C and includes not only coupling amplitudes that depend on frequency but also the so-called frequency-shift terms. A master equation equivalent to the Langevin equation (4.27) is recovered neglecting the frequency dependence of the coupling amplitudes as well as the frequency-shift terms. The master equation has then the form

$$\begin{aligned}\dot{\rho} = -\mathrm{i}\sum_{\lambda} \omega_\lambda [a_\lambda^\dagger a_\lambda, \rho] + (1 + n_{\mathrm{th}}) \sum_{\lambda\lambda'} \Gamma_{\lambda\lambda'}\big([a_{\lambda'}, \rho a_\lambda^\dagger] + [a_{\lambda'}\rho, a_\lambda^\dagger]\big) \\ + n_{\mathrm{th}} \sum_{\lambda\lambda'} \Gamma_{\lambda\lambda'}\big([a_\lambda^\dagger, \rho a_{\lambda'}] + [a_\lambda^\dagger \rho, a_{\lambda'}]\big).\end{aligned} \tag{4.53}$$

This equation generalizes the familiar quantum optical master equation for a single damped harmonic oscillator to many oscillators coupled by the (off-diagonal elements of the) damping matrix $\Gamma_{\lambda\lambda'}$. The latter coupling is important when the damping is strong enough to cause spectral overlap of modes. The first double sum, proportional to $1 + n_{\mathrm{th}}$ ($n_{\mathrm{th}} = [\exp(\hbar\omega/kT) - 1]^{-1}$), describes spontaneous and induced emission of photons towards the outside while the second double sum, proportional only to n_{th}, describes absorption from the outside; that interpretation is easily checked by employing the Fock representation, i.e., the representation in terms of eigenstates of the photon number operators $a_\lambda^\dagger a_\lambda$.

Systematic and stochastic forces are not as clearly separated here as in the Langevin equation. In order to bring about such distinction here as well, we may imagine the density operator $\rho(t)$ at time t anti-normally ordered in the annihilation and creation operators (all a's to the left of all $a^\dagger$'s); further, we rearrange the commutators in the right-hand side of the master equation (4.53) such that $\dot\rho$ becomes anti–normally ordered provided $\rho(t)$ is,

$$\dot\rho = -\mathrm{i}\sum_\lambda \omega_\lambda\big([a_\lambda,\rho a_\lambda^\dagger] - [a_\lambda\rho, a_\lambda^\dagger]\big) + \sum_{\lambda\lambda'}\Gamma_{\lambda\lambda'}\big([a_{\lambda'},\rho a_\lambda^\dagger] + [a_{\lambda'}\rho, a_\lambda^\dagger]\big) \\ + 2n_{\mathrm{th}}\sum_{\lambda\lambda'}\Gamma_{\lambda\lambda'}[[a_{\lambda'},\rho],a_\lambda^\dagger]\,. \quad (4.54)$$

The latter form of the master equation preserves anti–normal ordering of $\rho(t)$ at all times. Moreover, we have now separated reversible drift terms (proportional to the frequencies ω_λ), irreversible drift terms ($\propto \Gamma_{\lambda\lambda'}$) not involving the thermal number of quanta n_{th}, and noise generated diffusion terms ($\propto n_{\mathrm{th}}$); the latter interpretation will become obvious in the next section where a representation based on coherent states will be employed.

4.4 Fokker–Planck Equation

A powerful technique to find solutions of quantum Markov processes are the so-called phase space methods [39, 78, 77] in which the system operators are degraded to c-numbers and the system density operator is represented by a quasiprobability function. For Markov processes the c-number equation of motion found for the quasiprobability function is usually of the Fokker–Planck form and standard analytical methods may be used to solve it.

In this section we employ the Glauber–Sudarshan P-function to describe the cavity field. Starting from the master equation derived in the previous section, we obtain a Fokker–Plank equation for the time evolution of the P-function and find its steady state solution. In addition, we establish the equivalence of this Fokker–Plank equation with the Langevin equation (4.27).

4.4.1 Derivation of the Fokker–Planck Equation

If we consistently stick to antinormal ordering of $\rho(t)$ we may write the commutators in the master equation (4.54) as differential operators [39] as $[a,(\cdot)] \to (\partial/\partial a^\dagger)(\cdot)$ and $[(\cdot),a^\dagger] \to (\partial/\partial a)(\cdot)$. We may then just as well degrade all creation and annihilation operators to complex c-number variables

$$a_\lambda \to \alpha_\lambda, \qquad a_\lambda^\dagger \to \alpha_\lambda^*, \tag{4.55}$$

and introduce the P-function to represent the density operator,

$$\rho(t) \to P(\{\alpha,\alpha^*\},t). \tag{4.56}$$

The P-function has as its moments expectation values of normally ordered observables,

$$\Big\langle \prod_\lambda (a_\lambda^\dagger)^{m_\lambda}\prod_{\lambda'}(a_{\lambda'})^{n_{\lambda'}}\Big\rangle(t) = \int\prod_\lambda \mathrm{d}^2\alpha_\lambda\;(\alpha_\lambda^*)^{m_\lambda}(\alpha_\lambda)^{n_\lambda}P(\{\alpha,\alpha^*\},t). \tag{4.57}$$

Here the differential volume element is to be interpreted according to

$$\mathrm{d}^2\alpha_\lambda = \mathrm{dRe}(\alpha_\lambda)\mathrm{dIm}(\alpha_\lambda) = \mathrm{d}\alpha_\lambda \mathrm{d}\alpha_\lambda^*/2\mathrm{i}\,. \tag{4.58}$$

The master equation (4.54) then becomes the Fokker–Planck equation (with the shorthand $\partial/\partial\alpha_\lambda \equiv \partial_\lambda$, $\partial/\partial\alpha_\lambda^* \equiv \partial_\lambda^*$)

$$\dot{P} = \left[-\mathrm{i}\sum_\lambda \omega_\lambda(\partial_\lambda^*\alpha_\lambda^* - \partial_\lambda\alpha_\lambda) + \sum_{\lambda\lambda'} \Gamma_{\lambda\lambda'}(\partial_\lambda^*\alpha_{\lambda'}^* + \partial_{\lambda'}\alpha_\lambda + 2n_{\mathrm{th}}\partial_{\lambda'}\partial_\lambda^*)\right]P. \tag{4.59}$$

At this point the interpretation of the various terms in the master equation (4.54) given earlier becomes obvious.

The c-number Langevin equation equivalent to (4.59) is [39, 126]

$$\dot{\alpha}_\lambda(t) = -\frac{\mathrm{i}}{\hbar}\sum_{\lambda'} \mathcal{H}_{\lambda\lambda'}\alpha_{\lambda'}(t) + \varphi_\lambda(t), \tag{4.60}$$

where the random forces $\varphi(t)$ have a Gaussian statistics and a white spectrum according to

$$\langle \varphi_\lambda^*(t)\varphi_{\lambda'}(t')\rangle = 2n_{\mathrm{th}}\Gamma_{\lambda'\lambda}\,\delta(t-t'), \tag{4.61}$$

while holding on to $\langle\varphi(t)\rangle = \langle\varphi_\lambda(t)\varphi_{\lambda'}(t')\rangle = 0$. We notice that Eq. (4.60) is precisely the c-number equation that we would have obtained by degrading the operators in the quantum Langevin equation (4.27) to c-numbers and making the correspondence $F(t) \to \varphi(t)$ for the noise operators. Thus, the Fokker–Plank equation (4.59) is equivalent to the quantum Langevin equation (4.27).

4.4.2 Stationary Solution of the Master Equation

The linearity of the drift coefficients and the constancy of the diffusion tensor in the Fokker-Planck equation (4.59) indicates that we are facing a stochastic process of the Ornstein–Uhlenbeck type. Then the general time dependent solution of (4.59) can be constructed [126]. The Gaussian distribution of the noise together with the linear evolution equation (4.60) imply that the stochastic variables must be Gaussian distributed. In particular, the stationary P-function is immediately checked to be

$$\bar{P}(\{\alpha,\alpha^*\}) = \prod_\lambda \frac{1}{\pi n_{\mathrm{th}}}\exp(-\alpha_\lambda^*\alpha_\lambda/n_{\mathrm{th}}). \tag{4.62}$$

The dissipative coupling of the system modes is no longer visible in the stationary state; rather, we encounter the thermal equilibrium state one would also find in the absence of spectral overlap.

4.5 Cavity Resonances Representation Using Nonorthogonal Modes

So far we have described the resonator field dynamics in terms of eigenmodes of a conveniently chosen *closed* system, for which the associated mode operators $\{a_\lambda, a_\lambda^\dagger\}$

obey canonical commutation relations. It turns out, that the cavity field dynamics is generated by the non-Hermitian effective Hamiltonian $\mathcal{H}$ defined in Eq. (4.29). Hence, one should expect the equations of motion for the cavity field to look simpler provided the field is described in terms of the operator $\mathcal{H}$. The complex eigenvalues of $\mathcal{H}$ are the *open* cavity resonances in the presence of the coupling to the bath, while its right and left eigenvectors form a biorthogonal set of modes representing the resonances of the open cavity. If one assumes this set of modes to be complete, one can employ it to represent the intracavity field. In what follows we show how such a representation can be implemented by introducing a new set of operators associated with the cavity resonance modes. We will see that the field dynamics looks simpler in terms of these new operators, but that the new operators obey noncanonical commutation rules.

Assuming the eigenvalues of $\mathcal{H}$ are nondegenerate, $\mathcal{H}$ can be diagonalized by a similarity transformation

$$\omega = \frac{1}{\hbar} T^{-1} \mathcal{H} T. \tag{4.63}$$

The diagonal matrix ω comprises the complex eigenvalues of $\mathcal{H}/\hbar$ with

$$\omega_k = \Omega_k - i\kappa_k, \tag{4.64}$$

where Ω_k is the resonance frequency and κ_k is the resonance broadening. The entries of the matrix T are the overlapping integrals

$$T_{\lambda k} = \langle \boldsymbol{u}_\lambda | \boldsymbol{R}_k \rangle \text{ and } T^{-1}_{k\lambda} = \langle \boldsymbol{L}_k | \boldsymbol{u}_\lambda \rangle. \tag{4.65}$$

Here $\boldsymbol{u}_\lambda$ are the modes of the closed system while $\boldsymbol{R}_k$ and $\boldsymbol{L}_k$ are, respectively, the set of right and left eigenmodes of $\mathcal{H}$. They satisfy $\mathcal{H}|\boldsymbol{R}_k\rangle = \hbar\omega_k|\boldsymbol{R}_k\rangle$ and $\mathcal{H}^\dagger|\boldsymbol{L}_k\rangle = \hbar\omega_k^*|\boldsymbol{L}_k\rangle$, from which it follows

$$\langle \boldsymbol{L}_l | \boldsymbol{R}_k \rangle = \delta_{lk}. \tag{4.66}$$

We chose this particular normalization because it implies the completeness relations

$$\sum_k |\boldsymbol{L}_k\rangle\langle \boldsymbol{R}_k| = \sum_k |\boldsymbol{R}_k\rangle\langle \boldsymbol{L}_k| = \mathbb{1}. \tag{4.67}$$

The most prominent feature of this nonorthogonal basis is that in general $\langle \boldsymbol{R}_l | \boldsymbol{R}_k \rangle \neq 0$ and $\langle \boldsymbol{L}_l | \boldsymbol{L}_k \rangle \neq 0$. A measure of the nonorthogonality is given by the mode Petermann factor K, defined by

$$K_k = \langle \boldsymbol{R}_k | \boldsymbol{R}_k \rangle \langle \boldsymbol{L}_k | \boldsymbol{L}_k \rangle\,. \tag{4.68}$$

Using Schwartz inequality one can easily show that $K \geq 1$ for all modes; the equality only holds for orthogonal modes. For general non-Hermitian matrices, eigenvalues and eigenvectors are correlated. In particular, large values of K are expected for almost degenerated modes. The nonorthogonality of the cavity resonance modes has physical observable consequences. The linewidth in lasers based on nonorthogonal modes is enhanced by a factor K [22, 24, 25] with respect to the value predicted by the Schawlow–Townes formula. So far values up to $K \approx 500$ have been measured for transverse modes in unstable cavities [29, 30]; recently, investigating the location of resonance degeneracies, Berry [127] has propose that unstable cavity configurations exist for which K takes arbitrarily large values.

Associated with the kth right and left eigenmodes of $\mathcal{H}$, respectively, are the operators

$$d_k = \sum_\lambda T^{-1}_{k\lambda} a_\lambda, \tag{4.69a}$$

$$e^\dagger_k = \sum_\lambda a^\dagger_\lambda T_{\lambda k}. \tag{4.69b}$$

The representation of the fields inside the cavity in terms of the new operators and the modes of the open cavity is obtained in the rotating wave approximation from the field expansion (3.61) and the definitions (4.69),

$$\boldsymbol{A}(\boldsymbol{r}, t) = \sum_k \left(\frac{\hbar}{2\Omega_k}\right)^{1/2} [d_k \boldsymbol{R}_k(\boldsymbol{r}) + e^\dagger_k \boldsymbol{L}^*_k(\boldsymbol{r})], \tag{4.70a}$$

$$\boldsymbol{E}(\boldsymbol{r}, t) = \mathrm{i} \sum_k \left(\frac{\hbar\Omega_k}{2}\right)^{1/2} [d_k \boldsymbol{R}_k(\boldsymbol{r}) - e^\dagger_k \boldsymbol{L}^*_k(\boldsymbol{r})], \tag{4.70b}$$

where we used that $\omega_k \sim \Omega_k$ and $\Omega_k \gg \kappa_k$. The new operators do not represent bosonic creation and annihilation operators. Instead they satisfy the following commutation relations

$$\begin{aligned} &[d_l, d_k] = 0, \qquad [e_l, e_k] = 0, \qquad [d_l, e_k] = 0, \\ &[d_l, d^\dagger_k] = (T^{-1}T^{-1\dagger})_{lk} = \langle \boldsymbol{L}_l | \boldsymbol{L}_k \rangle, \\ &[e_l, e^\dagger_k] = (T^\dagger T)_{lk} = \langle \boldsymbol{R}_l | \boldsymbol{R}_k \rangle, \\ &[d_l, e^\dagger_k] = \delta_{lk}, \end{aligned} \tag{4.71}$$

which are easily checked using the definitions (4.69) and the commutation relations (3.58) for the operators $\{a_\lambda, a^\dagger_\lambda\}$. The new operators $\{d_k, e^\dagger_k\}$ coincide with the set of operators introduced by Lamprecht and Ritsch [61, 62] for the non-orthogonal modes of unstable cavities. These authors did not derive dynamical equations for the novel operators. That dynamics will be addressed below.

4.5.1 Langevin Equations

The Heisenberg equations of motion for the operators d_k are obtained by differentiating definition (4.69a) with respect to t and using the Heisenberg equations of motion (4.27) for the operators a_λ. The result is

$$\dot{d}_k(t) = -\mathrm{i}\omega_k d_k(t) + F_k(t). \tag{4.72}$$

The fact that these equations of motion decouple from each other is hardly surprising since the operators d_k were introduced for that purpose. The noise forces are given by

$$F_k(t) = \sum_\lambda T^{-1}_{k\lambda} F_\lambda(t) = -2\pi\mathrm{i} \sum_m (T^{-1}\mathcal{W})_{km} b^{\mathrm{in}}_m(t), \tag{4.73}$$

displaying their dependence on the input field. Here the coupling amplitudes $\mathcal{W}_{\lambda m}$ form an $N \times M$ matrix $\mathcal{W}$ ($M = M(\omega)$ is the number of open channels at frequency ω and the number of cavity modes N is taken to infinity at the end of the calculations) and T is the $N \times N$ linear transformation defined in Eq. (4.65). The Langevin equations of motion follow from the Heisenberg equations of motion (4.72) by considering noise forces with a white spectrum, such that $\langle F_k(t)\rangle = 0$, and the correlation functions different from zero are given by

$$\langle F_l^\dagger(t)F_k(t')\rangle = \mathrm{i}\langle L_l|L_k\rangle(\omega_l - \omega_k^*)n_{\mathrm{th}}\,\delta(t-t'), \tag{4.74a}$$

$$\langle F_k(t)F_l^\dagger(t')\rangle = \mathrm{i}\langle L_l|L_k\rangle(\omega_l - \omega_k^*)(n_{\mathrm{th}}+1)\,\delta(t-t'), \tag{4.74b}$$

with the thermal number of photons $n_{\mathrm{th}} = [\exp(\hbar\bar{\omega}/kT) - 1]^{-1}$. Thus, although the deterministic part of the dynamics does not couple the open cavity modes, the noise terms for different modes are correlated.

Input–Output Relation

The input-output relation can be expressed in terms of the new set of operator. In the time domain, one obtains the relation

$$b_m^{\mathrm{out}}(t) - b_m^{\mathrm{in}}(t) = -\mathrm{i}\sum_k (\mathcal{W}^\dagger T)_{mk} d_k(t')\,. \tag{4.75}$$

After Fourier transformation the above equations yield

$$b_m^{\mathrm{out}}(\omega) - b_m^{\mathrm{in}}(\omega) = -\mathrm{i}\sum_k (\mathcal{W}^\dagger T)_{mk} d_k(\omega). \tag{4.76}$$

These conditions are obtained from the input–output relations (4.30) and (4.31) employing the inverse of the definition (4.69a).

4.5.2 Master Equation

The operators $\{d, e^\dagger\}$ may be employed to express the cavity field dynamics in the Schrödinger picture. In terms of these operators the master equation (4.54) takes the form

$$\dot{\rho} = -\mathrm{i}\sum_k \Big\{\omega_k\big([e_k^\dagger, d_k\rho] - n_{\mathrm{th}}[[d_k,\rho], e_k^\dagger]\big) - \omega_k^*\big([\rho d_k^\dagger, e_k] - n_{\mathrm{th}}[[e_k,\rho], d_k^\dagger]\big)\Big\}. \tag{4.77}$$

Here we used the relations $\omega_\lambda\delta_{\lambda\lambda'} = \frac{1}{2\hbar}(\mathcal{H}_{\lambda\lambda'} + \mathcal{H}_{\lambda\lambda'}^\dagger)$ and $\Gamma_{\lambda\lambda'} = \frac{i}{2\hbar}(\mathcal{H}_{\lambda\lambda'} - \mathcal{H}_{\lambda\lambda'}^\dagger)$, together with the representation (4.63) of $\mathcal{H}$, and the definitions (4.69) of the operators $\{d, e^\dagger\}$. We notice that in the limit $kT \ll \hbar\bar{\omega}$ the master equation (4.77) can be recast as

$$\dot{\rho} = -\frac{\mathrm{i}}{\hbar}(\mathcal{H}\rho - \rho\mathcal{H}^\dagger) + \mathrm{i}\sum_{kl}\langle \boldsymbol{R}_l|\boldsymbol{R}_k\rangle(\omega_k - \omega_l^*)d_k\rho d_l^\dagger, \tag{4.78}$$

with $\mathcal{H} = \sum_k \hbar\omega_l e_k^\dagger d_k$. This is the master equation proposed by Lamprecht and Ritsch [62, 34]. Our derivation provides a microscopic basis for this equation and proves the equivalence to the master equations (4.53) and (4.54) in the limit $kT \ll \hbar\bar{\omega}$.

4.A Formal Solution of the Field Equations of Motion

In this section we give the exact solutions to the equations of motion for the electromagnetic field in open optical cavities. Two cases are considered: The exact dynamics generated by the Hamiltonian (3.59) and the dynamics in the *rotating wave approximation* generated by the Hamiltonian (4.17).

Exact Dynamics

The solutions of the field equations of motion for the exact dynamics are obtained in a rather simple way if one uses the position and momentum operators to describe the field. The modes-of-the-universe Hamiltonian (3.13) corresponds to a set of independent harmonic oscillators,

$$q_m(\omega,t) = q_m(\omega,t_0)\cos(\omega(t-t_0)) + \frac{1}{\omega}p_m^\dagger(\omega,t_0)\sin(\omega(t-t_0)), \tag{4.A.1a}$$

$$p_m^\dagger(\omega,t) = p_m^\dagger(\omega,t_0)\cos(\omega(t-t_0)) - \omega q_m(\omega,t_0)\sin(\omega(t-t_0)), \tag{4.A.1b}$$

where q and $p^\dagger$ are the position and the adjoint momentum operator for the exact modes of Maxwell's equations. The solutions for the cavity and channel operators are obtained by substitution of Eq. (4.A.1) into definitions (3.49) and (3.50), and using the inverse relations (3.54) for the operators at the initial time t_0. The result for the position operators is

$$\begin{aligned} Q_\lambda(t) = {} & \sum_{\lambda'} \left[\dot{X}_{\lambda\lambda'}(t-t_0)Q_{\lambda'}(t_0) + X_{\lambda\lambda'}(t-t_0)P_{\lambda'}^\dagger(t_0)\right] \\ & + \sum_m \int_{\omega_m}^{\infty} \mathrm{d}\omega \left[\dot{X}_{\lambda m}(\omega,t-t_0)Q_m(\omega,t_0) + X_{\lambda m}(\omega,t-t_0)P_m^\dagger(\omega,t_0)\right], \end{aligned} \tag{4.A.2a}$$

$$\begin{aligned} Q_m(\omega,t) = {} & \sum_{\lambda} \left[\dot{X}^*_{\lambda m}(\omega,t-t_0)Q_\lambda(t_0) + X^*_{\lambda m}(\omega,t-t_0)P_\lambda^\dagger(t_0)\right] \\ & + \sum_{m'} \int_{\omega_{m'}}^{\infty} \mathrm{d}\omega' \left[\dot{X}_{mm'}(\omega,\omega',t-t_0)Q_{m'}(\omega',t_0) + X_{mm'}(\omega,\omega',t-t_0)P_{m'}^\dagger(\omega',t_0)\right], \end{aligned} \tag{4.A.2b}$$

while the momenta follow from

$$P_\lambda^\dagger(t) = \dot{Q}_\lambda(t), \qquad P_m^\dagger(\omega,t) = \dot{Q}_m(\omega,t). \tag{4.A.3}$$

The matrix elements of the time evolution transformation X are defined by

$$X_{\lambda\lambda'}(t) = \sum_n \int_{\omega_n}^{\infty} \mathrm{d}\omega'' \; \alpha_{n\lambda}(\omega'')\alpha^*_{n\lambda'}(\omega'')\frac{1}{\omega''}\sin(\omega'' t), \tag{4.A.4a}$$

$$X_{\lambda m}(\omega, t) = \sum_n \int_{\omega_n}^{\infty} \mathrm{d}\omega'' \; \alpha_{n\lambda}(\omega'')\beta^*_{nm}(\omega'', \omega)\frac{1}{\omega''}\sin(\omega'' t), \tag{4.A.4b}$$

$$X_{mm'}(\omega, \omega', t) = \sum_n \int_{\omega_n}^{\infty} \mathrm{d}\omega'' \; \beta_{nm}(\omega'', \omega)\beta^*_{nm'}(\omega'', \omega')\frac{1}{\omega''}\sin(\omega'' t). \tag{4.A.4c}$$

Using the results given in Appendix 3.A for the integrals involving the expansion coefficients α and β, one can easily check that

$$\begin{aligned}
X_{\lambda\lambda'}(0) &= 0, & \dot{X}_{\lambda\lambda'}(0) &= \delta_{\lambda\lambda'}, & \ddot{X}_{\lambda\lambda'}(0) &= 0,\\
X_{\lambda m}(\omega, 0) &= 0, & \dot{X}_{\lambda m}(\omega, 0) &= 0, & \ddot{X}_{\lambda m}(\omega, 0) &= 0,\\
X_{mm'}(\omega, \omega', 0) &= 0, & \dot{X}_{mm'}(\omega, \omega', 0) &= \delta_{mm'}\,\delta(\omega - \omega'), & \ddot{X}_{mm'}(\omega, \omega', 0) &= 0.
\end{aligned} \tag{4.A.5}$$

The solutions for the bosonic operators for the cavity and channel field are obtained as linear combinations of Eqs. (4.A.2) and (4.A.3), by means of Eq. (3.57).

Dynamics in the Rotating Wave Approximation

The solutions of the Heisenberg equations of motion (4.18a) and (4.18b) are

$$a_\lambda(t) = \sum_{\lambda'} Y_{\lambda\lambda'}(t - t_0)a_{\lambda'}(t_0) + \sum_m \int \mathrm{d}\omega Y_{\lambda m}(\omega, t - t_0)b_m(\omega, t_0), \tag{4.A.6a}$$

$$b_m(\omega, t) = \sum_{\lambda} Y^*_{\lambda m}(\omega, t - t_0)a_\lambda(t_0) + \sum_{m'} \int \mathrm{d}\omega' Y_{mm'}(\omega, \omega', t - t_0)b_{m'}(\omega', t_0). \tag{4.A.6b}$$

Here the time evolution operator Y has the matrix elements

$$Y_{\lambda\lambda'}(t) = \sum_n \int \mathrm{d}\omega'' \; \alpha_{n\lambda}(\omega'')\alpha^*_{n\lambda'}(\omega'')\mathrm{e}^{-\mathrm{i}\omega'' t}, \tag{4.A.7a}$$

$$Y_{\lambda m}(\omega, t) = \sum_n \int \mathrm{d}\omega'' \; \alpha_{n\lambda}(\omega'')\beta^*_{nm}(\omega'', \omega)\mathrm{e}^{-\mathrm{i}\omega'' t}, \tag{4.A.7b}$$

$$Y_{mm'}(\omega, \omega', t) = \sum_n \int \mathrm{d}\omega'' \; \beta_{nm}(\omega'', \omega)\beta^*_{nm'}(\omega'', \omega')\mathrm{e}^{-\mathrm{i}\omega'' t}; \tag{4.A.7c}$$

and the expansion coefficients α and β are to be taken in the rotating wave approximation. Using the results in Appendix 3.A, one finds the initial values

$$Y_{\lambda\lambda'}(0) = \delta_{\lambda\lambda'}, \qquad Y_{\lambda m}(\omega, 0) = 0 \qquad \text{and} \qquad Y_{mm'}(\omega, \omega', 0) = \delta_{mm'}\,\delta(\omega - \omega'). \tag{4.A.8}$$

Within the rotating wave approximation Eq. (3.B.8) reduces to

$$(\omega - \omega_\lambda)\, \alpha_{m\lambda}(\omega) = \sum_n \int \mathrm{d}\omega'\; \mathcal{W}_{\lambda n}(\omega')\beta_{mn}(\omega,\omega'), \tag{4.A.9a}$$

$$(\omega - \omega')\, \beta_{mn}(\omega,\omega') = \sum_\lambda \mathcal{W}^*_{\lambda n}(\omega')\alpha_{m\lambda}(\omega), \tag{4.A.9b}$$

Direct substitution shows that the expressions (4.A.6) are solutions of the equations of motion (4.18).

4.B Corrections to the Rotating Wave Approximation

For resonators with overlapping modes the time scale set by the inverse of the mean frequency spacing $1/\Delta\omega$ is comparable to the damping time $1/\Gamma$. Therefore the Langevin or master equation must be used if they provide a *nonperturbative* description of damping and noise (in the sense that the mode decay rates Γ may exceed the mode spacing).

In this section we show that the Langevin equations (4.27) and the master equations (4.53) and (4.54) are nonperturbative in the above mentioned sense. To this end we address again the exact field equations of motion and illustrate how they can be used to compute corrections to the dynamics in the Markov approximation of Sec. 4.2.1. We start from Eq. (4.6), which describes the exact time evolution of the cavity modes operators a_λ,

$$\dot{a}_\lambda(t) = -\mathrm{i}\omega_\lambda a_\lambda(t) + \sum_{\lambda'} \int_{t_0}^{t} \mathrm{d}t' \tilde{C}_{\lambda\lambda'}(t-t') \left[a_{\lambda'}(t') + \sum_{\lambda'} \mathcal{N}^\dagger_{\lambda'\lambda''} a^\dagger_{\lambda''}(t') \right] + \tilde{F}_\lambda(t), \tag{4.B.1}$$

and consider it in the rotating wave approximation made in Sec. 4.2.1. That is, we restrict our analysis to a frequency bandwidth which is small compared to the central frequency $\bar{\omega}$, and consider the time evolution only for times larger than the bath correlation times τ_{bath}. In addition, we assume the coupling to be such that the typical damping rate $\bar{\Gamma}$ for the cavity modes are much smaller than $\bar{\omega}$, but of the same order than the mean frequency spacing $\Delta\omega$ of the cavity modes in the frequency range considered.

We first move to a rotating frame

$$a_\lambda(t) = \mathrm{e}^{-\mathrm{i}\bar{\omega}t}\bar{a}_\lambda(t), \tag{4.B.2}$$

where $\bar{a}_\lambda(t)$ are slowly varying variables. Specifically, $\bar{a}_\lambda(t)$ does not change much on the time scale of the order τ_{bath} in which $\tilde{C}_{\lambda\lambda'}(t)$ decays to zero. Substituting the operators (4.B.2) into Eq. (4.B.1) and replacing $\bar{a}_\lambda(t')$ with $\bar{a}_\lambda(t)$, one obtains the equation of motion for the slowly varying operators $\bar{a}_\lambda(t)$,

$$\dot{\bar{a}}_\lambda(t) = \\ -\sum_\lambda \left[\tilde{C}_{\lambda\lambda'}(\omega_{\lambda'})\mathrm{e}^{-\mathrm{i}(\omega_{\lambda'}-\bar{\omega})t}\bar{a}_{\lambda'}(t) + \tilde{C}_{\lambda\lambda'}(-\omega_{\lambda'})\mathrm{e}^{\mathrm{i}(\omega_{\lambda'}+\bar{\omega})t} \sum_{\lambda'\lambda''} \mathcal{N}_{\lambda'\lambda''}\bar{a}^\dagger_{\lambda''}(t) \right] + \mathrm{e}^{\mathrm{i}\omega_\lambda t}\tilde{F}_\lambda(t). \tag{4.B.3}$$

Here the channel response matrix in the frequency domain is given by

$$\begin{aligned}\tilde{C}_{\lambda\lambda'}(\pm\omega) &= \int_{-\infty}^{t} \mathrm{d}t'\, \tilde{C}_{\lambda\lambda'}(t-t')\mathrm{e}^{\pm\mathrm{i}\omega(t-t')} \\ &= -\frac{\mathrm{i}}{\pi}\mathcal{P}\int_{\omega_m}^{\infty} \mathrm{d}\omega'\, \frac{\Gamma_{\lambda\lambda'}(\omega')}{\omega'-\omega} \pm \Gamma_{\lambda\lambda'}(\omega) + \mathcal{O}(\gamma/2\bar{\omega}),\end{aligned} \tag{4.B.4}$$

where we set $t_0 \to -\infty$ in the integration limits because we are only considering times t such that $t - t_0 \gg \tau_{\mathrm{bath}}$. The second term inside the brackets in the Eq. (4.B.3) oscillates very fast, with a frequency $\sim 2\bar{\omega}$, and can be neglected in the rotating wave approximation. Equation (4.B.3) then reduces to Eq. (4.26), from which the Langevin equation follows. The neglected terms provide corrections of order $|C(\bar{\omega})|/2\bar{\omega} \sim \Gamma/2\bar{\omega}$ which are very small for the systems of interest in quantum optics. We note that there are no corrections of order $\Gamma/\Delta\omega$; thus our field dynamics correctly describes the regime of overlapping resonances.

4.C Complete Master Equation

The master equation (4.53) was obtained upon neglecting both the frequency dependence of the coupling amplitudes as well as possible frequency shift terms. Dropping these last approximations, the more general master equation is given by

$$\begin{aligned}\dot{\rho} = &-\mathrm{i}\sum_{\lambda}\omega_\lambda[a^\dagger_\lambda a_\lambda, \rho] \\ &+\sum_{\lambda\lambda'}(1+n_{\mathrm{th}}(\omega_\lambda))\big(\Gamma_{\lambda\lambda'}(\omega_\lambda)[a_{\lambda'}, \rho a^\dagger_\lambda] + \Gamma^*_{\lambda\lambda'}(\omega_\lambda)[a_\lambda\rho, a^\dagger_{\lambda'}]\big) \\ &+\sum_{\lambda\lambda'} n_{\mathrm{th}}(\omega_\lambda)\big(\Gamma_{\lambda\lambda'}(\omega_\lambda)[a^\dagger_\lambda\rho, a_{\lambda'}] + \Gamma^*_{\lambda\lambda'}(\omega_\lambda)[a^\dagger_{\lambda'}, \rho a_\lambda]\big) \\ &+\frac{\mathrm{i}}{\pi}\sum_{\lambda\lambda'}\left(\mathcal{P}\int \mathrm{d}\omega\, \frac{\Gamma_{\lambda\lambda'}(\omega)n_{\mathrm{th}}(\omega)}{\omega-\omega_\lambda}[a_{\lambda'}, [\rho, a^\dagger_\lambda]] - \mathcal{P}\int \mathrm{d}\omega\, \frac{\Gamma^*_{\lambda\lambda'}(\omega)n_{\mathrm{th}}(\omega)}{\omega-\omega_\lambda}[a^\dagger_{\lambda'}, [\rho, a_\lambda]]\right) \\ &+\frac{\mathrm{i}}{\pi}\sum_{\lambda\lambda'}\left(\mathcal{P}\int \mathrm{d}\omega\, \frac{\Gamma_{\lambda\lambda'}(\omega)}{\omega-\omega_\lambda}[a_{\lambda'}, \rho a^\dagger_\lambda] - \mathcal{P}\int \mathrm{d}\omega\, \frac{\Gamma^*_{\lambda\lambda'}(\omega)}{\omega-\omega_\lambda}[a_\lambda\rho, a^\dagger_{\lambda'}]\right).\end{aligned} \tag{4.C.1}$$

The most relevant terms in this master equation are contained in the first three lines, accounting for the oscillations, the damping and the noise in the field dynamics. The last two lines contain the so-called frequency shift terms which are, due to the principal part integrals, small corrections to the oscillating part of the master equation. The terms in the fourth line proportional to n_{th} constitute the *Stark* shift which has its origin in thermal fluctuations. The terms on the last line are the *Lamb* shift which is due to vacuum fluctuations. Contrary to the *Stark* shift, the *Lamb* shift is present even at zero temperature.

Chapter 5

Laser Equations with Overlapping Resonances

In this chapter we employ the quantum description of the electromagnetic field in open optical resonators developed in *Chapters 3* and *4* to study the interaction of the field with a two-level atomic medium filling the resonator. The results are used to develop a quantum theory for multi-mode fields in resonators with overlapping resonances. We derive laser Lagenvin equations that generalize the standard laser theory [10, 11, 36] to account for lasing in weakly confining cavities.

Before attempting a derivation of the laser equations, and in order to gain some physical insight into the atom-field interaction, we study the effect of the field on a single atom. As a simple but nontrivial problem we consider the spontaneous emission of a two-level atom inside a cavity. This problem has attracted considerable interest [103, 128]; and it was found that the cavity may drastically modify the rate of spontaneous emission from its free space value. The origin of the effect is the modification due to the cavity of the local density of modes at the position of the atom. Most investigations of the spontaneous emission rate assumed cavities of regular shape (see Ref. [128] and references therein), but recently [61, 62, 129] also unstable and chaotic cavities were addressed. We show below that our system-and-bath Hamiltonian reproduces the standard result for the atomic decay rate within the Wigner–Weisskopf approximation. We express the result in terms of left and right eigenmodes of a non-Hermitean matrix and demonstrate that for chaotic resonators a statistical analysis of the decay rate is possible using random matrix theory.

We consider resonators filled with a large number of two-level atoms and derive generalized laser Langevin equations suitable for overlapping modes. We present two set of equivalent laser Langevin equations related by a linear transformation: One in terms of orthogonal modes corresponding to the close cavity problem, and the other in terms of the resonance modes of the empty open cavity. The obtained multi-mode laser equations differ from the standard laser equations in a fundamental feature: due to the resonator losses the noise forces associated with different cavity modes are correlated. This feature is characteristic of systems with overlapping resonances and, as we show in *Chapter 6*, is responsible for the excess noise found in this kind of systems.

We use the multi-mode field equations to describe the laser operation below the lasing threshold. In this regime the field amplitude is small and nonlinear terms on the equations of motion might be neglected; the laser then behaves like a linear amplifier. Using the resulting linear set of equations we determine the laser threshold which gives the value of pumping above which the linear description breaks down. Then the input-output theory is utilized to evaluate the laser power emission spectrum and express it in terms of the system S matrix. Finally, we consider the emission spectrum close to threshold and show that for overlapping modes the linewidth of the dominating contribution coming from the mode with the smallest loss is enhanced by the Petermann excess noise factor.

5.1 Atom-Field Interaction

Consider an open resonator of arbitrary shape filled with a large number $\mathcal{N}$ of homogeneously broadened two-level atoms with transition frequency ν. The dipole strength of the atomic transition is given by $\boldsymbol{d} = \langle 0|e\boldsymbol{r}_{\text{el}}|1\rangle$, where e is the elementary charge, $\boldsymbol{r}_{\text{el}}$ denotes the electron position operator, and $|0\rangle$ and $|1\rangle$ the ground state and the excited state of the atom, respectively. To describe the atoms we use the lowering and rising operators $\sigma_- = |0\rangle\langle 1|$ and $\sigma_+ = |1\rangle\langle 0|$, which introduce transitions between the atomic levels $|0\rangle$ and $|1\rangle$, and the Pauli σ_z matrix, $\sigma_z = |1\rangle\langle 1| - |0\rangle\langle 0|$. These operators obey the usual algebra for two-level systems

$$\sigma_\pm^2 = 0, \quad [\sigma_\pm, \sigma_z] = \mp 2\sigma_\pm, \quad [\sigma_+, \sigma_-]_+ = \mathbb{1}, \quad \text{and} \quad [\sigma_+, \sigma_-] = \sigma_z. \tag{5.1}$$

Each atom is located at a position $\boldsymbol{r}_p$ inside the cavity and does not interact with any other atom; we use the index p to label the atoms.

The interaction between the cavity electromagnetic field and the atoms is described using two approximations [11, 10]: The dipole approximation and the rotating wave approximation. For the first approximation we assume the size of the atoms to be much smaller than the wavelength of the field, allowing us to take the field constant over the atomic size. The second approximation amounts to neglecting the rapidly oscillating nonresonant terms in the atom-field interaction. The total Hamiltonian for the field and atoms then has the form

$$H = H_{\text{SB}} + \sum_p \hbar\omega_0\sigma_{zp} + \hbar\sum_\lambda\sum_p [g_{\lambda p}a_\lambda\sigma_{+p} + g_{\lambda p}^* a_\lambda^\dagger\sigma_{-p}]. \tag{5.2}$$

Here H_{SB} is the system–and–bath Hamiltonian (4.17), the second term on the right hand side represents the free Hamiltonian of the atoms, and the last term accounts for the interaction between the atoms and the cavity modes with the coupling amplitudes

$$g_{\lambda p} = -\mathrm{i}\frac{\nu}{\sqrt{2\hbar\omega_\lambda}}\boldsymbol{d}\cdot\boldsymbol{u}_\lambda(\boldsymbol{r}_p), \tag{5.3}$$

where $\boldsymbol{u}_\lambda$ is the wave function of the λth cavity field mode and ω_λ its oscillation frequency.

5.2 Atomic Spontaneous Emission

We investigate the effect of the intracavity field on a single atom[1]. Since the cavity resonances overlap we can accurately describe the atomic spontaneous emission in the perturbative regime [128] following a Wigner-Weisskopf approach. We assume that initially the atom, which is located at position $\boldsymbol{r}_0$ inside the cavity, is in the excited state while there is no photon in the radiation field. Hence, the state of the total system at time $t = 0$ is given by $|1, \mathrm{vac}\rangle$, where vac represents the vacuum state of the electromagnetic field. Since the Hamiltonian (5.2) conserves the total number of atom and field excitations, the time-dependent solution of the Schrödinger equation can be written in the form

$$|\Phi(t)\rangle = c(t)|1, \mathrm{vac}\rangle + \sum_\lambda c_\lambda(t)|0, 1_\lambda\rangle + \sum_m \int \mathrm{d}\omega\; c_m(\omega, t)|0, 1_m(\omega)\rangle, \tag{5.4}$$

where $c_\lambda(t)$ and $c_m(\omega, t)$ are, respectively, the probability amplitude to find a single photon in the cavity mode λ and in channel m with frequency ω. The time evolution of the amplitudes $c(t)$, $c_\lambda(t)$ and $c_m(\omega, t)$ follows from the Schrödinger equation; an exact solution can be obtained using Laplace transformation. However, within the framework of the Wigner–Weisskopf approximation $c(t)$ decays exponentially

$$c(t) = \exp\left(-\mathrm{i}(\nu + \delta\nu)t - \frac{\gamma_{\mathrm{at}}}{2}t\right) c(0), \tag{5.5}$$

where $\delta\nu$ is a frequency shift and γ_{at} the decay rate of the intensity $|c(t)|^2$. We note that an exponential decay is only found if the local density of modes is smooth on the scale of the atomic decay rate. The decay rate is given by

$$\gamma_{\mathrm{at}} = \lim_{\epsilon \longrightarrow 0} \mathrm{Re}\left[\frac{2}{\hbar^2} \sum_{ij} d_i d_j^* \mathcal{C}_{ij}(\nu + i\epsilon)\right], \tag{5.6}$$

where i, j label the components of the dipole matrix element. Here $C_{ij}(\nu + i\epsilon)$ is the Fourier transform of the two time correlation function of the electric field

$$\mathcal{C}_{ij}(t - t') \equiv \Theta(t - t') \left\langle E_i^+(\boldsymbol{r}_0, t) E_j^-(\boldsymbol{r}_0, t')\right\rangle_{\mathrm{vac}}, \tag{5.7}$$

$E^\pm$ denote the positive and negative frequency part of the electric field, $\Theta(t - t')$ is the step function, and the average $\langle \cdots \rangle_{\mathrm{vac}}$ is the quantum average over the initial state of the field.

The electric field is connected with the canonical momentum field through the relation $\mathbf{E}(\boldsymbol{r}, t) = -c\boldsymbol{\Pi}(\boldsymbol{r}, t)$. Inside the cavity both can be expanded in terms of the cavity modes using Eq. (3.61b). Substitution into Eq. (5.7) reduces the field correlation function to a sum over the Green functions of the cavity modes,

$$\mathcal{C}_{ij}(\tau) = \mathrm{i} \sum_{\lambda\lambda'} \frac{\hbar\sqrt{\omega_\lambda \omega_{\lambda'}}}{2} u_{\lambda i}(\boldsymbol{r}_0) u_{\lambda' j}^*(\boldsymbol{r}_0) G_{\lambda\lambda'}(\tau), \tag{5.8a}$$

$$G_{\lambda\lambda'}(\tau) \equiv -\mathrm{i}\Theta(\tau)\langle a_\lambda(\tau) a_{\lambda'}^\dagger(0)\rangle_{\mathrm{vac}}. \tag{5.8b}$$

[1]The result in this section have been reported in Ref. [97].

To compute the Green functions, we differentiate Eq. (5.8b) with respect to τ and use the equations of motion (4.19) of the cavity operators a_λ. This yields the equations of motion of the Green functions

$$\dot{G}_{\lambda\lambda'}(\tau) = \delta(\tau)G_{\lambda\lambda'}(0) - \mathrm{i}\omega_\lambda G_{\lambda\lambda'}(\tau) - \frac{1}{\pi}\int \mathrm{d}\omega \int_0^\tau \mathrm{d}t\, \mathrm{e}^{-\mathrm{i}\omega(\tau-t)}[\Gamma(\omega)G(t)]_{\lambda\lambda'} . \tag{5.9}$$

There is no contribution from the noise term in Eq. (4.19) as $\langle b_m(\omega, 0)a_\lambda^\dagger(0)\rangle_{\mathrm{vac}} = 0$. The initial condition at $\tau = 0$ is $G_{\lambda\lambda'}(0) = -\mathrm{i}\delta_{\lambda\lambda'}$. Equation (5.9) is readily solved by Fourier transformation. The result is

$$G(\omega) = D^{-1}(\omega), \tag{5.10}$$

where the non-Hermitean matrix D was defined in Eq. (4.33). Substituting the result into the Fourier transform of Eq. (5.8a), we obtain the field correlation function in the frequency domain,

$$\mathcal{C}_{ij}(\omega) = \frac{\mathrm{i}\hbar\nu}{2} \sum_{\lambda\lambda'} u_{\lambda i}(\boldsymbol{r}_0)u^*_{\lambda' j}(\boldsymbol{r}_0) \left[D^{-1}(\omega)\right]_{\lambda\lambda'} , \tag{5.11}$$

where we again made use of the rotating wave approximation to replace $\sqrt{\omega_\lambda\omega_{\lambda'}} \simeq \nu$. The decay rate follows upon substitution of Eq. (5.11) into Eq. (5.6),

$$\gamma_{\mathrm{at}} = -\frac{\nu}{\hbar}\mathrm{Im}\left[\sum_{ij} d_i d_j^* \sum_{\lambda\lambda'} u_{\lambda i}(\boldsymbol{r}_0)[D^{-1}(\nu)]_{\lambda\lambda'} u^*_{\lambda' j}(\boldsymbol{r}_0)\right]. \tag{5.12}$$

The sum over modes may be simplified in the eigenbasis of the non-Hermitean matrix D. In this basis, the double sum over the mode functions $\boldsymbol{u}_\lambda$ reduces to a summation over the left and right eigenmodes of the wave equation of the open cavity,

$$\gamma_{\mathrm{at}} = \frac{\pi\nu d^2}{\hbar}\rho(\nu, \boldsymbol{r}_0), \tag{5.13a}$$

$$\rho(\nu, \boldsymbol{r}_0) = \frac{1}{\pi}\mathrm{Im}\left[\sum_l \frac{L_l^*(\boldsymbol{r}_0, \nu)R_l(\boldsymbol{r}_0, \nu)}{\Omega_l - \nu - \mathrm{i}\kappa_l}\right]. \tag{5.13b}$$

Here, $\rho(\nu, \boldsymbol{r}_0)$ is the local density of modes at the position of the atom, L_l, R_l denote the component along $\mathbf{d}$ in the left and right mode l, and Ω_l, κ_l are the mode frequency and the mode broadening.

Equations (5.13) are the final result for the decay rate. They describe spontaneous emission not only in cavities with quasi-discrete modes but also in unstable resonators with strongly overlapping modes. In the latter case, the left eigenfunctions of the cavity may differ strongly from the corresponding right eigenfunctions. Our result agrees with the decay rate derived in Refs. [62, 64] using a field expansion in terms of non–orthogonal modes. Equations (5.13) have recently [129] been used to calculate the distribution $P(\gamma_{\mathrm{at}})$ of decay rates for a two–level atom inside a chaotic cavity. The local density of modes also determines the photo-dissociation rate of small molecules with chaotic internal dynamics [130].

Our derivation of the decay rate was based on the system-and-bath Hamiltonian (4.17) which describes the cavity field dynamics in the rotating wave approximation. This approximation is valid for the (typical) case in which the broadening of the resonator modes is much smaller than the atomic transition frequency. When the mode broadening is of the order of the transition frequency, one can still compute the decay rate in the Wigner-Weisskopf approximation provided the coupling between the field and the atom is sufficiently small. Then Eq. (5.13a) still holds, but the local density of states must be evaluated using the complete Hamiltonian (3.59) for the field. The calculation is done in Appendix 5.A.

5.3 Laser Langevin Equations

We now extend our theory to many atoms and consider nonlinear effects. The resulting laser model of open cavities with overlapping resonances is a generalization of the theory of Hacken [11] for lasing in cavities with isolated resonances. The laser Langevin equations are obtained by accounting for the atom-field interaction in the electric–dipole and rotating wave approximations. Additionally, we take the field losses in the Markovian approximation and neglect the frequency dependence of the outcoupling amplitudes $\mathcal{W}(\omega)$. To model pumping and losses for the atoms (e.g., due to nonradiative transitions out of the excited level) we couple them to external pumping and loss baths. This model leads to the following set of coupled Heisenberg-Langevin equations

$$\dot{a}_\lambda(t) = -\frac{\mathrm{i}}{\hbar}\sum_{\lambda'}\mathcal{H}_{\lambda\lambda'}a_{\lambda'}(t) - \mathrm{i}\sum_p g^*_{\lambda p}\sigma_{-p}(t) + F_\lambda(t), \tag{5.14a}$$

$$\dot{\sigma}_{-p}(t) = -(\mathrm{i}\nu+\gamma_\perp)\sigma_{-p}(t) + \mathrm{i}\sum_\lambda g_{\lambda p}a_\lambda(t)\sigma_{zp}(t) + F_{\perp p}(t), \tag{5.14b}$$

$$\dot{\sigma}_{zp}(t) = \gamma_\parallel(\Lambda_p - \sigma_{zp}(t)) + 2\mathrm{i}\sum_\lambda[g^*_{\lambda p}a^\dagger_\lambda(t)\sigma_{-p}(t) - g_{\lambda p}\sigma_{+p}(t)a_\lambda(t)] + F_{\parallel p}(t), \tag{5.14c}$$

where λ labels the close resonator modes and p the atoms. The dynamics of the resonator field is damped by the coupling to the external radiation field and is described by the non-Hermitian matrix $\mathcal{H}$ defined in Eq. (4.29). Likewise, the atomic polarization and inversion are damped with damping amplitudes $\gamma_\perp$ and $\gamma_\parallel$. The atomic polarization oscillates with frequency ν, and Λ_p is a parameter for the pump strength which is assumed to be time independent. The coupling amplitudes $g_{\lambda p}$ between atoms and field are defined in Eq. (5.3). Finally, the operators F_λ, $F_{\perp p}$, and $F_{\parallel p}$ represent quantum noise due to the coupling to external baths. The presence of such noise terms is a consequence of the fluctuation-dissipation theorem.

In order to complete the equations of motion (5.14) the statistics of the Langevin force operators should be specify. All noise operators are treated as Gaussian random variables with zero mean and are therefore fully defined by their second-order moments. The nonzero correlations functions of the field Langevin force F_λ are specified in Eq. (4.28). In this thesis we are mainly interested in the optical domain where $\hbar\nu \gg kT$. Hence, we take the cavity bath to be at temperature $T = 0$ so that the average number of thermal photons n_{th} in the cavity is zero. According to the simple relation between the field noise operator and the bath-input, $F_\lambda = -2\pi\mathrm{i}\sum_m \mathcal{W}_{\lambda m} b_m^{\mathrm{in}}$, the above assumption corresponds to the situation in which there is no external illumination.

The correlation functions for the atomic noise operators $F_{\perp p}$ and $F_{\parallel p}$ are obtained using the generalized Einstein relations and correspond to the ones used in the standard laser theory [10, 11]. The correlation functions different from zero are written down in the Appendix 5.B.

The main difference between our Langevin equations and the independent-oscillator equations of the standard laser theory [11, 10] is the coupling among the modes by the matrix $\mathcal{H}$. As discussed before, this coupling is due to the leakage of energy from the cavity through the opening, and its most important consequence is that the Langevin forces for different modes are correlated. In Sec. 4.5 we showed that the field cavity dynamics simplifies if one uses the modes of the open cavity to represent the field. In terms of such modes the equations of motion decouple ($\mathcal{H}$ becomes diagonal). The correlation between the noise for different modes, however, does not disappear and can be interpreted as a consequence of the nonorthogonality of the open cavity modes. The laser equations in terms of the operators d, associated with the modes of the open cavity, are obtained from Eqs. (5.14) with the help of the linear transformation (4.69a). They read

$$\dot{d}_k(t) = -\mathrm{i}\omega_k d_k(t) - \mathrm{i}\int d\boldsymbol{r}\, g_k^{L*}(\boldsymbol{r}) S_-(\boldsymbol{r},t) + F_k(t), \tag{5.15a}$$

$$\dot{S}_-(\boldsymbol{r},t) = -(\mathrm{i}\nu + \gamma_\perp) S_-(\boldsymbol{r},t) + \mathrm{i}\sum_k g_k^R(\boldsymbol{r}) d_k(t) S_z(\boldsymbol{r},t) + F_\perp(\boldsymbol{r},t), \tag{5.15b}$$

$$\begin{aligned}\dot{S}_z(\boldsymbol{r},t) &= \gamma_\parallel(\Lambda(\boldsymbol{r}) - S_z(\boldsymbol{r},t)) \\ &\quad + 2\mathrm{i}\sum_k [g_k^{R*}(\boldsymbol{r}) d_k^\dagger(t) S_-(\boldsymbol{r},t) - g_k^R(\boldsymbol{r}) S_+(\boldsymbol{r},t) d_k(t)] + F_\parallel(\boldsymbol{r},t),\end{aligned} \tag{5.15c}$$

where ω_k are the complex eigenvalues of $\mathcal{H}/\hbar$ defined in Eq. (4.64). Additionally, we now describe the atoms in terms of the atomic polarization and inversion densities operators

$$S_-(\boldsymbol{r},t) = \sum_p \sigma_{-p}(t)\,\delta(\boldsymbol{r} - \boldsymbol{r}_p), \tag{5.16a}$$

$$S_z(\boldsymbol{r},t) = \sum_p \sigma_{zp}(t)\,\delta(\boldsymbol{r} - \boldsymbol{r}_p), \tag{5.16b}$$

and the pump strength density

$$\Lambda(\boldsymbol{r}) = \sum_p \Lambda_p(t)\,\delta(\boldsymbol{r} - \boldsymbol{r}_p). \tag{5.17}$$

Since the linear transformation (4.69a) is not unitary there are two coupling amplitudes for each laser mode k,

$$g_k^R(\boldsymbol{r}) = -\mathrm{i}\sqrt{\frac{\nu}{2\hbar}}\boldsymbol{d}\cdot\boldsymbol{R}_k(\boldsymbol{r}) \quad \text{and} \quad g_k^L(\boldsymbol{r}) = -\mathrm{i}\sqrt{\frac{\nu}{2\hbar}}\boldsymbol{d}\cdot\boldsymbol{L}_k(\boldsymbol{r}), \tag{5.18}$$

associated with the kth right and left mode, $\boldsymbol{R}_k$, and $\boldsymbol{L}_k$, respectively. The field Langevin forces F_k are related with the input field through Eq. (4.73), their second order correlation functions are given by Eq. (4.74), while the correlation functions for the atomic Langevin density forces $F_{\|}(\boldsymbol{r},t) = \sum_p F_{\|p}(t)\,\delta(\boldsymbol{r}-\boldsymbol{r}_p)$ and $F_{\perp}(\boldsymbol{r},t) = \sum_p F_{\perp}(t)\,\delta(\boldsymbol{r}-\boldsymbol{r}_p)$ are given in Appendix 5.B. The proposed multi-mode laser equations (5.15) describe the laser phenomena in resonators with overlapping resonances. In the limiting case of weak damping they reduce to the standard laser equations [11]; then the set of left and right modes coincide and form an orthonormal basis, the operators d reduce to the operators a, and the coupling amplitudes $g^{L/R}$ equals the coupling amplitude g for orthogonal modes. Similar laser equations for nonorthogonal modes were introduce recently by Cheng and Siegman [35]. Earlier, Langevin laser equations in terms of non-orthogonal transverse modes of unstable cavities were deduced by Dutra et al [131, 132] using c-number representation instead of operators.

5.4 Below Threshold Operation

Before dealing with the complete non-linear dynamics of the laser equations we consider the operation below the laser threshold. This regime has previously been considered for one-dimensional cavities with arbitrary large couplings to the external field [133], in semiclassical studies of excess quantum noise [94], and in statistical studies of on the Petermann factor in chaotic cavities by Beenakker and coworkers [75, 73, 74]. In this section we estimate the laser threshold and evaluate the linear amplifier emission spectrum. Close to threshold the emission spectrum is dominated by the resonance with the smallest loss and its linewidth is seen to be enhanced by the Petermann excess noise factor as compare with its Schawlow–Townes value [23].

Below threshold the atomic and field operators are basically driven by the noise forces. The field exhibits big amplitude and phase fluctuations. In the steady-state the field is weak as it is generated only from spontaneous emission [11, 36]. The photonic population on the electromagnetic modes is then characterized by a thermal distribution and, inasmuch as the field intensity is small, the non-linear interaction in Eq. (5.14) between the field operators and the atomic inversion can be neglected. The inversion population S_z is then well approximated by its steady-state value

$$S_z(\boldsymbol{r},t) = \Lambda(\boldsymbol{r}), \tag{5.19}$$

determined just by the pumping process. Hence the field equations of motions (5.14) reduce to the linear coupled equations

$$\dot{d}_k(t) = -\mathrm{i}\omega_k d_k(t) - \mathrm{i}\int d\boldsymbol{r}\, g_k^{L*}(\boldsymbol{r}) S_-(\boldsymbol{r},t) + F_k(t), \tag{5.20a}$$

$$\dot{S}_-(\boldsymbol{r},t) = -(\mathrm{i}\nu + \gamma_\perp) S_-(\boldsymbol{r},t) + \mathrm{i}\Lambda \sum_k g_k^R(\boldsymbol{r}) d_k(t) + F_\perp(\boldsymbol{r},t). \tag{5.20b}$$

Here we assumed that the atomic medium fills the cavity uniformly and that the pumping is isotropic, so that $\Lambda(\boldsymbol{r}) = \Lambda$. This linear system of equations can be solved immediately by Fourier transformation. Introducing the operators in the frequency domain through

$$d_k(t) = \frac{1}{2\pi}\int \mathrm{d}\omega\, \mathrm{e}^{-\mathrm{i}\omega t} d_k(\omega), \tag{5.21}$$

$$S_-(\boldsymbol{r},t) = \frac{1}{2\pi}\int \mathrm{d}\omega\, \mathrm{e}^{-\mathrm{i}\omega t} S_-(\boldsymbol{r},\omega), \tag{5.22}$$

and in a similar fashion the noise operators, we may solve the resulting set of algebraic equations. To keep the notation simple the same symbol is used for both members of the Fourier transformed pair, the partners will be distinguished through their arguments. Provided all the poles of the resolvent lay in the lower half of the complex plane, the steady–state solution for the field is given by

$$d(\omega) = \mathrm{i}D^{-1}(\omega)G(\omega), \tag{5.23}$$

where we combined the mode operators and the noise operators to N-component vectors. The noise vector $G(\omega)$ has the elements

$$G_k(\omega) = F_k(\omega) + F_{\perp k}(\omega) \tag{5.24}$$

with

$$F_{\perp k}(\omega) = -\frac{\mathrm{i}}{\gamma_\perp + \mathrm{i}(\nu-\omega)}\int \mathrm{d}\boldsymbol{r} g_k^{L*}(\boldsymbol{r})F_\perp(\boldsymbol{r},t). \tag{5.25}$$

The inverse of the $N\times N$ resolvent matrix $D^{-1}(\omega)$ has elements

$$D_{kl}(\omega) = \delta_{kl}\left(\omega - \omega_k - \frac{\mathrm{i}Vg^2\Lambda}{\gamma_\perp + \mathrm{i}(\nu-\omega)}\right). \tag{5.26}$$

Here V is the cavity volume, $g^2 = \nu|\boldsymbol{d}|^2/(2\hbar V)$, and we used

$$\int d\boldsymbol{r}\, g_k^{L*}(\boldsymbol{r})g_l^R(\boldsymbol{r}) = Vg^2\delta_{kl}, \tag{5.27}$$

which is evaluated using the definitions (5.18) and the biorthogonality of left and right modes of the open cavity. The diagonal form of $D(\omega)$ in this representation is a consequence of our assumption of uniform gain over the cavity volume. The spatially uniform population inversion does not affect the spatial profile of the cold cavity modes and hence the eigenvectors of $\mathcal{H}$ and $D(\omega)$ coincide. The complex eigenfrequencies of oscillation, notwithstanding, differ according to Eq. (5.26).

For a given pumping value a description of the dynamics in the time domain is recovered from Eq. (5.23) by contour integration with a path closed in the lower half of the complex plane. In the linear regime the dynamics is then determined by the resonances $\bar{\omega}_k = \bar{\Omega}_k - \mathrm{i}\bar{\kappa}_k$ of the filled cavity. The cavity resonances are complex frequencies satisfying

$$\det[D(\bar{\omega})] = 0, \tag{5.28}$$

which are easily evaluated using the explicit form (5.26) for the elements of $D(\omega)$. For $\Lambda = 0$ all resonances of the filled cavity lay in the lower half of the complex plane and

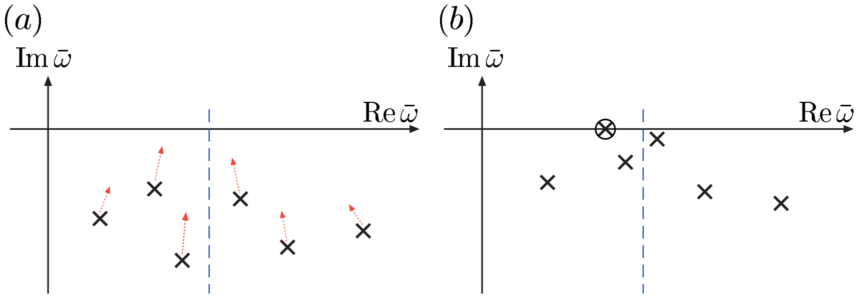

Figure 5.1: (a) Schematic illustration of the resonances (crosses) of the linear amplifier in the complex frequency plane. With increasing pump the resonances move towards the real axis as indicated by the arrows. The dashed line represents the center of the gain spectrum. (b) The lasing threshold is reached when the first resonance hits the real axis.

coincide with the empty cavity resonances, $\bar{\omega}_k = \omega_k$. As the pump increases the gain experienced by the resonance modes grows, and all resonances move towards the real axis. Additionally a frequency pulling by the active medium takes place and all resonances experience a shift towards the center of the Lorentzian gain profile. Resonances closer to the center of the gain profile move upward faster than those far from the it. The linear solution (5.23) breaks down when the first resonance reaches the real axis, and a steady–state solution no longer exists. Figure 5.1 illustrates schematically the resonance shift as function of the pump.

5.4.1 Laser Threshold

The solution (5.23) to the linear equations (5.20) gives an accurate description of the laser below threshold as long as the amplification of the noise is small; then the modes losses dominate and a steady–state solution exits. However, if the pump strength is increased such that the gain in the system overcomes the losses for any of the oscillating modes, an instability in the mode dynamics arises, the nonlinear terms neglected in going from Eq. (5.15) to Eq. (5.20) become relevant and the linear theory breaks down. The minimum value of the pumping parameter Λ for which this happens defines the laser threshold.

The k-mode will start to lase when its resonance reaches the real axis. Thus in order to find its threshold value one must look for real solutions, $\bar{\omega}_k = \bar{\omega}_k^* = \bar{\Omega}_k$, of Eq. (5.28). Using the definition (5.26) of the matrix $D(\omega)$, one must solve

$$\omega - \omega_k - \frac{\mathrm{i}Vg^2\Lambda}{\gamma_\perp + \mathrm{i}(\nu - \omega)} = 0 \tag{5.29}$$

for real ω. From the real part of this equation we obtain the resonance oscillating frequency

$$\bar{\Omega}_k = \frac{\gamma_\perp \Omega_k + \kappa_k \nu}{\gamma_\perp + \kappa_k}, \tag{5.30}$$

which for the lasing mode mode will determined the laser frequency. The imaginary part of Eq. (5.29) yields the value of pumping necessary for the k-resonance to reach the real axis,

$$\Lambda_k = \frac{\kappa_k \gamma_\perp}{V g^2} \left[1 + \left(\frac{\nu - \Omega_k}{\gamma_\perp + \kappa_k} \right)^2 \right]. \tag{5.31}$$

The laser threshold is given by the minimum value of all Λ_k,

$$\Lambda_{\rm th} = \min_k \Lambda_k, \tag{5.32}$$

and the corresponding mode will be the first to lase. Equation (5.31) shows that the laser threshold is fixed by the interplay between the empty cavity resonances and the gain provided by the atomic medium. Generally, however, one expects the lasing mode to be close to the center of the gain profile where the amplifying spectrum can be approximated by a flat spectrum. Then the second term in Eq. (5.31) can be neglected, and the lasing threshold is given by the condition that the lasing mode gain should equal its loss, $Vg^2\Lambda_{\rm th}/\gamma_\perp = \kappa_l$. Using this condition Beenakker and coworkers determined the distribution of the laser threshold for lasers in chaotic open cavities with overlapping [74] and isolated [129] resonances. For the latter they found the threshold distribution to be wide, its mean value being much smaller that the pumping rate necessary to compensate for the average loss.

5.4.2 Emission Power Spectrum

Below threshold the field dynamics inside the resonator is linear and the emission spectrum is easily recovered from the steady state solution (5.23) using the input-output formalism for linear amplifiers developed in Sec. 4.2.3. The emission power spectrum is defined in terms of the Wienier–Khintchine theorem [78]

$$\mathcal{S}(\omega) = \sum_m^{M(\omega)} \int_{-\infty}^{\infty} \mathrm{d}t\, \mathrm{e}^{-i\omega t} \langle b_m^{\rm out\dagger}(t) b_m^{\rm out}(0) \rangle. \tag{5.33}$$

The bosonic operators $b^{\rm out}$ and $b^{\rm out\dagger}$ are the creation and annihilation operators of the output field, m indexes the exterior channels, $M(\omega)$ is the number of open channels at frequency ω, and $\langle \ldots \rangle$ denotes the quantum average respect to the initial state of the output electromagnetic field. Using the definitions (4.10), the above expression reduces to

$$\mathcal{S}(\omega) = \frac{1}{2\pi} \sum_m^{M(\omega)} \langle b_m^{\rm out\dagger}(\omega) b_m^{\rm out}(\omega) \rangle. \tag{5.34}$$

The output field operators are related with the cavity field operators through the input-output relations (4.76). Combining Eqs. (4.76), (5.23), and (5.24) we may express the output field operators in terms of the input operators and the cavity field noise,

$$b^{\rm out}(\omega) = S(\omega) b^{\rm in}(\omega) + V(\omega) T F_\perp(\omega), \tag{5.35}$$

where we combined the input and output operators at frequency ω to M-component vectors and the noise operators to an N-component vector, $V(\omega) = \mathcal{W}^\dagger T D^{-1}(\omega) T^{-1}$ is an $M \times N$ matrix, and the $M \times M$ scattering matrix is given by

$$S(\omega) = \mathbb{1} - 2\pi\mathrm{i} \mathcal{W}^\dagger T D^{-1}(\omega) T^{-1} \mathcal{W}. \tag{5.36}$$

The linear amplifier emission spectrum is obtained by substituting Eq. (5.35) into Eq. (5.34) and performing the quantum average. In the absence of external illumination ($\langle b^{\mathrm{in}\dagger} b^{\mathrm{in}} \rangle = 0$) the emission spectrum reduces to

$$\mathcal{S}(\omega) = \frac{1}{2\pi} \sum_{kl} [T^\dagger V^\dagger(\omega) V(\omega) T]_{kl} \langle F^\dagger_{\perp k}(\omega) F_{\perp l}(\omega) \rangle. \tag{5.37}$$

For an atomic medium uniformly distributed over the cavity volume the correlation function of the noise operators reduces to,

$$\langle F^\dagger_{\perp k}(\omega) F_{\perp l}(\omega') \rangle = \frac{4\pi V g^2 \gamma_\perp \overline{S_1}}{\gamma_\perp^2 + (\nu - \omega)^2} \langle \boldsymbol{L}_l | \boldsymbol{L}_k \rangle \delta(\omega - \omega'), \tag{5.38}$$

where we used the relations in Appendix 5.B. Taking into account that $\langle \boldsymbol{L}_l | \boldsymbol{L}_k \rangle = (T^{-1} T^{-1\dagger})_{lk}$, the emission spectrum can be written as

$$\mathcal{S}(\omega) = \frac{2V g^2 \gamma_\perp \overline{S_1}}{\gamma_\perp^2 + (\nu - \omega)^2} \,\mathrm{Tr}[V^\dagger(\omega) V(\omega)]. \tag{5.39}$$

Using the definition (5.36) of the scattering matrix, one easily shows that $S(\omega) S^\dagger(\omega) - \mathbb{1} = \big(4\pi V g^2 \gamma_\perp S_0 / (\gamma_\perp^2 + (\nu - \omega)^2)\big) V(\omega) V^\dagger(\omega)$, so that the emission spectrum can be expressed in terms of the system scattering matrix,

$$\mathcal{S}(\omega) = \frac{\overline{S_1}}{2\pi(\overline{S_1} - \overline{S_0})} \,\mathrm{Tr}[S(\omega) S^\dagger(\omega) - \mathbb{1}]. \tag{5.40}$$

Here $\overline{S_1}$ and $\overline{S_0}$ are the mean atomic population operators for the upper and lower atomic levels, and we used $\Lambda = \overline{S_1} - \overline{S_0}$, which holds below threshold, to express the spectrum in terms of the incomplete population inversion. This result for the emission spectrum corresponds to *Kirchkoff's law*, relating the thermal emission with the amplification [69, 74].

It is illustrative to write down the emission spectrum (5.39) in terms of the complex eigenfrequencies and non-orthogonal eigenmodes of the open empty cavity. After a straight forward calculation one obtains

$$\mathcal{S}(\omega) = \frac{2V g^2 \gamma_\perp \overline{S_1}}{\pi[\gamma_\perp^2 + (\nu - \omega)^2]} \left[\sum_l \frac{\kappa_l K_l}{|D_{ll}(\omega)|^2} + \sum_k \sum_{l<k} \mathrm{Im} \left[\frac{(\omega_l^* - \omega_k) \langle \boldsymbol{R}_l | \boldsymbol{R}_k \rangle \langle \boldsymbol{L}_k | \boldsymbol{L}_l \rangle}{D_{kk}(\omega) D_{ll}^*(\omega)} \right] \right], \tag{5.41}$$

where K_l is the Petermann factor associated with the l-mode as defined in Eq. (4.68). The first sum inside the brackets is the contribution to the emission spectrum from the individual resonances, and is the only term one could anticipate from the standard theory of lasers [11]. Each term in this sum is approximated by a Lorentzian centered on the resonance frequency $\mathrm{Re}\big(\bar{\omega}_l(\Lambda)\big)$ and with fullwidth at half maximum given by $2\mathrm{Im}\big(\bar{\omega}_l(\Lambda)\big)$. Each of these contributions is proportional to the Petermann factor. This last feature is solely due to the non-orthogonal character [24, 25] of the field modes, and is absent in the case of isolated resonances. The main difference between our result and the emission spectrum expected from standard laser theory is the presence of the double sum term inside the brackets. It accounts for the correlation among the different modes and is proportional to their overlap $\langle \boldsymbol{R}_l|\boldsymbol{R}_k\rangle\langle \boldsymbol{L}_k|\boldsymbol{L}_l\rangle$. In the limit of orthogonal modes, right and left eigenmodes coincide and form an orthogonal set, the cross terms contribution vanish, and the Petermann factor is equal one. In this limit, Eq. (5.41) reduces to the emission spectrum for a linear amplifier with isolated resonances.

Excess Noise and Linewidth

Close to threshold the gain experienced by the lasing mode, say the mode with $k = 0$, almost completely compensates its losses. The emission spectrum is then mainly determined by this mode and we need to retain only its diagonal contribution. For a mode close to the center of the gain profile, the emission spectrum is then approximated by the Lorentzian

$$\mathcal{S}(\omega) \simeq \frac{2K_0\kappa_0\overline{S_1}}{\pi\Lambda[(\omega-\bar{\Omega}_0)^2+\frac{1}{4}\delta\omega^2]}, \tag{5.42}$$

with full width at half maximum $\delta\omega$. Here we used $Vg^2/\gamma_\perp \sim \kappa_l/\Lambda$, which holds close to threshold for modes in the center of the gain profile.

It is possible to express $\delta\omega$ in terms of the total output photon current. The later follows from Eq. (5.42) upon integrating over frequency,

$$I_{\text{out}} = \frac{4K_0\kappa_0^2\overline{S_1}}{\Lambda\delta\omega}. \tag{5.43}$$

If we now recall the Schawlow–Townes formula for the linewidth $\delta\omega_{\text{ST}} = 2\kappa_0^2/I_{\text{out}}$, it follows from Eq. (5.43) that the linewidth of the lasing mode is given by

$$\delta\omega = 2K_0\frac{\overline{S_1}}{\Lambda}\delta\omega_{\text{ST}}, \tag{5.44}$$

where an enhancement as compared with the Schawlow–Townes value is observed. The factor two in the relation is consequence of the below threshold calculation in which both phase and amplitude fluctuations are included; above threshold the non-linearities greatly suppress the amplitude fluctuations reducing the linewidth by a factor two [11]. The remaining two other factors are generally named excess noise factors. The factor $\overline{S_1}/\Lambda = \overline{S_1}/(\overline{S_1}-\overline{S_0})$ accounts for an extra noise due to the incomplete population inversion. The enhancement due to the Petermann factor, was discussed above, and is a signature of the nonorthogonal nature of the electromagnetic modes. A similar below threshold approach to excess noise was followed by Beenakker and co-workers in their statistical analysis of the Petermann factor in chaotic cavities [73, 74, 75]. A derivation of the linewidth enhancement for a lasing mode above threshold is presented in the following chapter.

5.A Atomic Decay Rate

Here we derive the atomic decay rate $\gamma_{\rm at}$ dropping the rotating wave approximation for the field dynamics. Our starting point is Eq. (5.7), which when written in terms of the exact modes of the total system takes the form [95]

$$C_{ij}(t-t') = \Theta(t-t') \sum_m \int_{\omega_m}^{\infty} \mathrm{d}\omega \; \frac{\hbar\omega}{2} f_{mi}(\omega, \boldsymbol{r}_0) f^*_{mj}(\omega, \mathbf{r}_0) \mathrm{e}^{-\mathrm{i}\omega(t-t')}. \tag{5.A.1}$$

The Fourier transform of this equation is readily evaluated,

$$C_{ij}(\nu + \mathrm{i}\epsilon) = \mathrm{i} \sum_m \int_{\omega_m}^{\infty} \mathrm{d}\omega \frac{\hbar\omega}{2} \frac{f_{mi}(\omega, \boldsymbol{r}_0) f^*_{mj}(\omega, \boldsymbol{r}_0)}{(\nu - \omega) + \mathrm{i}\epsilon}. \tag{5.A.2}$$

Substitution into Eq. (5.6) yields the golden rule result

$$\gamma_{\rm at} = \frac{\pi}{\hbar^2} \sum_{ij} \sum_m \int_{\omega_m}^{\infty} \mathrm{d}\omega \; \hbar\omega [d_i d^*_j f_{mi}(\omega, \boldsymbol{r}_0) f^*_{mj}(\omega, \boldsymbol{r}_0) \delta(\omega - \nu)]. \tag{5.A.3}$$

The atom is located inside the cavity. Therefore, we can use the mode expansion (3.47) to replace the modes of the total system by the cavity modes,

$$\gamma_{\rm at} = \frac{\pi}{\hbar^2} \sum_{ij} \int_{\omega_m}^{\infty} \mathrm{d}\omega \; \hbar\omega \; d_i d^*_j \left[\sum_{\lambda\lambda'} \sum_m u_{\lambda i}(\boldsymbol{r}_0) u^*_{\lambda' j}(\boldsymbol{r}_0) \alpha_{\lambda m}(\omega) \alpha^*_{\lambda' m}(\omega) \right] \delta(\omega - \nu). \tag{5.A.4}$$

The quantity in square brackets is proportional to the local density of states $\rho(\omega, \boldsymbol{r}_0)$ (see Eq. (3.C.4)), which can be written in terms of the Green's function projected onto the resonator space (3.43),

$$\rho(\omega_0, \boldsymbol{r}_0) = -\frac{2\nu}{\pi c^2} \mathrm{Im} \langle \boldsymbol{r}_0 | \mathcal{G}_{\mathcal{QQ}}(\omega_0) | \boldsymbol{r}_0 \rangle \, . \tag{5.A.5}$$

Hence, the atomic decay rate has the same form as in Eq. (5.13a) but with a modified local density of modes

$$\rho(\nu, \boldsymbol{r}_0) = \frac{2\nu}{\pi c^2} \mathrm{Im} \left[\sum_k \frac{l^*_k(\nu, \boldsymbol{r}_0) r_k(\nu, \boldsymbol{r}_0)}{\sigma^2_k(\nu) - \frac{\nu^2}{c^2}} \right], \tag{5.A.6}$$

where l_k and r_k are the left and right eigenmodes and σ_k^2 the eigenvalues of the non-Hermitian operator $L_{\rm eff}(\nu)$. Equation (5.13) is recovered in the rotating wave approximation. Then the eigenmodes of $L_{\rm eff}$ are simply related to the eigenmodes of the non–Hermitean matrix D^{-1}, $l_k \approx L_k$ and $r_k \approx R_k$, and the eigenvalues of $L_{\rm eff}(\nu)$ can be approximated by

$$\sigma^2_k \approx \left(\frac{\Omega_k}{c} \right)^2 - \frac{i2\nu}{c^2} \kappa_k, \tag{5.A.7}$$

where Ω_k and κ_k are the mode frequency and the mode broadening, respectively.

5.B Noise Correlation Functions

The correlation functions for the atomic noise operators $F_{\perp p}$ and $F_{\parallel p}$ in the laser equations (5.14) can be found in [10, 11]. Those different from zero are

$$\langle F^{\dagger}_{\perp p}(t)F_{\perp p}(t')\rangle = \Big(\frac{\gamma_{\parallel}}{2}(\Lambda_p - \langle\sigma_{zp}(t)\rangle) + 2\gamma_{\perp}\langle\sigma_{1p}(t)\rangle\Big)\,\delta(t-t'), \tag{5.B.1a}$$

$$\langle F_{\perp p}(t)F^{\dagger}_{\perp p}(t')\rangle = \Big(-\frac{\gamma_{\parallel}}{2}(\Lambda_p - \langle\sigma_{zp}(t)\rangle) + 2\gamma_{\perp}\langle\sigma_{0p}(t)\rangle\Big)\,\delta(t-t'), \tag{5.B.1b}$$

$$\langle F_{\perp p}(t)F_{\parallel p}(t')\rangle = \gamma_{\parallel}(1-\Lambda_p)\langle\sigma_{-p}(t)\rangle\,\delta(t-t'), \tag{5.B.1c}$$

$$\langle F_{\parallel p}(t)F_{\perp p}(t')\rangle = -\gamma_{\parallel}(1+\Lambda_p)\langle\sigma_{-p}(t)\rangle\,\delta(t-t'), \tag{5.B.1d}$$

$$\langle F^{\dagger}_{\perp p}(t)F_{\parallel p}(t')\rangle = -\gamma_{\parallel}(1+\Lambda_p)\langle\sigma^{\dagger}_{-p}(t)\rangle\,\delta(t-t'), \tag{5.B.1e}$$

$$\langle F_{\parallel p}(t)F^{\dagger}_{\perp p}(t')\rangle = \gamma_{\parallel}(1-\Lambda_p)\langle\sigma^{\dagger}_{-p}(t)\rangle\,\delta(t-t'), \tag{5.B.1f}$$

$$\langle F_{\parallel p}(t)F^{\dagger}_{\parallel p}(t')\rangle = 2\gamma_{\parallel}(1-\Lambda_p\langle\sigma_{zp}(t)\rangle)\,\delta(t-t'), \tag{5.B.1g}$$

where $\langle\sigma_{1p}(t)\rangle$ and $\langle\sigma_{0p}(t)\rangle$ are the atomic mean population in the upper and lower atomic state, respectively. In the case of two–level atoms they are defined through the relations $\langle\sigma_{1p}(t)\rangle + \langle\sigma_{0p}(t)\rangle = 1$ and $\langle\sigma_{1p}(t)\rangle - \langle\sigma_{0p}(t)\rangle = \langle\sigma_{zp}(t)\rangle$.

The correlation functions for the atomic Langevin density forces

$$F_{\parallel}(\boldsymbol{r},t) = \sum_p F_{\parallel p}(t)\,\delta(\boldsymbol{r}-\boldsymbol{r}_p) \quad \text{and} \quad F_{\perp}(\boldsymbol{r},t) = \sum_p F_{\perp}(t)\,\delta(\boldsymbol{r}-\boldsymbol{r}_p) \tag{5.B.2}$$

in the laser equations (5.15), follow from the correlation functions (5.B.1),

$$\langle F^{\dagger}_{\perp}(\boldsymbol{r},t)F_{\perp}(\boldsymbol{r}',t')\rangle = \Big(\frac{\gamma_{\parallel}}{2}(\Lambda(\boldsymbol{r}) - \overline{S_z(\boldsymbol{r},t)}) + 2\gamma_{\perp}\overline{S_1(\boldsymbol{r},t)}\Big)\,\delta(\boldsymbol{r}-\boldsymbol{r}')\,\delta(t-t') \tag{5.B.3a}$$

$$\langle F_{\perp}(\boldsymbol{r},t)F^{\dagger}_{\perp}(\boldsymbol{r}',t')\rangle = \Big(-\frac{\gamma_{\parallel}}{2}(\Lambda(\boldsymbol{r}) - \overline{S_z(\boldsymbol{r},t)}) + 2\gamma_{\perp}\overline{S_0(\boldsymbol{r},t)}\Big)\,\delta(\boldsymbol{r}-\boldsymbol{r}')\,\delta(t-t'), \tag{5.B.3b}$$

$$\langle F_{\perp}(\boldsymbol{r},t)F_{\parallel}(\boldsymbol{r}',t')\rangle = \gamma_{\parallel}(1-\Lambda(\boldsymbol{r}))\overline{S_-(\boldsymbol{r},t)}\,\delta(\boldsymbol{r}-\boldsymbol{r}')\,\delta(t-t'), \tag{5.B.3c}$$

$$\langle F_{\parallel}(\boldsymbol{r},t)F_{\perp}(\boldsymbol{r}',t')\rangle = -\gamma_{\parallel}(1+\Lambda(\boldsymbol{r}))\overline{S_-(\boldsymbol{r},t)}\,\delta(\boldsymbol{r}-\boldsymbol{r}')\,\delta(t-t'), \tag{5.B.3d}$$

$$\langle F^{\dagger}_{\perp}(\boldsymbol{r},t)F_{\parallel}(\boldsymbol{r}',t')\rangle = -\gamma_{\parallel}(1+\Lambda(\boldsymbol{r}))\overline{S_+(\boldsymbol{r},t)}\,\delta(\boldsymbol{r}-\boldsymbol{r}')\,\delta(t-t'), \tag{5.B.3e}$$

$$\langle F_{\parallel}(\boldsymbol{r},t)F^{\dagger}_{\perp}(\boldsymbol{r}',t')\rangle = \gamma_{\parallel}(1-\Lambda(\boldsymbol{r}))\overline{S_+(\boldsymbol{r},t)}\,\delta(\boldsymbol{r}-\boldsymbol{r}')\,\delta(t-t'), \tag{5.B.3f}$$

$$\langle F_{\parallel}(\boldsymbol{r},t)F^{\dagger}_{\parallel}(\boldsymbol{r}',t')\rangle = 2\gamma_{\parallel}(1-\Lambda(\boldsymbol{r})\overline{S_z(\boldsymbol{r},t)})\,\delta(\boldsymbol{r}-\boldsymbol{r}')\,\delta(t-t'), \tag{5.B.3g}$$

where $\overline{S_1(\boldsymbol{r})}$ and $\overline{S_0(\boldsymbol{r})}$ are the mean atomic population density operators for the upper and lower atomic levels. All other correlation functions involving one or two noise operators vanish.

Chapter 6

Laser with Overlapping Resonances: Single-Mode Operation

Lasers in cavities with overlapping resonances exhibit unusual noise properties. This fact, by now extensively confirmed by experiments [27, 29, 30], was first noticed by Petermann [22] in his semiclassical analysis of the fundamental linewidth in gain-guided semiconductor lasers. This kind of lasers exhibit a greatly enhanced linewidth as compared with the Schawlow-Townes value; the associated excess noise factor was later named after Petermann. Later, Siegman[24, 25] attributed the origin of the Petermann excess noise factor to the nonorthogonality of the modes in cavities with overlapping resonances, showing that excess noise is the fingerprint of optical systems with nonorthogonal modes. Although Siegman's semiclassical theory provides a detailed description of excess noise, to the best of our knowledge, a complete quantum laser theory of that phenomenon was lacking. We address this problem in this chapter.

We use the laser Langevin equations for overlapping resonances derived in *Chapter 5* to study the emission power spectrum of a single-mode laser oscillator. Excess noise emerges in our equations as a consequence of the correlations between noise forces corresponding to different modes. Excess noise thus is, in essence, a multi-mode phenomenon. In order to properly account for that phenomenon we not only consider the lasing mode but also the below threshold modes, retaining the full multi-mode character of the problem. In that respect our approach differs from other studies [25] of excess noise which neglect the below threshold modes altogether arguing that they are overwhelmed by the intensity of the lasing mode. We show that this argument, derived from the knowledge in standard lasers, must be reformulated when applied to lasers with overlapping resonances. Indeed, while in standard lasers contributions to the emission spectrum arise only from the autocorrelation functions of the modes, additional contributions are obtained in lasers with overlapping resonances from the nonvanishing correlations between different modes. The autocorrelation functions are proportional to the mode intensities, so that modes below threshold typically contribute negligible to the output intensity. The same holds for most of the cross-correlation contributions, namely for those that involve two below threshold modes. There are, however, cross-correlation functions that involve the lasing mode and a below threshold mode, which are therefore only linear in the below threshold mode amplitude. Such correlation functions comprise the effects of the below threshold modes on the lasing mode noise properties. In this chapter we show that such contributions may introduce dramatic changes to the laser spectrum lineshape.

Our evaluation of the emission spectrum proceed by first considering the contributions from the lasing mode. We recover a Lorentzian lineshape with a linewidth enhanced by the Petermann factor. Next we evaluate the contributions from cross-correlations between the lasing mode and the below threshold modes. These contributions to the spectrum are show to be important above threshold, where they lead to deviations of the lineshape from Lorentzian form. Such deviations are most important when both below threshold modes are close to threshold and have frequencies close to the laser frequency. Our result for the emission spectrum can be tested in unstable cavities, but is also important for single-mode lasers in chaotic cavities and random media.

6.1 Laser Equations

In this chapter we are mainly interested in the effects that the nonorthogonality of the open cavity modes may have on the power spectrum of a single-mode laser oscillation. To exhibit these effects most clearly, we shall introduce some approximations to the laser model presented in *Chapter 5*. The first approximation is to assume the atomic population inversion to be spatially uniform[1] and replace it by its average over the cavity volume,

$$S_z(t) = \frac{1}{V} \int \mathrm{d}\boldsymbol{r}\, S_z(\boldsymbol{r}, t). \tag{6.1}$$

Physically this approximation amounts to neglecting spatial hole burning, thereby inhibiting mode competition and effectively allowing only for single-mode laser operation above threshold [36]. In addition, we also take the pumping to be isotropic and uniform all over the cavity volume, $\Lambda(\boldsymbol{r}) = \Lambda$. The major simplification that these approximations yield is that the modes of the load cavity, i.e., the modes of the cavity filled with the active medium, coincide with the modes of the empty cavity for all values of the pumping. The second approximation consist in restricting our study to lasers for which the dipole relaxation rate of the active medium is much larger than both the inversion relaxation rate and the characteristic decay rate of the open cavity modes, $\gamma_\perp \gg \gamma_\parallel, \bar{\kappa}$; this is an approximation valid for most solid-state lasers. The atomic polarization can thus be adiabatically eliminated from the equations of motions (5.15). As a consequence, the polarization

$$S_-(\boldsymbol{r}, t) = \mathrm{i} \sum_k \frac{g_k^R(\boldsymbol{r}) d_k(t) S_z(t)}{\gamma_\perp + \mathrm{i}(\nu - \bar{\Omega}_k)} + \frac{1}{\gamma_\perp} F_\perp(\boldsymbol{r}, t), \tag{6.2}$$

[1] This approximation is quite reasonable for gas lasers in which the atoms, due to the rapid thermal motion, diffuse fast enough to destroy spatial hole burning [131, 132]. The argument, however, should be used with caution. In order to destroy hole burning the minimum atomic velocity is given by $v \approx D/\lambda \gg \lambda\gamma_\perp$, where D is the diffusion constant and λ the light wave length. If v is too large, the motion of the atoms may lead to an inhomogeneously broadened gain line due to the Doppler effect, a situation not covered by our laser equations.

follows instantaneously the phase of the cavity field. The frequencies $\bar{\Omega}_k$ are the real part of the complex oscillation frequencies $\bar{\omega}_k = \bar{\Omega}_k - \mathrm{i}\bar{\kappa}_k$ of the cavity modes in the presence of the active medium; they are still to be determined. Substituting this expression into the remaining equations for the field operators and the atomic inversion, one obtains the simplified laser equations

$$\dot{d}_k(t) = \big[-\mathrm{i}\omega_k + W_k S_z(t)\big] d_k(t) + G_k(t), \tag{6.3a}$$

$$\dot{S}_z(t) = \gamma_{\|}(\Lambda - S_z(t)) - \frac{2}{V}\sum_{kl}\big(W_k^* + W_l\big)\langle \boldsymbol{R}_k|\boldsymbol{R}_l\rangle d_k^\dagger(t) d_l(t) S_z(t) + G_{\|}(t)\,, \tag{6.3b}$$

where

$$W_k = \frac{V g^2}{\big(\gamma_\perp + \mathrm{i}(\nu - \bar{\Omega}_k)\big)}. \tag{6.4}$$

The noise terms for the field amplitudes are now given by

$$G_k(t) = F_k(t) + F_{\perp k}(t)\,, \tag{6.5a}$$

with

$$F_{\perp k}(t) \equiv -\frac{\mathrm{i}}{\gamma_\perp}\int d\boldsymbol{r}\, g_k^{L*}(\boldsymbol{r}) F_\perp(\boldsymbol{r},t), \tag{6.5b}$$

and the Langevin forces for the population inversion are

$$G_{\|}(\boldsymbol{r},t) = F_{\|}(\boldsymbol{r},t) + \frac{2\mathrm{i}}{V\gamma_\perp}\sum_k \int \mathrm{d}\boldsymbol{r}\,\big[g_k^{R*}(\boldsymbol{r}) d_k^\dagger(t) F_\perp(\boldsymbol{r},t) - g_k^R(\boldsymbol{r}) F_\perp^\dagger(\boldsymbol{r},t) d_k(t)\big]. \tag{6.6}$$

These new noise operators are easily shown to still provide a noise with a white spectrum. Their second moments are evaluated using the definitions (4.28), (6.5a), (6.6), and the correlations functions for the atomic noise forces listed in Appendix 5.B. The nonvanishing correlation functions for the field noise forces $G_k(t)$ are given in the Appendix 6.A.

6.2 Single-Mode Laser Operation

The semiclassical laser equations obtained from Eq. (6.3) by averaging over the state of the system were shown by Hacken[36] to have only a single stable steady–state solution for all values of pumping above the threshold. This solution corresponds to a selfsustained laser oscillation in a single-mode of the open cavity. The existence of this single solution is a consequence of neglecting spatial hole burning, as the lasing mode deflects the atomic inversion uniformly over the cavity inhibiting other modes from lasing. In what remains of this chapter, we use the laser equations (6.3) to determine the emission spectrum in the lasing regime.

6.2.1 Steady-State Solution

In the lasing regime only a single cavity mode, say the mode with $k = 0$, is above threshold, while all other modes, with $k \neq 0$, remain below threshold. We decompose the field amplitudes and the atomic population inversion into their classical steady-state value and their quantum fluctuations[2],

$$d_k(t) = (\overline{d_k} + \delta d_k(t))\mathrm{e}^{-\mathrm{i}\bar{\omega}_k t}, \tag{6.7a}$$

$$S_z(t) = \overline{S_z} + \delta S_z(t). \tag{6.7b}$$

In a single-mode laser there is a selfsustained oscillation in the laser mode with frequency $\bar{\omega}_0 = \bar{\Omega}_0$. Sufficiently far above threshold its amplitude is much in excess of the amplitudes in any of the other modes that remain below threshold. The steady-state field amplitudes are given by $\overline{d_0} \neq 0$, and $\overline{d_k} = 0$ for $k \neq 0$. Consequently, the atomic medium only "sees" the lasing mode, and the classical steady-state solutions for the laser mode amplitude and the atomic population satisfy the following equations

$$\left[\mathrm{i}(\bar{\Omega}_0 - \Omega_0) - \kappa_0 + W_0\overline{S_z}\right]\overline{d_0} = 0, \tag{6.8a}$$

$$\gamma_{\|}(\Lambda - \overline{S_z}) - \frac{4}{V}\mathcal{L}_0\overline{I}_0\overline{S_z} = 0. \tag{6.8b}$$

Here we have introduced the Lorentzian function $\mathcal{L}_0 = \mathrm{Re}[W_0]$ and the steady-state field intensity $\overline{I_0} = \langle \boldsymbol{R}_0|\boldsymbol{R}_0\rangle|\overline{d_0}|^2$. Separating the expression inside the brackets in Eq. (6.8a) into its real an imaginary parts, we obtain the steady-state value for the population inversion and the laser oscillation frequency,

$$\overline{S_z} = \frac{\kappa_0}{\mathcal{L}_0} = \Lambda_{\mathrm{th}}\,, \tag{6.9}$$

$$\bar{\Omega}_0 = \frac{\gamma_\perp\Omega_0 + \kappa_0\nu}{\gamma_\perp + \kappa_0} \simeq \Omega_0 + \frac{\kappa_0}{\gamma_\perp}\nu\,, \tag{6.10}$$

which coincide with the threshold conditions Eqs. (5.31) and (5.32) obtained in the study of the below threshold problem in Sec. 5.4. The steady-state solution for the field intensity follows from Eq. (6.8b),

$$\overline{I}_0 = \frac{V\gamma_{\|}}{4\mathcal{L}_0}\left(\frac{\Lambda}{\overline{S_z}} - 1\right). \tag{6.11}$$

We notice that the mean optical phase of the laser field does not enter the steady-state solutions. This is related with the fact that in the steady-state the optical phase of the laser mode is randomly distributed between 0 and 2π. We can then conveniently choose the arbitrary mean value of the phase to be equal to 0, since then the steady-state field amplitude $\overline{d_0}$ becomes real.

[2]That decomposition is always possible whenever the number of atoms inside the cavity is large $\mathcal{N} \gg 1$ and the medium is distributed over the whole cavity. Then, the field intensity and the atomic variables scale proportional to $\mathcal{N}$ while the noise forces scale as $\sqrt{\mathcal{N}}$. Accordingly the noise terms become much smaller than the deterministic terms in the limit $\mathcal{N} \gg 1$ [134, 39].

6.2.2 Dynamics of the Field Fluctuations

The equations of motion for the quantum fluctuations follow upon linearization of the laser equations (6.3) around the steady–state solution. The result is

$$\delta\dot{d}_k(t) = \tilde{G}_k(t); \qquad (k \neq 0)\,, \tag{6.12a}$$

$$\delta\dot{d}_0(t) = W_0\overline{d_0}\delta S_z(t) + \tilde{G}_0(t)\,, \tag{6.12b}$$

$$\delta\dot{S}_z(t) = -\gamma_\parallel \frac{\Lambda}{\overline{S_z}}\delta S_z(t) - \frac{2\overline{d_0 S_z}}{V}\sum_k \left[(W_0 + W_k^*)\langle \boldsymbol{R}_k|\boldsymbol{R}_0\rangle \delta d_k + \text{ H.c. }\right] + G_\parallel(t)\,. \tag{6.12c}$$

Here we used $\overline{d_0} = \overline{d_0^*}$ and defined $\tilde{G}_0(t) = \mathrm{e}^{\mathrm{i}\bar{\Omega}_0 t}G_0(t)$ and $\tilde{G}_k(t) = \mathrm{e}^{\mathrm{i}\bar{\omega}_k t}G_k(t)$. We note that the equations of motion for the field modes below threshold decouple and can be solve immediately; they correspond to the equations of motion of a linear amplifier studied in Sec. 5.4. It follows that the complex oscillation frequencies $\bar{\omega}_k$ of the below threshold modes are solutions of the equation $\mathrm{i}(\bar{\omega}_k - \omega_k) + W_k\overline{S}_z = 0$. The linear set of equations (6.12) can be solved exactly by Fourier transformation. We define the field fluctuation operators in the frequency domain through

$$\delta d_k(t) = \frac{1}{2\pi}\int \mathrm{d}\omega\, \mathrm{e}^{\mathrm{i}\omega t}\delta d_k(\omega), \tag{6.13}$$

and analogous for the population inversion operator and the noise operators. For notational simplicity we again use the same symbol for both members of the Fourier transformed pair. The new variables obey the algebraic set of equations

$$-\mathrm{i}\omega\delta d_k(\omega) = \tilde{G}_k(\omega)\,; \qquad (k \neq 0)\,, \tag{6.14a}$$

$$-\mathrm{i}\omega\delta d_0(\omega) = W_0\overline{d_0}\delta S_z(\omega) + \tilde{G}_0(\omega)\,, \tag{6.14b}$$

$$\begin{aligned} -\mathrm{i}\omega\delta S_z(\omega) &= -\gamma_\parallel \frac{\Lambda}{\overline{S_z}}\delta S_z(\omega) \\ &\quad - \frac{2\overline{d_0 S_0}}{V}\sum_k \left[(W_0 + W_k^*)\langle \boldsymbol{R}_k|\boldsymbol{R}_0\rangle \delta d_k(\omega) + \text{ H.c. }\right] + G_\parallel(\omega)\,. \end{aligned} \tag{6.14c}$$

The solution of these coupled equations is easily obtained. The correlation functions for the ω-dependent fluctuation forces, can be evaluated using the relations given in Appendix 5.B.

6.2.3 Field Quadratures

Since we are mainly interested on the laser field fluctuations, the relevant quantities to be determined are the amplitude and phase quadrature components of the lasing mode fluctuations. For our choice of phase for the field steady-state solution, these quadratures are defined by [77, 135, 134]

$$\delta X_0(\omega) = \frac{1}{2}\big(\delta d_0(\omega) + \delta d_0^\dagger(-\omega)\big)\,, \tag{6.15a}$$

$$\delta Y_0(\omega) = \frac{1}{2\mathrm{i}}\big(\delta d_0(\omega) - \delta d_0^\dagger(-\omega)\big)\,. \tag{6.15b}$$

Using Eq. (6.14b), the quadrature components can be written as

$$\delta X_0(\omega) = \frac{\mathrm{i}}{2\omega}\left[2\overline{d}_0\mathrm{Re}[W_0]\delta S_z(\omega) + \tilde{G}(\omega) + \tilde{G}_0^\dagger(-\omega)\right], \tag{6.16a}$$

$$\delta Y_0(\omega) = \frac{1}{2\omega}\left[2\mathrm{i}\overline{d}_0\mathrm{Im}[W_0]\delta S_z(\omega) + \tilde{G}(\omega) - \tilde{G}_0^\dagger(-\omega)\right], \tag{6.16b}$$

where we used that $\delta S_z(t)$ is a Hermitian operator, so that $\delta S_z(\omega) = \delta S_z^\dagger(-\omega)$. We notice that for a detuned laser $\mathrm{Im}[W_0] \neq 0$, and amplitude and phase fluctuations couple. Sufficiently far above threshold the laser amplitude stabilizes and its fluctuations become negligible, then the laser field emission power spectrum is determined solely from the phase fluctuations. For a detuned laser, due to the coupling to the amplitude fluctuations, the phase fluctuations are enhanced [136]. This yield the well-known enhancement factor $(1+\alpha^2)$ in the emission linewidth. The dimensionless detuning parameter α is defined as the ratio $(\nu - \bar{\Omega}_0)/\gamma_\perp$ and is formally equivalent [137] to the Henry parameter [138, 139] in semiconductor lasers; the latter originates from the coupling between amplitude and phase fluctuations induced by changes in the refractive index due to the relaxation oscillations that follow a spontaneous emission event. The complete effect of detuning between the laser and the atomic medium can be encoded in the Henry factor. In what remains of the chapter we assume the laser to be on resonance and defer the discussion of our results for the detune case to the Appendix 6.C.

6.2.4 Phase Diffusion Coefficient

Far above threshold the laser power spectrum is determined from the phase fluctuations. Small phase fluctuations are related to the phase quadrature component of the field fluctuations by

$$\delta\phi(t) = \frac{1}{\overline{d}_0}\delta Y_0(t), \tag{6.17}$$

which, after using Eq.(6.16b), for a laser with zero detuning reduces to

$$\delta\phi(\omega) = \frac{1}{2\omega\overline{d}_0}\left(\tilde{G}_0(\omega) - \tilde{G}_0^\dagger(-\omega)\right). \tag{6.18}$$

The phase fluctuations are therefore linear superpositions of Gaussian random variables and thus behave like random Gaussian variables themselves. We notice that the phase fluctuations diverge when $\omega \to 0$. This divergence is related to the phase diffusion process encountered far above threshold. In order to see this, let us first consider the second order phase correlation function

$$\begin{aligned}\langle\delta\phi(\omega)\delta\phi(\omega')\rangle &= -\frac{1}{4\omega\omega'\overline{d}_0^2}\langle\tilde{G}_0(\omega)\tilde{G}_0^\dagger(-\omega') + \tilde{G}_0^\dagger(-\omega)\tilde{G}_0(\omega')\rangle \\ &= 2\pi[\delta\phi^2]_\omega\delta(\omega+\omega').\end{aligned} \tag{6.19}$$

Here, for the first line we used $\langle\tilde{G}_0(\omega)\tilde{G}_0(\omega')\rangle = \langle\tilde{G}_0^\dagger(-\omega)\tilde{G}_0^\dagger(-\omega')\rangle = 0$, and the second line follows from the correlations functions (6.A.3). The phase diffusion coefficient is given by

$$[\delta\phi^2]_\omega = \frac{\langle \boldsymbol{L}_0|\boldsymbol{L}_0\rangle}{4\omega^2\overline{d_0^2}}(2\mathcal{D}_{00}^A + 2\mathcal{D}_{00}^N)$$
$$= \frac{\langle \boldsymbol{L}_0|\boldsymbol{L}_0\rangle}{2\omega^2\overline{d_0^2}}\left(\kappa_0 + \frac{Vg^2}{\gamma_\perp}(\overline{S_1}+\overline{S_0})\right). \tag{6.20}$$

If we now use the steady-state solution (6.9) for the population inversion density, and the fact that $\overline{S_z} = \overline{S_1} - \overline{S_0}$, the phase diffusion coefficient may be written as

$$[\delta\phi^2]_\omega = \frac{K_0\delta\omega_{\mathrm{ST}}}{\omega^2}, \tag{6.21}$$

where $\delta\omega_{\mathrm{ST}}$ is the Schawlow–Townes diffusion coefficient [10]

$$\delta\omega_{\mathrm{ST}} = \frac{Vg^2\overline{S_1}}{\gamma_\perp \overline{I_0}}. \tag{6.22}$$

According to Eq.(6.21) the diffusion coefficient for a laser with nonorthogonal modes is enhanced as compared to a standard laser with orthogonal modes by the Petermann factor $K_0 = \langle \boldsymbol{L}_0|\boldsymbol{L}_0\rangle\langle \boldsymbol{R}_0|\boldsymbol{R}_0\rangle > 1$. This enhancement has its origin in the nonorthogonality of the open resonator modes, leading to a faster diffusion of the laser phase fluctuations. The diffusive behavior of the phase fluctuations is obtained by calculating the time dependent mean-square variance of the phase. One obtains

$$\langle\delta\phi^2(t)\rangle = \int_0^t \mathrm{d}t_1 \int_0^t \mathrm{d}t_2 \, \langle\delta\dot{\phi}(t_1)\delta\dot{\phi}(t_2)\rangle$$
$$= \frac{1}{2\pi}\int_0^t \mathrm{d}t_1 \int_0^t \mathrm{d}t_2 \int \mathrm{d}\omega \, \mathrm{e}^{-\mathrm{i}\omega(t_1-t_2)}\omega^2[\delta\phi^2]_\omega \tag{6.23}$$
$$= K_0\delta\omega_{\mathrm{ST}}|t|,$$

which shows that the phase fluctuations grows linearly with time. As we will see in the following section this linear increase of the phase fluctuations with time leads to a Lorentzian laser lineshape.

6.3 Laser Emission Spectrum

We now turn to the evaluation of the emission spectrum for a single mode laser in a cavity with overlapping resonances. The laser emission spectrum is given by Eq. (5.33), in terms of the Wienier–Khintchine theorem [78] for the output field. Using the input-output relations (4.9) in the absence of external illumination, we obtain the emission spectrum

$$\mathcal{S}(\omega) = \frac{\mathrm{i}}{2\pi}\sum_{kl}(\omega_l - \omega_k^*)\langle \boldsymbol{R}_k|\boldsymbol{R}_l\rangle \int_{-\infty}^{\infty} \mathrm{d}t \, \mathrm{e}^{-\mathrm{i}\omega t}\langle d_k^\dagger(t)d_l(0)\rangle\,, \tag{6.24}$$

where we used the general identity

$$
\begin{aligned}
(T^{\dagger}\mathcal{W}\mathcal{W}^{\dagger}T)_{kl} &= \frac{\mathrm{i}}{2\pi\hbar}\langle \boldsymbol{R}_k|(\mathcal{H}-\mathcal{H}^{\dagger})|\boldsymbol{R}_l\rangle \\
&= \frac{\mathrm{i}}{2\pi}(\omega_l-\omega_k^*)\langle \boldsymbol{R}_k|\boldsymbol{R}_l\rangle\,,
\end{aligned}
\tag{6.25}
$$

which follows from the properties of the non-Hermitian operator $\mathcal{H}$ and its right eigenvectors $\{|\boldsymbol{R}_k\rangle\}$ with complex eigenvalues ω_k.

Let us first discuss the above emission spectrum in the limit of isolated resonances. In this limit the right eigenmodes become an orthonormal set of functions and the result reduces to the emission spectrum for almost closed cavities with contributions coming only from the diagonal terms with $k = l$. In particular, for a single-mode laser with an amplitude much larger than the amplitude of the modes below threshold, we recovers a Lorentzian lineshape with a full width at half maximum given by the Schawlow–Townes formula (6.22) [23, 36, 78].

For a laser with overlapping resonances the spectrum has a much richer structure. As an example, we recall the emission spectrum (5.41) for a linear amplifier in a cavity with large outcoupling to the outside world. Due to the nondiagonal terms accounting for correlations among the modes, this spectrum differs dramatically from a sum of Lorentzians expected for isolated modes. In the laser regime we expect the laser amplitude far exceeds the amplitudes of the below threshold modes. Therefore, similarly to the case of isolated resonances, we can neglect contributions which are second order in the below threshold mode amplitudes. For overlapping modes, however, contributions linear in the below threshold mode amplitudes are present and contribute to the emission spectrum for a laser not too far above threshold. Our main purpose in this chapter is to study the effects that such contributions may have on the laser lineshape. Correlations between different modes are the fingerprint of overlapping modes, they imply that the excess noise found in systems with nonorthogonal modes is spectrally colored [140, 32, 141, 142, 94]. In particular, correlations between a single laser mode and modes below threshold have been measured in cavities with overlapping resonances by Poizat, Chang and Grangier [143] and van der Lee et al [116], and were found to hamper the noise reduction on the laser amplitude. Taking into account these contributions the laser emission spectrum is given by

$$
\mathcal{S}(\omega) = \mathcal{S}_{00}(\omega) + \sum_{k\neq 0}(\mathcal{S}_{0k}(\omega)+\mathcal{S}_{k0}(\omega))\,, \tag{6.26}
$$

where the diagonal and nondiagonal contributions are defined, respectively, by

$$
\mathcal{S}_{00}(\omega) = \frac{\kappa_0}{\pi}\langle \boldsymbol{R}_0|\boldsymbol{R}_0\rangle \int_{-\infty}^{\infty} \mathrm{d}t\, \mathrm{e}^{-\mathrm{i}\omega t}\langle d_0^{\dagger}(t)d_0(0)\rangle\,, \tag{6.27}
$$

$$
\mathcal{S}_{0k}(\omega) = (\omega_k-\omega_0^*)\langle \boldsymbol{R}_0|\boldsymbol{R}_k\rangle \int_{-\infty}^{\infty} \mathrm{d}t\, \mathrm{e}^{-\mathrm{i}\omega t}\langle d_0^{\dagger}(t)d_k(0)\rangle\,, \tag{6.28}
$$

and $\mathcal{S}_{k0}(\omega)$ is obtained from (6.28) by interchanging the indices $k \leftrightarrow 0$. We now turn to the evaluation of the different contributions to the laser spectrum.

6.3.1 Laser Linewidth

We first consider Eq. (6.27) yielding the dominant contribution to the emission spectrum. For this calculation we follow the usual steps for evaluating the laser lineshape for a single-mode laser [10, 11]. Far above threshold the laser amplitude fluctuations are small compared with the laser amplitude steady-state value; following Haken [11] we approximate the laser field amplitude by

$$d_0 = \overline{d_0} \exp\big(- \mathrm{i}[\overline{\Omega}_0 t - \delta\phi(t)]\big). \tag{6.29}$$

Substitution into Eq. (6.27) and using the Gaussian properties of the laser phase fluctuations $\delta\phi(t)$, one obtains

$$\mathcal{S}_{00} = \frac{\overline{I}_{\mathrm{out}}}{2\pi} \int\limits_{-\infty}^{\infty} \mathrm{d}t \, \exp\Big(-\mathrm{i}(\omega - \Omega_0)t - \frac{1}{2}\langle \delta\phi^2(t)\rangle\Big), \tag{6.30}$$

where we introduced the mean outgoing laser photocurrent $\overline{I}_{\mathrm{out}} = 2\kappa_0 \overline{I_0}$. Using Eq. (6.23) for the mean-square variance of the phase we find

$$\begin{aligned} \mathcal{S}_{00} &= \frac{\overline{I}_{\mathrm{out}}}{2\pi} \int\limits_{-\infty}^{\infty} \mathrm{d}t \, \exp\Big(-\mathrm{i}(\omega - \Omega_0)t - \frac{1}{2} K_0 \delta\omega_{\mathrm{ST}} |t|\Big) \\ &= \frac{\overline{I}_{\mathrm{out}}}{\pi} \frac{K_0 \delta\omega_{\mathrm{ST}}/2}{(\omega - \overline{\Omega}_0)^2 + \frac{1}{4}(K_0 \delta\omega_{\mathrm{ST}})^2} \, . \end{aligned} \tag{6.31}$$

Thus, like for a standard laser, we recovered a laser line given by a Lorentzian. In this case, however, the full width at half maximum is given by $K_0\delta\omega_{\mathrm{ST}}$, which presents an enhancement by a factor K_0 with respect to the standard linewidth $\delta\omega_{\mathrm{ST}}$. In the limit of a cavity with orthogonal modes the Petermann factor K_0 equals one and we recover the standard result. We will show below that provided the enhancement of the laser linewidth is large enough ($K_0 \gg 1$), the total laser lineshape may differ from a Lorentzian.

Finally, let us mention that recently Lamprecht and Ritsch [62], and Cheng and Siegman [35] proposed alternative quantum laser theories within which the laser linewidth enhancement due to the excess noise can be derived. Although in these theories the Langevin equations considered are similar to ours the quantization field scheme on which they are based is completely different to system-and-bath underlaying our theory.

6.3.2 Cross Correlation Contributions

We now evaluate the contributions to the emission spectrum arising from the correlation between the laser mode and the modes below threshold. Substitution of Eq. (6.29) into Eq. (6.28) yields

$$\mathcal{S}_{0k}(\omega) = \frac{\mathrm{i}}{2\pi}(\omega_k - \omega_0^*)\langle \boldsymbol{R}_0 | \boldsymbol{R}_k\rangle \overline{d_0} \int\limits_{-\infty}^{\infty} \mathrm{d}t \, \exp\big(-\mathrm{i}(\omega - \bar{\Omega}_0)t\big) \big\langle \exp(-\mathrm{i}\delta\phi(t))\delta d_k(0)\big\rangle \, , \tag{6.32}$$

where we used the below threshold amplitudes $d_k(t) = \delta d_k \mathrm{e}^{-\mathrm{i}\bar{\omega}_k t}$. The correlation function $\langle \exp(-\mathrm{i}\delta\phi(t))\delta d_k(0)\rangle$ can be evaluated using that both the laser phase fluctuations as well as the below threshold mode amplitudes are driven by Gaussian random noises. Hence phase fluctuations and below threshold amplitudes are themselves Gaussian random variables. Employing Wick's theorem, in Appendix 6.B is shown that the correlation function $\langle \exp(-\mathrm{i}\delta\phi(t))\delta d_k(0)\rangle$ reduces to

$$\langle \exp(-\mathrm{i}\delta\phi(t))\delta d_k(0)\rangle = -2\mathrm{i}\exp\Big(-\frac{1}{2}\langle\delta\phi^2(t)\rangle\Big)\left[\langle\delta\phi(t)\delta d_k(0)\rangle + \langle\delta d_k(0)\delta\phi(t)\rangle\right]. \quad (6.33)$$

It is left to evaluate the simpler correlation functions $\langle\delta\phi(t)\delta d_k(0)\rangle$ and $\langle\delta d_k(0)\delta\phi(t)\rangle$. To this end, we write

$$\begin{aligned}\langle\delta\phi(t)\delta d_k(0)\rangle &= \int_0^t \mathrm{d}t'\,\langle\dot{\delta\phi}(t')\delta d_k(0)\rangle \\ &= \frac{1}{(2\pi)^2}\int_0^t \mathrm{d}t' \int \mathrm{d}\omega \int \mathrm{d}\omega'\,\mathrm{e}^{-\mathrm{i}\omega t'}(-\mathrm{i}\omega)\langle\delta\phi(\omega)\delta d_k(\omega')\rangle\,.\end{aligned} \quad (6.34)$$

The remaining correlation function is easily computed using a Fourier transformation and relations in Appendix 6.A. The result is

$$\langle\delta\phi(\omega)\delta d_k(\omega')\rangle = -\frac{2\pi\mathrm{i}}{\overline{d_0}\omega\omega'}\mathcal{D}^N_{0k}\langle\boldsymbol{L}_k|\boldsymbol{L}_0\rangle\,\delta(\omega+\omega'-\bar{\Omega}_0+\bar{\omega}_k)\,. \quad (6.35)$$

Substituting the result into Eq. (6.34) and performing the integrals, one obtains

$$\langle\delta\phi(t)\delta d_k(0)\rangle = -\frac{\mathcal{D}^N_{0k}\langle L_k|L_0\rangle}{\overline{d_0}(\bar{\Omega}_0-\bar{\omega}_k)}\Theta(-t)\left[\mathrm{e}^{-\mathrm{i}(\bar{\Omega}_0-\bar{\omega}_k)t}-1\right], \quad (6.36)$$

where $\Theta(x)$ is the step function which is equal to one if $x > 0$ and vanishes otherwise. In a similar fashion one can show

$$\langle\delta d_k(0)\delta\phi(t)\rangle = -\frac{\mathcal{D}^A_{k0}\langle L_k|L_0\rangle}{\overline{d_0}(\bar{\Omega}_0-\bar{\omega}_k)}\Theta(-t)\left[\mathrm{e}^{-\mathrm{i}(\bar{\Omega}_0-\bar{\omega}_k)t}-1\right]. \quad (6.37)$$

Substituting Eq. (6.33) into Eq. (6.32), and performing the time integration using the results (6.36) and (6.37), one obtains the cross correlation contributions to the emission spectrum

$$\mathcal{S}_{0k}(\omega) = -\frac{\mathrm{i}(\omega_k-\omega_0^*)(\mathcal{D}^N_{0k}+\mathcal{D}^A_{k0})\langle\boldsymbol{R}_0|\boldsymbol{R}_k\rangle\langle\boldsymbol{L}_k|\boldsymbol{L}_0\rangle}{\pi\left[\frac{1}{2}K_0\delta\omega_{\mathrm{ST}}-\mathrm{i}(\omega-\bar{\Omega}_0)\right]\left[\frac{1}{2}K_0\delta\omega_{\mathrm{ST}}+\bar{\kappa}_k-\mathrm{i}(\omega-\bar{\Omega}_k)\right]}, \quad (6.38)$$

where we have split the complex frequencies $\bar{\omega}_k = \bar{\Omega}_k - \mathrm{i}\bar{\kappa}_k$ into their real an imaginary parts. A calculation following the same steps as the one presented for $\mathcal{S}_{0k}(\omega)$ yields for $\mathcal{S}_{k0}(\omega)$,

$$\mathcal{S}_{k0}(\omega) = \mathcal{S}^*_{0k}(\omega)\,. \quad (6.39)$$

The cross correlations contributions to the laser power spectrum (6.38) are the key result of this chapter. Their presence is a consequence of the mode nonorthogonality and leads to changes in the laser line, causing the spectrum to deviate from a Lorentzian shape. The magnitude of these contributions is determined by two features. First, the numerator on the right hand side of Eq. (6.38) that depends on the correlation between the laser mode and the $k \neq 0$ non-lasing mode: For strongly correlated modes the product of overlap integrals $\langle \boldsymbol{R}_0 | \boldsymbol{R}_k \rangle \langle \boldsymbol{L}_k | \boldsymbol{L}_0 \rangle$ is large. In contrast, modes with small correlations have small spatial overlap, the extreme case being orthogonal modes for which the overlap integral vanishes. Second, their frequency dependence through the complex denominator. This denominator allows for large values of the cross correlation terms at frequencies different from that of the laser mode, introducing more structure to the laser line provided the non-lasing modes are close to (but below) threshold, with $\bar{\kappa}_k$ not to large. In order to discuss these features more clearly, it is convenient to write down the complete power spectrum.

6.3.3 Emission Power Spectrum

The total emission power spectrum for a single-mode laser in a cavity with overlapping resonances is obtained by substituting the results (6.31), (6.38), and (6.39) into Eq.(6.26). The final expression takes the form

$$\begin{aligned} \mathcal{S}(\omega) = {} & \frac{\overline{I}_{\mathrm{out}}}{\pi} \frac{\delta\omega/2}{(\omega - \overline{\Omega}_0)^2 + (\delta\omega/2)^2} \\ & \times \left\{ 1 - 8 \sum_{k \neq 0} \mathrm{Re} \left(\left[\frac{\frac{1}{2}\delta\omega + \mathrm{i}(\omega - \bar{\Omega}_0)}{\frac{1}{2}\delta\omega + \bar{\kappa}_k - \mathrm{i}(\omega - \bar{\Omega}_k)} \right] \right. \right. \\ & \times \left. \left. \left[\frac{\mathrm{i}(\omega_k - \omega_0^*)(\mathcal{D}_{0k}^N + \mathcal{D}_{k0}^A) \langle \boldsymbol{R}_0 | \boldsymbol{R}_k \rangle \langle \boldsymbol{L}_k | \boldsymbol{L}_0 \rangle}{2\kappa_0 K_0 (\mathcal{D}_{00}^N + \mathcal{D}_{00}^A)} \right] \right) \right\} , \end{aligned} \tag{6.40}$$

where the total linewidth is given by $\delta\omega = K_0 \delta\omega_{\mathrm{ST}}$, which includes the Petermann enhancement factor K_0.

The first term inside the curved brackets on the right hand side of Eq. (6.40) accounts for the lasing mode contribution to the power spectrum. It corresponds to a Lorentzian with linewidth $\delta\omega$ that incorporates the effects of excess noise. As discussed in Sec. 6.3.2, this term is the dominant contribution to spectrum provided the correlation between the lasing mode and the non-lasing modes are negligible. In case of strong correlations, due to the second term inside the brackets, the power spectrum will deviate significantly from a Lorentzian provided some non-lasing modes are close to (but below) threshold. Indeed, close to threshold $\bar{\kappa}_k \approx 0$ for non-lasing modes, and the contribution arising from the cross correlations term is large if ω is close to the oscillation frequencies of the non-lasing modes. Far above threshold, cross correlation contributions become negligible. Then, $\delta\omega$ is very small (see Eq. (6.22)), and the laser line reduces to a very sharp Lorentzian. Any deviation arising from the cross correlation terms is suppressed by the small values of the Lorentzian at the wings of the spectrum.

6.4 Discussion and Outlook

In this chapter we derived the power spectrum of a laser with overlapping resonances in the regime of single-mode laser oscillation. To this end, we used the quantum Langevin equations derived in *Chapter 5*, and demonstrated that they can account for a quantum description of the Petermann excess noise. Our quantum description of phase diffusion accounts for the laser linewidth enhancement by the Petermann factor. Additionally, we found that excess noise plays a more significant role in the determination of the laser spectrum. In contrast to the power spectrum of standard lasers for which the only contribution arises from the lasing mode autocorrelation, we showed that in lasers with overlapping resonances cross-correlations exist between the lasing mode and close-by non-lasing modes. Their contribution to the spectrum can become of the same order as the lasing mode autocorrelation contribution and cannot be neglected for pumpings no too far above threshold. The origin of these contributions lays only in the nonorthogonal character of the laser modes. Due to these contributions the laser line deviates from the Lorentzian shape expected from standard laser theory.

So far most of the experimental and theoretical studies of excess noise has been restricted to lasers in optical cavities with simple geometries (see Sec. 1.3). Overlapping modes, however, are a generic property of random lasers with weak disorder, and therefore one should expect excess noise to be at least partially responsible for the complex structure displayed by the power spectra of random lasers (see Fig. 1.2). Investigations in this direction, to the best of our knowledge, have not been yet carried out. We briefly discuss how random matrix theory, may be applied in this context.

The power spectrum (6.40) can be used to evaluate the emission spectrum of chaotic lasers with overlapping resonances in the regime of a single laser oscillation. For this some simplifications are convenient. Since we expect the laser mode to be close to the center of the amplification spectrum, i.e., to be almost at resonance, the effective gain seen by it and by the close-by below threshold modes can be assumed to be $Vg^2\overline{S_z}/\gamma_\perp = \kappa_0$ which holds at the center of the amplification line. Close to the center of the gain profile we may also neglect the gain frequency pulling. Then the resonances of the filled cavity are trivially related to the cold cavity resonances by

$$\bar{\Omega}_0 = \Omega_0 \,, \tag{6.41a}$$

$$\bar{\omega}_k = \omega_k + \mathrm{i}\kappa_0 = \Omega_k - \mathrm{i}(\kappa_k - \kappa_0)\,. \tag{6.41b}$$

Upon substitution into Eq. (6.40), the power spectrum simplifies and can be written in terms of the passive cavity resonances,

$$\begin{aligned} \mathcal{S}(\omega) = {} & \frac{\overline{I}_{\mathrm{out}}}{\pi} \frac{\delta\omega/2}{(\omega-\Omega_0)^2 + \frac{1}{4}(\delta\omega)^2} \\ & \times \left\{ 1 - 8 \sum_{k\neq 0} \mathrm{Re}\left(\left[\frac{\frac{1}{2}\delta\omega + \mathrm{i}(\omega-\Omega_0)}{\frac{1}{2}\delta\omega + (\kappa_k-\kappa_0) - \mathrm{i}(\omega-\Omega_k)} \right] \right.\right. \\ & \times \left.\left. \left[\frac{\mathrm{i}(\omega_k-\omega_0^*)(\mathcal{D}^N_{0k}+\mathcal{D}^A_{k0})\langle \boldsymbol{R}_0|\boldsymbol{R}_k\rangle\langle \boldsymbol{L}_k|\boldsymbol{L}_0\rangle}{2\kappa_0 K_0(\mathcal{D}^N_{00}+\mathcal{D}^A_{00})} \right] \right) \right\} , \end{aligned} \tag{6.42}$$

where the total linewidth is given by $\delta\omega = K_0\delta\omega_{\mathrm{ST}}$. As a consequence of the chaotic scattering at the resonator mirrors the resonator right and left modes become chaotic, and both the resonances frequencies Ω_k and widths κ_k become random quantities. Their statistics can be obtained from the random-matrix model for chaotic scattering [122]: The passive resonator dynamics is assumed to be generated by the non-Hermitian random matrix $\mathcal{H}/\hbar$, with the form given in Eq. (4.29). Its Hermitian part is taken from the orthogonal Gaussian ensemble. Although, due to its complexity an analytical treatment of the spectrum (6.42) may not be possible at present, a numerical random matrix study is feasible.

6.A Field Noise Correlation Functions

Here we list the nonvanishing correlation functions of the field noise operators defined in Eq. (6.5a). Combining the correlation function in the Appendix 5.B and the correlation functions (4.28), one obtains

$$\langle G_k(t)G_l^\dagger(t')\rangle = 2\mathcal{D}_{kl}^A\langle \boldsymbol{L}_k|\boldsymbol{L}_l\rangle\,\delta(t-t')\,, \tag{6.A.1a}$$

$$\langle G_k^\dagger(t)G_l(t')\rangle = 2\mathcal{D}_{kl}^N\langle \boldsymbol{L}_l|\boldsymbol{L}_k\rangle\,\delta(t-t')\,, \tag{6.A.1b}$$

$$\tag{6.A.1c}$$

where the diffusion constants are defined by

$$2\mathcal{D}_{kl}^A = \mathrm{i}(\omega_k-\omega_l^*) - \frac{Vg^2}{2\gamma_\perp^2}\big(\gamma_\parallel(\Lambda-\overline{S_z}) - 4\gamma_\perp\overline{S_0}\big)\,, \tag{6.A.2a}$$

$$2\mathcal{D}_{kl}^N = \frac{Vg^2}{2\gamma_\perp^2}\big(\gamma_\parallel(\Lambda-\overline{S_z}) + 4\gamma_\perp\overline{S_1}\big)\,. \tag{6.A.2b}$$

The correlation functions for the slowly varying noises in the frequency domain $\tilde{G}_k(\omega)$ are easily obtained from the above results using $\tilde{G}_k(\omega) = \int \mathrm{d}t\,\mathrm{e}^{-\mathrm{i}(\omega-\omega_k)t}G_k(t)$. They read

$$\langle \tilde{G}_k(\omega)\tilde{G}_l^\dagger(-\omega')\rangle = 4\pi\mathcal{D}_{kl}^A\langle \boldsymbol{L}_k|\boldsymbol{L}_l\rangle\,\delta(\omega+\omega'-\bar{\omega}_l^*+\bar{\omega}_k)\,, \tag{6.A.3a}$$

$$\langle \tilde{G}_k^\dagger(-\omega)\tilde{G}_l(\omega')\rangle = 4\pi\mathcal{D}_{kl}^N\langle \boldsymbol{L}_l|\boldsymbol{L}_k\rangle\,\delta(\omega+\omega'-\bar{\omega}_k^*+\bar{\omega}_l)\,. \tag{6.A.3b}$$

6.B Lasing-Nonlasing Modes Correlations

Here we derive Eq. (6.33). The whole calculation is based on the fact that both the laser phase fluctuations and the amplitude of the below threshold modes are Gaussian random variables. We star from

$$\langle\,\exp(-\mathrm{i}\delta\phi(t))\delta d_k(0)\rangle = \sum_{l=0}^{+\infty}\frac{(-\mathrm{i})^l}{l!}\langle[\delta\phi(t)]^l\delta d_k(0)\rangle. \tag{6.B.1}$$

Employing Wick's theorem, one can show that only terms with odd values l will contribute to the sum on the right hand side. Hence

$$\langle\,\exp(-\mathrm{i}\delta\phi(t))\delta d_k(0)\rangle = \sum_{n=0}^{+\infty}\frac{(-\mathrm{i})^{2n+1}}{(2n+1)!}\langle[\delta\phi(t)]^{2n+1}\delta d_k(0)\rangle. \tag{6.B.2}$$

The correlation functions on the right side are evaluated upon summation of all the $(2n+2)!/(2^{n+1}(n+1)!)$ possible contractions. For the correlation function of order $2n+2$, this yields

$$\langle[\delta\phi(t)]^{2n+1}\delta d_k(0)\rangle = \frac{(2n+2)!}{2^n(n+1)!}\langle\delta\phi^2(t)\rangle^n\big[\langle\delta\phi(t)\delta d_k(0)\rangle + \langle\delta d_k(0)\delta\phi(t)\rangle\big]\,. \tag{6.B.3}$$

Substituting Eq. (6.B.3) into Eq. (6.B.2), and after some straight forward calculation, one recovers Eq. (6.33).

6.C Off-Resonance Case: Henry Factor

In Sec. 6.3 we assumed the laser mode to be on resonance with the atomic medium. Here we address the modifications to our results that arise when this assumption is dropped. As is evident from Eqs. (6.16a) and (6.16b), in a detuned laser, where $\mathrm{Im}[W_0] \neq 0$, amplitude and phase fluctuations are coupled. Hence, the evaluation of the phase fluctuations must take into account the excess noise originating in the coupling to the amplitude fluctuations. Following Lax [136], we will show that the consequences of detuning can be quantified by an excess noise factor. That factor depends in a simple manner on the detuning, provided the laser is operating far above threshold so that the amplitude fluctuations can be neglected as compared with the steady-state laser amplitude. This excess noise factor is mathematically equivalent to the Henry factor [138] arising in semiconductor laser, where the coupling between amplitude and phase fluctuations also plays a significant role.

Let us then start by writing Eqs. (6.16a) and (6.16b) for the amplitude and phase quadrature components in the way

$$\delta X_0(\omega) = \frac{\mathrm{i}}{2\omega}\big(r\cos(\beta)\delta S_z(\omega) + \tilde{G}(\omega) + \tilde{G}_0^\dagger(-\omega)\big)\,, \tag{6.C.1a}$$

$$\delta Y_0(\omega) = \frac{1}{2\omega}\big(\mathrm{i}r\sin(\beta)\overline{d}_0\delta S_z(\omega) + \tilde{G}(\omega) - \tilde{G}_0^\dagger(-\omega)\big)\,. \tag{6.C.1b}$$

Thus amplitude and phase fluctuations are coupled through the atomic population inversion fluctuations. Here the two new parameters r and β are defined by

$$r = 2\overline{d_0}|W_0|\,, \tag{6.C.2}$$

$$\beta = \mathrm{Arg}[W_0] = \mathrm{Arctan}\left(\frac{-(\nu-\bar{\Omega}_0)}{\gamma_\perp}\right)\,. \tag{6.C.3}$$

We now define

$$\eta(\omega) = \cos(\beta)\delta Y_0(\omega) - \sin(\beta)\delta X_0(\omega)\,, \tag{6.C.4}$$

which can be written explicitly in terms of the noise operators using Eqs. (6.C.1a) and (6.C.1b),

$$\eta(\omega) = \frac{1}{2\omega}\big(\mathrm{e}^{-\mathrm{i}\beta}\tilde{G}_0(\omega) - \mathrm{e}^{\mathrm{i}\beta}\tilde{G}_0^\dagger(\omega)\big)\,. \tag{6.C.5}$$

We notice that the new variable η is a linear combination of the laser mode noise forces. Any dependence on the population inversion fluctuation has been eliminated. For small phase fluctuations, one can express them in terms of the phase quadrature component as $\delta\phi(\omega) = \delta Y_0(\omega)/\overline{d_0}$. Using Eq. (6.C.4), we may write the phase fluctuations as

$$\delta\phi(\omega) = \frac{1}{\overline{d_0}\cos(\beta)}\big(\eta(\omega) + \sin(\beta)\delta X_0(\omega)\big) \simeq \frac{\eta(\omega)}{\overline{d_0}\cos(\beta)}\,, \tag{6.C.6}$$

where the last relation holds for a laser far above threshold where $\delta X_0 \ll \overline{d_0}$. We can use the above equations to evaluate the phase fluctuations diffusion coefficient $[\delta\phi]_\omega$, which ultimately determines the laser line width. Following the same reasoning that led to Eq. (6.20), one obtains, starting from Eq. (6.C.6), the result

$$[\delta\phi]_\omega = \frac{K_0\delta\omega_{\mathrm{ST}}}{\cos^2(\beta)\omega^2} = \frac{K_0(1+\alpha^2)\delta\omega_{\mathrm{ST}}}{\omega^2}\,, \tag{6.C.7}$$

where we have written $\cos^2(\beta) = (1+\alpha^2)^{-1}$. Here, $\alpha = (\nu - \bar{\Omega}_0)/\gamma_\perp$ is the Henry parameter [138]. According to Eq. (6.C.7) the effect on the detuning on the laser linewidth is an enhancement by the factor $1+\alpha^2$.

The total emission spectrum for a detuned laser is obtained following the same reasoning that led to the emission spectrum (6.40), however one should now use the following correlation functions

$$\langle \delta\phi^2(t)\rangle = \frac{1}{\cos^2(\beta)}\langle \delta\phi^2(t)\rangle_{\text{tune}}\,, \tag{6.C.8}$$

$$\langle \delta\phi(t)\delta d_k(0)\rangle = \frac{\mathrm{e}^{\mathrm{i}\beta}}{\cos(\beta)}\langle \delta\phi(t)\delta d_k(0)\rangle_{\text{tune}}\,, \tag{6.C.9}$$

$$\langle \delta d_k(0)\delta\phi(t)\rangle = \frac{\mathrm{e}^{\mathrm{i}\beta}}{\cos(\beta)}\langle \delta d_k(0)\delta\phi(t)\rangle_{\text{tune}}\,, \tag{6.C.10}$$

which now hold for a detuned laser and that are evaluated using the phase fluctuations (6.C.6), and . Here $\langle\ldots\rangle_{\text{tune}}$ refers to the results obtained for the laser on resonance in Sec. 6.3. The emission spectrum then reads

$$\begin{aligned}\mathcal{S}(\omega) = {} & \frac{\overline{I}_{\text{out}}}{\pi}\frac{\delta\omega/2}{(\omega-\overline{\Omega}_0)^2+\frac{1}{4}(\delta\omega)^2} \\ & \times\left\{1-8\sum_{k\neq 0}\mathrm{Re}\left(\left[\frac{\frac{1}{2}\delta\omega+\mathrm{i}(\omega-\bar{\Omega}_0)}{\frac{1}{2}\delta\omega+\bar{\kappa}_k-\mathrm{i}(\omega-\bar{\Omega}_k)}\right]\right.\right. \\ & \times\left.\left.\left[\frac{\mathrm{i}(\omega_k-\omega_0^*)(\mathcal{D}^N_{0k}+\mathcal{D}^A_{k0})\langle \boldsymbol{R}_0|\boldsymbol{R}_k\rangle\langle \boldsymbol{L}_k|\boldsymbol{L}_0\rangle\cos(\beta)\mathrm{e}^{\mathrm{i}\beta}}{2\kappa_k K_0(\mathcal{D}^N_{00}+\mathcal{D}^A_{00})}\right]\right)\right\}\,,\end{aligned} \tag{6.C.11}$$

where the total linewidth is given by $\delta\omega = K_0\delta\omega_{\text{ST}}/\cos^2(\beta)$, which includes the Petermann enhancement factor K_0 and the Henry factor $1/\cos^2(\beta)$.

Bibliography

[1] H. Cao, Lasing in random media, Wave Random Media 13 (2003) R1.

[2] H. Cao, Lasing in disordered media, Progress in Optics 45 (2003) 317.

[3] H. Cao, Y. G. Zhao, S. T. Ho, J. Y. Dai, J. Y. Wu, R. P. H. Chang, Ultraviolet lasing in resonators formed by scattering in semiconductor polycrystalline films, Appl. Phys. Lett. 73 (1998) 3656.

[4] H. Cao, Y. G. Zhao, S. Ho, E. W. Seelig, Q. H. Wang, R. P. H. Chang, Random laser action in semiconductor powder, Phys. Rev. Lett. 82 (1999) 2278.

[5] H. Cao, D. Z. Zhang, S. H. Chang, S. T. Ho, E. W. Seelig, X. Liu, R. P. H. Chang, Spatial confinement of laser light in active random media, Phys. Rev. Lett. 84 (2000) 5584.

[6] H. Cao, J. Y. Xu, E. W. Seelig, R. P. H. Chang, Microlaser made of disordered media, Appl. Phys. Lett. 76 (2000) 2997.

[7] H. Cao, J. Y. Xu, S. H. Chang, S. T. Ho, Transition from amplified spontaneous emission to laser action in strongly scattering media, Phys. Rev. E 61 (2000) 1985.

[8] G. Zacharakis, N. A. Papadogiannis, G. Filippidis, T. G. Papazoglou, Photon statistics of laserlike emission from polymeric scattering gain media, Opt. Lett. 25 (2000) 923.

[9] H. Cao, Y. Ling, J. Y. Xu, C. Q. Cao, P. Kumar, Photon statistics of random lasers with resonant feedback, Phys. Rev. Lett. 86 (2001) 4524.

[10] M. Sargent III, M. O. Scully, W. E. Lamb, Laser physics, Addison-Wesley, 1974.

[11] H. Haken, Laser theory, 2nd Edition, Springer, Berlin, 1984.

[12] A. Siegman, Lasers, Oxford University Press, 1986.

[13] V. S. Letokhov, Generation of light by scattering medium with negative resonance absoption, Sov. Phys.–JETP 26 (1968) 835.

[14] V. S. Letokhov, Noncoherent feedback in space masers and stellar lasers, in: R. Y. Chiao (Ed.), Amazing Light, Springer, Berlin, 1996, p. 409.

[15] M. C. W. van Rossum, T. M. Nieuwenhuizen, Multiple scattering of classical waves: microscopy, mesoscopy, and diffusion, Rev. Mod. Phys. 71 (1999) 313.

[16] S. John, G. Pang, Theory of lasing in a multiple-scattering medium, Phys. Rev. A 54 (1996) 3642.

[17] R. M. Balachandran, N. M. Lawandy, J. A. Moon, Theory of laser action in scattering gain media, Opt. Lett. 22 (1997) 319.

[18] N. M. Lawandy, R. M. Balachandran, A. S. L. Gomes, E. Sauvain, Laser action in strongly scattering media, Nature 368 (1994) 436.

[19] W. L. Sha, C.-H. Liu, R. R. Alfano, Spectral and temporal measurements of laser action of Rhodamine 640 dye in strongly scattering media, Opt. Lett. 23 (1994) 19.

[20] N. M. Lawandy, R. M. Balachandran, Random laser?, Nature 373 (1995) 204.

[21] W. Zhang, N. Cue, K. M. Yoo, Effect of random multiple light scattering on the laser action in a binary-dye mixture, Opt. Lett. 20 (1995) 1023.

[22] K. Petermann, Calculated spontaneus emission factor for double heterostructure injection laser with gain-induced waveguiding, IEEE J. Quantum. Electron. 15 (1979) 566.

[23] A. L. Schawlow, C. H. Townes, Infrared and optical masers, Phys. Rev. 112 (1958) 1940.

[24] A. E. Siegman, Excess spontaneous emission in non-Hermitian optical systems. I. Laser amplifiers, Phys. Rev. A 39 (1989) 1253.

[25] A. E. Siegman, Excess spontaneous emission in non-Hermitian optical systems. II. Laser oscillators, Phys. Rev. A 39 (1989) 1264.

[26] W. A. Hamel, J. P. Woerdman, Nonorthogonality of the longitudinal eigenmodes of a laser, Phys. Rev. A 40 (1989) 2785.

[27] W. A. Hamel, J. P. Woerdman, Observation of enhanced fundamental linewidth of a laser due to nonorthogonality of its longitudinal eigenmodes, Phys. Rev. Lett. 64 (1990) 1506.

[28] Å. M. Lindberg, M. A. van Eijkelenborg, K. Joosten, G. Nienhuis, J. P. Woerdman, Observation of excess quantum noise in geometrically stable laser, Phys. Rev. A 57 (1998) 3036.

[29] Y.-J. Cheng, C. G. Fanning, A. E. Siegman, Experimental observation of a large excess quantum noise factor in the linewidth of a laser oscillator having nonorthogonal modes, Phys. Rev. Lett. 77 (1996) 627.

[30] M. A. van Eijkelenborg, Å. M. Lindberg, M. S. Thijssen, J. P. Woerdman, Resonance of quantum noise in an unstable cavity laser, Phys. Rev. Lett. 77 (1996) 4314.

[31] A. M. van der Lee, N. J. van Druten, A. L. Mieremet, M. A. van Eijkelenborg, r. M. Lindberg, M. P. van Exter, J. P. Woerdman, Excess quantum noise due to nonorthogonal polarization modes, Phys. Rev. Lett. 79 (1997) 4357.

[32] A. M. van der Lee, A. L. Mierement, M. P. van Exter, N. J. van Druten, J. P. Woerdman, Quantum noise in a laser with nonorthogonal polarization modes, Phys. Rev. A 61 (2000) 033812.

[33] G. Hackenbroich, C. Viviescas, F. Haake, Field quantization for chaotic resonators with overlapping modes, Phys. Rev. Lett. 89 (2002) 083902.

[34] C. Lamprecht, H. Ritsch, Theory of excess noise in unstable resonator lasers, Phys. Rev. A. 66 (2002) 053808.

[35] Y.-J. Cheng, A. E. Siegman, Generalized radiation-field quantization method and the Petermann factor, Phys. Rev. A 68 (2003) 043808.

[36] H. Haken, Light, North-Holland, Amsterdam, 1985.

[37] I. R. Senitzky, Dissipation in quantum mechanics. The harmonic oscillator, Phys. Rev. 119 (1959) 670.

[38] I. R. Senitzky, Dissipation in quantum mechanics. The harmonic oscillator. II, Phys. Rev. 124 (1960) 642.

[39] C. W. Gardiner, P. Zoller, Quantum noise, 2nd Edition, Vol. 56 of Springer series in synergetics, Springer, Berlin, 2000.

[40] A. G. Fox, T. Li, Resonant modes in a maser interferometer, Bell Tech. J. 40 (1961) 453.

[41] V. I. Kukulin, V. M. Krasnopol'sky, J. Horáček, Theory of resonances, Kluwer, London, 1989.

[42] R. Lang, M. O. Scully, W. E. Lamb Jr., Why is the laser line so narrow? a theory of single–quasimode laser operation, Phys. Rev. A 7 (1973) 1788.

[43] K. Ujihara, Quantum theory of a one–dimensional optical cavity with output coupling, Phys. Rev. A 12 (1975) 148.

[44] K. Ujihara, Quantum theory of a one–dimensional laser with output coupling. Linear theory, Phys. Rev. A 16 (1977) 652.

[45] K. Ujihara, Quantum theory of a one-dimensional optical cavity with output coupling. II. Thermal radiation field and the fluctuation-dissipation theorem, Phys. Rev. A 18 (1978) 659.

[46] M. Ley, R. Loudon, Quantum theory of high-resolution length measurement with Fabry-Perot interferometer, J. Mod. Opt. 34 (1987) 227.

[47] X. P. Feng, K. Ujihara, Quantum theory of spontaneous emission in a one-dimensional optical cavity with two-side output coupling, Phys. Rev. A 41 (1990) 2668.

[48] J. Gea-Banacloche, N. Lu, L. M. Pedrotti, S. Prasad, M. O. Scully, K. Wódkiewicz, Treatment of the spectrum of squeezing based on the modes of the universe. I. Theory and a physical picture, Phys. Rev. A 41 (1990) 369.

[49] J. Gea-Banacloche, N. Lu, L. M. Pedrotti, S. Prasad, M. O. Scully, K. Wódkiewicz, Treatment of the spectrum of squeezing based on the modes of the universe. II. Applications, Phys. Rev. A 41 (1990) 381.

[50] L. Knöll, W. Vogel, D. G. Welsch, Resonators in quantum optics: A first principle approach, Phys. Rev. A 43 (1991) 543.

[51] R. W. F. van der Plank, L. G. Suttorp, Generalization of damping theory for cavities with mirrors of finite transmittivity, Phys. Rev. A 53 (1996) 1791.

[52] B. J. Dalton, S. M. Barnett, P. L. Knight, Quasi mode theory of macroscopic canonical quantization in quantum optics and cavity quantum electrodynamics, J. Mod. Opt. 46 (1999) 1315.

[53] B. J. Dalton, S. M. Barnett, P. L. Knight, Macroscopic canonical quantization in quantum optics: Properties of quasi mode annihilation and creation operators, J. Mod. Opt. 46 (1999) 1495.

[54] B. J. Dalton, S. M. Barnett, P. L. Knight, Quasi mode theory of the beam splitter a quantum scattering theory approach, J. Mod. Opt. 46 (1999) 1559.

[55] B. J. Dalton, P. L. Knight, The standard model in cavity quantum electrodynamics. I. General features of mode functions for a Fabry-Perot cavity, J. Mod. Opt. 46 (1999) 1817.

[56] B. J. Dalton, P. L. Knight, The standard model in cavity quantum electrodynamics. ii. coupling constants and atom field interaction, J. Mod. Opt. 46 (1999) 1839.

[57] S. A. Brown, B. J. Dalton, Generalized quasi mode theory of macroscopic canonical quantization in cavity quantum electrodynamics and quantum optics I. Theory, J. Mod. Opt. 48 (2001) 597.

[58] S. A. Brown, B. J. Dalton, Generalized quasi mode theory of macroscopic canonical quantization in cavity quantum electrodynamics and quantum optics II. Application to reflection and refraction at a dielectric interface, J. Mod. Opt. 48 (2001) 639.

[59] K. C. Ho, P. T. Leung, A. Maasen van den Brink, K. Young, Second quantization of open systems using quasinormal modes, Phys. Rev. E 58 (1998) 2965.

[60] E. S. C. Ching, A. Leung, P. T. Maassen van den Brink, W. M. Suen, S. S. Tong, K. Young, Quasinormal-mode expansion for waves in open systems, Rev. Mod. Phys. 70 (1998) 1545.

[61] C. Lamprecht, H. Ritsch, Quantized atom-field dynamics in unstable cavities, Phys. Rev. Lett. 82 (1999) 3787.

[62] C. Lamprecht, H. Ritsch, Unexpected role of excess noise in spontaneous emission, Phys. Rev. A. 65 (2002) 023803.

[63] S. M. Dutra, G. Nienhuis, Quantized mode of a leaky cavity, Phys. Rev. A 62 (2000) 063805.

[64] S. A. Brown, B. J. Dalton, Field quantization, photons and non-Hermitean modes, J. Mod. Opt. 49 (2002) 1009.

[65] T. Gruner, D.-G. Welsch, Quantum-optical input-output relations for dispersive and lossy multilayer dielectric plates, Phys. Rev. A 54 (1996) 1661.

[66] T. Gruner, D.-G. Welsch, Green-function approach to the radiation-field quantization for homogeneous and inhomogeneous Kramers-Kronig dielectrics, Phys. Rev. A 53 (1996) 1818.

[67] M. Artoni, R. Loudon, Quantum theory of optical pulse propagation through an absorbing and dispersive slab, Phys. Rev. A 55 (1997) 1347.

[68] C. W. J. Beenakker, Thermal radiation and amplified emission from a random medium, Phys. Rev. Lett. 81 (1998) 1829.

[69] C. W. J. Beenakker, Photon statistics of a random laser, in: J. P. Fouque (Ed.), Diffuse Waves in Complex Media, Vol. 531 of NATO Science Series C, Kluwer, Dordrecht, 1999, p. 137.

[70] M. Patra, On quantum optics of random media, Ph.D. thesis, Universiteit Leiden (2000).

[71] E. G. Mishchenko, M. Patra, C. W. J. Beenakker, Frequency dependence of the photonic noise spectrum in an absorbing or amplifying diffusive medium, Eur. Phys. J. D 13 (2001) 289.

[72] C. W. J. Beenakker, M. Patra, P. W. Brouwer, Photonic excess noise and wave localization, Phys. Rev. A 61 (2000) R051801.

[73] K. M. Frahm, H. Schomerus, M. Patra, C. W. J. Beenakker, Large Petermann factor in chaotic cavities with many scattering channels, Europhys. Lett. 40 (2000) 48.

[74] H. Schomerus, K. M. Frahm, M. Patra, C. W. Beenakker, Quantum limit of the laser linewidth in chaotic cavities and statistics of residues of scattering matrix poles, Physica A 278 (2000) 469.

[75] M. Patra, H. Schomerus, C. W. J. Beenakker, Quantum–limited linewidth of a chaotic laser cavity, Phys. Rev. A 61 (2000) 023810.

[76] H. Feshbach, A unified theory of nuclear reactions. II, Ann. Phys. 19 (1962) 287.

[77] D. F. Wall, G. J. Milburn, Quantum Optics, Springer, Berlin, 1994.

[78] L. Mandel, E. Wolf, Optical coherence and quantum optics, Cambridge, New York, 1995.

[79] C. Gmachl, F. Capasso, E. E. Narimanov, J. U. Nöckel, A. D. Stone, J. Faist, D. L. Sivco, A. Y. Cho, High-power directional emission from microlasers with chaotic resonators, Science 280 (1998) 1556.

[80] G. Hackenbroich, C. Viviescas, B. Elattari, F. Haake, Photocount statistics of chaotic lasers, Phys. Rev. Lett. 86 (2001) 5262–5265.

[81] S. Deus, P. M. Koch, L. Sirko, Statistical properties of the eigenfrequency distribution of three-dimensional microwave cavities, Phys. Rev. E 52 (1995) 1146.

[82] H. Alt, H. D. Gräf, H. L. Harney, R. Hofferbert, H. Lengeler, A. Richter, P. Schardt, H. A. Weidenmüller, Gaussian orthogonal ensemble statistics in a microwave stadium billiard with chaotic dynamics: Porter-thomas distribution and algebraic decay of time correlations, Phys. Rev. Lett. 74 (1995) 62.

[83] H. Alt, C. Dembowski, H. D. Gräf, R. Hofferbert, H. Rehfeld, A. Richter, R. Schuhmann, T. Weiland, Wave dynamical chaos in a superconducting three-dimensional sinai billiard, Phys. Rev. Lett. 79 (1997) 1026.

[84] M. V. Berry, Regular and irregular semiclassical wavefunctions, J. Phys. A: Math. Gen. 10 (1977) 2083.

[85] F. Haake, Quantum Signatures of Chaos, 2nd Edition, Vol. 54 of Springer series in synergetics, Springer, Berlin, 2001.

[86] J. D. Urbina, K. Richter, Supporting random wave models: A quantum mechanical approach, J. Phys. A: Math. Gen. 36 (2003) L495.

[87] T. Guhr, A. Müller-Groeling, H. A. Weidenmüller, Random–matrix theories in quantum physics: Common concepts, Phys. Rep. 299 (1998) 189.

[88] C. W. Gardiner, M. J. Collett, Input and output in damped quantum systems: Quantum stochastic differential equations and the master equation, Phys. Rev. A 31 (1985) 3761.

[89] R. J. Glauber, Photon correlations, Phys. Rev. Lett. 10 (1963) 84.

[90] P. L. Kelley, W. H. Kleiner, Theory of electromagnetic field measurement and photoelectron counting, Phys. Rev. 136 (1964) A316.

[91] R. A. Jalabert, D. A. Stone, Y. Alhassid, Statistical theory of Coulomb blockade oscillations: Quantum chaos in quantum dots, Phys. Rev. Lett. 68 (1992) 3468.

[92] M. Patra, Theory for photon statistics of random lasers, Phys. Rev. A 65 (2002) 043809.

[93] E. G. Mishchenko, Fluctuations of radiation from a chaotic laser below threshold, Phys. Rev. A 69 (2004) 033802.

[94] M. P. van Exter, N. J. van Dutren, A. M. van der Lee, S. M. Dutra, G. Nienhuis, J. P. Woerdman, Semiclassical dynamics of excess quantum noise, Phys. Rev. A 63 (2001) 043801.

[95] R. J. Glauber, M. Lewenstein, Quantum optics of dielectric media, Phys. Rev. A 43 (1991) 467.

[96] D. V. Savin, V. V. Sokolov, H. J. Sommers, Is the concept of non-Hermitian effective Hamiltonian relevant in the case of potential scattering?, Phys. Rev. E 67 (2003) 026215.

[97] C. Viviescas, G. Hackenbroich, Field quantization for open optical cavities, Phys. Rev. A 67 (2003) 013805.

[98] C. Viviescas, G. Hackenbroich, Quantum theory of multimode fields: Applications to optical resonators, J. Opt. B 6 (2004) 211.

[99] W. Vogel, D.-G. Welsch, Lectures on quantum optics, Akademie Verlag, Berlin, 1994.

[100] J. D. Jackson, Classical Electrodynamics, Wiley, New York, 1975.

[101] U. Fano, Effects of configuration interaction on intensities and phase shifts, Phys. Rev. 124 (1961) 1866.

[102] F. M. Dittes, The decay of quantum systems with small number of open channels, Phys. Rep. 339 (2000) 215.

[103] C. Cohen-Tannoudji, J. Dupont-Roc, G. Grynberg, Atom–Photon Interactions: Basic Processes and Aplications, Wiley, New York, 1992.

[104] S. M. Barnett, P. M. Radmore, Quantum theory of cavity quasimodes, Opt. Commun. 68 (1988) 364.

[105] S. M. Dutra, G. Nienhuis, Derivation of a Hamiltonian for photon decay in a cavity, J. Opt. B 2 (2000) 584.

[106] S. M. Dutra, G. Nienhuis, A Hamiltonian for cavity decay, Acta Physica Slovaca 50 (2000) 275.

[107] P. L. Kapur, R. Peierls, The dispersion formula for nuclear reactions, Proc. Roy. Soc. Lond. A 166 (1938) 277.

[108] M. Hentschel, K. Richter, Quantum chaos in optical systems: The annular billiard, Phys. Rev. E 66 (2002) 056207.

[109] C. de Carvalho, H. Nussenzveig, Time delay, Phys. Rep. 364 (2002) 83.

[110] P. Ullersma, An exactly solvable model for brownian motion, Physica (Utrecht) 32 (1966) 27.

[111] P. S. Riseborough, P. Hänggi, U. Weiss, Exact results for a damped quantum–mechanical harmonic oscillator, Phys. Rev. A 31 (1985) 471.

[112] F. Haake, R. Reibold, Strong damping and low-temperature anomalies for the harmonic oscillator, Phys. Rev. A 32 (1985) 2462.

[113] P. J. Bardroff, S. Stenholm, Quantum theory of excess noise, Phys. Rev. A 60 (1999) 2529.

[114] P. J. Bardroff, S. Stenholm, Quantum Langevin theory of excess noise in lasers, Phys. Rev. A 61 (2000) 023806.

[115] P. J. Bardroff, S. Stenholm, Two-mode laser with excess noise, Phys. Rev. A 62 (2000) 023814.

[116] A. M. van der Lee, N. J. van Druten, M. P. van Exter, J. P. Woerdman, J.-P. Poizat, P. Grangier, Critical Petermann K factor for intensity noise squeezing, Phys. Rev. Lett. 85 (2000) 4711.

[117] G. Hackenbroich, C. Viviescas, F. Haake, Quantum statistics of overlapping modes in open resonators, Phys. Rev. A 68 (2003) 063805.

[118] C. Mahaux, H. A. Weidenmüller, Shell-Model Approach to Nuclear Reactions, North-Holland, Amsterdam, 1969.

[119] C. W. J. Beenakker, Random-matrix theory of quantum transport, Rev. Mod. Phys. 69 (1997) 731.

[120] M. Patra, C. W. J. Beenakker, Excess noise for coherent radiation propagating through amplifying random media, Phys. Rev. A 60 (1999) 4059.

[121] M. Patra, C. W. J. Beenakker, Propagation of squeezed radiation through amplifying absorbing random media, Phys. Rev. A 61 (2000) 063805.

[122] Y. V. Fyodorov, H.-J. Sommers, Statistics of resonance poles, phase shifts and time delays in quantum chaotic scattering: Random matrix approach for systems with broken time–reversal invariance, J. Math. Phys. 38 (1997) 1918.

[123] V. V. Sokolov, V. G. Zelevinsky, Dynamics and statistics of unstable quantum states, Nucl. Phys. A 504 (1989) 562.

[124] J. T. Chalker, B. Mehlig, Eigenvector statistics in non-Hermitian random matrix ensembles, Phys. Rev. Lett. 81 (1997) 3367.

[125] F. Haake, Statistical treatment of open systems by generalized master equations, in: G. Höhler (Ed.), Spring Tracts in Modern Physics, Vol. 66, Springer, Berlin, 1973, p. 98.

[126] H. Risken, The Fokker-Planck Equation, 2nd Edition, Springer, Berlin, 1989.

[127] M. V. Berry, Mode degeneracies and the Petermann excess-noise factor for unstable lasers, J. Mod. Opt. 50 (2003) 63.

[128] S. Haroche, Cavity quantum electrodynamics, in: J. Dalibard, R. J.-M., J. Zinn-Justin (Eds.), Fundamental Systems in Quantum Optics, Noth–Holland, Amsterdam, 1992, p. 767.

[129] T. S. Misirpashaev, P. W. Brouwer, C. W. J. Beenakker, Spontaneous emission in chaotic cavities, Phys. Rev. Lett. 79 (1997) 1841.

[130] Y. V. Fyodorov, Y. Alhassid, Photodissociation in quantum chaotic systems: Random-matrix theory of cross-section fluctuations, Phys. Rev. A 58 (1998) R3375.

[131] S. M. Dutra, K. Joosten, G. Nienhuis, N. J. van Dutren, A. M. van der Lee, M. P. van Exter, J. P. Woerdman, Maxwell–bloch approach to excess quantum noise, Phys. Rev. A 59 (1999) 4699.

[132] S. M. Dutra, K. Joosten, G. Nienhuis, J. P. Woerdman, Maxwell-bloch theory of excess quantum noise in lasers, J. Opt. B 2 (2000) 063805.

[133] S. Prasad, Theory of a homogeneously broadened laser with arbitrary mirror outcoupling: Intrinsic linewidth and phase diffusion, Phys. Rev. A 46 (1992) 1540.

[134] L. Davidovich, Sub-Poissonian processes in quantum optics, Rev. Mod. Phys. 68 (1996) 127.

[135] M. I. Kolobov, L. Davidovich, E. Giacobino, C. Fabre, Role of pumping statistics and dynamics of atomic polarization in quantum fluctuations of laser sources, Phys. Rev. A 47 (1993) 1431.

[136] M. Lax, Classical noise. V. Noise in self–sustained oscillators, Phys. Rev. 160 (1967) 290.

[137] P. Goldberg, P. W. Milonni, B. Sundaram, Theory of the fundamental laser linewidth. II, Phys. Rev. A 44 (1991) 4556.

[138] C. H. Henry, Theory of the linewidth of semiconductor lasers, IEEE J. Quantum Electron. QE-18 (1982) 259.

[139] C. H. Henry, Theory of the phase noise and power spectrum of a single mode injection laser, IEEE J. Quantum Electron. QE-19 (1983) 1391.

[140] A. M. van der Lee, N. J. van Druten, A. L. Mierement, M. P. van Exter, J. P. Woerdman, Excess quantum noise is colored, Phys. Rev. Lett. 81 (1998) 5121.

[141] P. Grangier, J. P. Poizat, A simple quantum picture for the Petermann excess noise factor, Eur. Phys. J. D 1 (1998) 97.

[142] P. Grangier, J. P. Poizat, Quantum derivation of the excess noise factor in lasers with non-orthogonal eigenmodes, Eur. Phys. J. D 7 (1999) 99.

[143] J.-P. Poizat, T. Chang, P. Grangier, Quantum intensity noise of laser diodes and nonorthogonal spatial eigenmodes, Phys. Rev. A 61 (2000) 043807.

Acknowledgements

During the period of my PhD studies I received the invaluable help and support of numerous colleagues and friends without which this work could not have been possible. I would like to thank all of them. *Gracias.*

It is a great pleasure to thank PD. Gregor Hackenbroich for the excellent guidance throughout the work. The open and continuous discussion we held during the course of the last years in which I felt my ideas were welcome and appreciated, and through which he exposed me to new and interesting topics and provided me with the support and encouragement to pursue research on them, led to fruitful work done together from which I took great satisfaction. The help and example he offered to me went beyond the academic and working environments and permeated other spheres of my life, I am particularly thankful for that.

I am grateful to Prof. Fritz Haake for his involvement in and collaborations to this work. I profited immensely from his in-depth knowledge of both quantum optics and quantum chaos through several insightful scientific discussions at different stages of my work. Witnessing his cheerful approach to research, always managed to motivate me.

The good working environment that I found in the "quantum chaos" group in Essen was without doubt the most positive and influential factor for the well development of my research work. I am grateful to all of its members. Dimitry V. Savin, by patiently answering to all of my questions, made clear to me most of the concepts of scattering theory that I needed for this thesis. I am in debt with him for the many fruitful discussions on open systems from which I always ended up taking much more than I put in. The work and comments of Prof. Hans-J. Sommers were crucial for my own understanding of the projection formalism and for the application of random matrix theory to open optical resonators presented in this work. On this last subject, the comments of Prof. Yan Fyodorov were also important. Special thanks goes to Prof. Petr A. Braun for the many delightful and illustrative scientific (and non-scientific) conversations. I would also like to say thanks to Holger Shaefers, Christopher Manderfeld, Dominique Spehner, Stefan Heusler, and Sebastian Müller for explaining me their work, sharing their ideas with me, and for many interesting discussions. I owe a large debt of gratitude to Ms. Monika Motzko for her generous help in dealing with every day administrative issues in and out of the university.

In the last years I have enjoyed the friendly atmosphere of the theoretical physical department in Essen. In particular, I thank Prof. Joachim Krug, Walter Strunz, Jouni Kallunki and Philipp Kuhn for enjoyable and interesting conversations.

I wish to express my deep gratitude to Prof. Thomas Dittrich for his constructive criticisms and wise counsels in scientific and non-scientific matters. I thank Prof. Uzy Smilansky for his interest in my work and for his hospitality during my visit to his group at the Weizmann Institute.

I am thankful to Juan Diego Urbina for his support, and for his insightful comments and critics to my work. I enjoy very much the exciting, and almost daily, exchanged of ideas of all sort that we kept during this period. I wish to thank Javier Madroñero for his unconditional help and interesting discussions.

I would like to say thank you to Annette Fiebig for her warm hospitality and valuable help since my first day in Essen. I am also thankful to Gabriela Baez and Rafael Méndez for making it so easy for me to get settled in Essen.

I want to express all my gratitude towards Esperanza, Fernando, and Federico for their unconditional support. Finally, I thank Olga for her priceless support, for keeping me close and letting me move along with her.

This work was supported by the SFB/TR 12 der Deutschen Forschungsgemeinschaft.

Curriculum Vitae

Name:	Carlos Leonardo Viviescas Ramírez
Born:	October 24, 1973 in Medellín (Colombia)
Marital status:	Married

Education

1990	High School degree at the Instituto Arturo Ramírez Montufar, Bogotá
1991	Military service
1992	Physics studies at Universidad Nacional de Colombia, Bogotá
1997	Physics degree at Universidad Nacional de Colombia
1998	Master studies in Physics at Universidad Nacional de Colombia, Bogotá
2000	Master in Physics at Universidad Nacional de Colombia
2000	PhD studies at Universität Essen–Duisburg

Scholarships

1998	Scholarship from Fundación MAZDA para la ciencia y el arte